NASA Tech Briefs

Official Publication of
National Aeronautics and
Space Administration
Volume 15 Number 7

Transferring Technology
to Industry and
Government
July 1991

Riding A Shock Wave

YOU CAN DEVELOP ADA CODE WITHOUT ADAMAT.™ OF COURSE, YOU CAN SKYDIVE WITHOUT THIS, TOO.

The fact is, when you write Ada code without using AdaMAT™ you're really putting the quality of your code at great risk. To be frank, you're actually inviting poorly written, unclear and inconsistent code that guarantees errors during development.

AdaMAT is quite simply, the most valuable and crucial software engineering tool that is available today to Ada program developers. It is the only tool for the prevention of errors during development. AdaMAT analyzes Ada code and evaluates it using key quality characteristics that are based on the most effective use of the language.

With the use of AdaMAT, potential errors are detected prior to testing. It lets programmers insure the quality of their code earlier in development when errors are much less time-consuming and costly to fix. So avoid the pitfalls.

Get your project in on time and right on budget. Write clean, consistent, accurate, reliable Ada code. And do it whether you're developing in the Rational, VAX, SUN, or SCO/UNIX environments. Call us today at 1-800-522-7321 for complete information. We'd jump at the chance to tell you all about the immediate benefits you'll receive using AdaMAT for your Ada development.

DRC® DYNAMICS RESEARCH CORPORATION

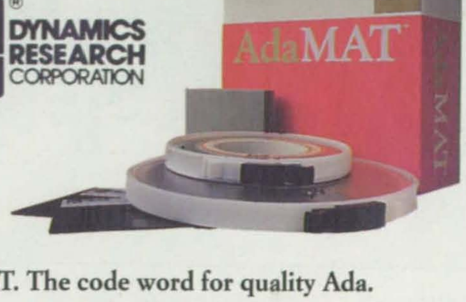

AdaMAT. The code word for quality Ada.

Dynamics Research Corporation, 60 Frontage Road, Andover, MA 01810

Circle Reader Action No. 601

2048 x 2048 Pixel, 12-Bit Digital CCD Camera

Photometrics introduces the world's first **2048 x 2048 pixel CCD camera** with a direct digital output and 12 bits per pixel (4096 gray levels). This ultra-high resolution camera interfaces directly to Macintosh II, 286/386 AT bus computers, or VME-based systems.

This camera features:

- A scientific-grade CCD image sensor with 2048 x 2048 pixels (Eastman Kodak KAF-4200)
- Thermoelectrically cooled camera head providing 12-bit dynamic range (4096 gray levels per pixel)
- A direct digital interface, plug-in programmable controller for Macintosh II, 286/386 AT bus, or VME computers
- Software for camera control, image acquisition, and calibration

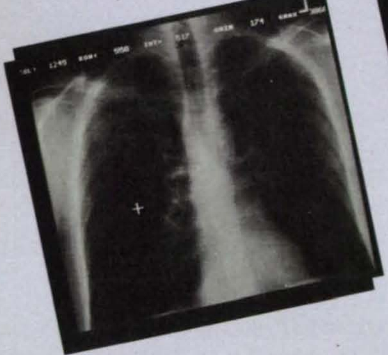

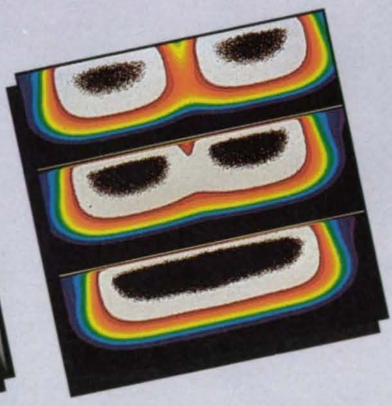

This camera can be used for high-resolution, low light applications including x-ray imaging and densitometry. (Image on right courtesy of the Medical College of Georgia.)

This new Photometrics camera is ideal for use in film digitization, electron and optical microscopy, medical diagnostic imaging (with phosphor screens), photodigitization, color separation, densitometry, and other applications demanding high resolution and high dynamic range.

Photometrics has a complete line of cooled CCD cameras from 512 x 512 to 2048 x 2048 pixels with 12, 14, or 16 bits per pixel. For end-user and OEM applications assistance, please call **(602) 889-9933**.

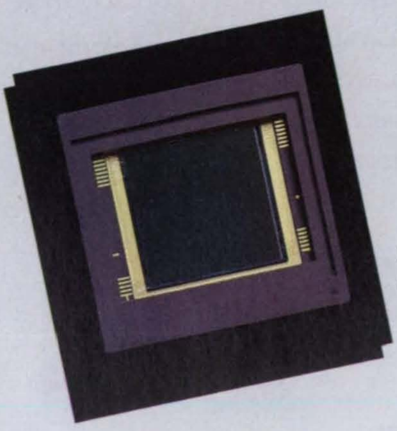

KAF-4200 CCD
(2048 x 2048 pixels)

Photometrics
World Leader in High Performance CCD Imaging

Circle Reader Action No. 619

Photometrics, Ltd.
3440 East Britannia Drive • Tucson, Arizona 85706
FAX: (602) 573-1944 • Telephone: (602) 889-9933

Also in Europe: Photometrics GmbH, Sollner Str. 61
D-8000 München 71, Germany, Telefax: 0 89-79-97-15, Telephone: 0 89-79-95-80
ARGENTINA: Laser Optics S.A., tel: 01-466-754 ■ **FRANCE:** Sofretec, tel: 1-34-23-30-00
ISRAEL: New Technology RK Ltd., tel: 03-324181 ■ **JAPAN:** Seki Technotron Corp., tel: 03-3820-1712
KOREA: Eusung International Corp., tel: 02-785-1368 ■ **TAIWAN:** Gorman Co., Ltd. tel: 02-392-3170
SINGAPORE: Astro Scientific Centre, tel: 567-4163

DATEL Redefines The Digital Panel Meter

DPM The Component

DATEL's new DMS-30PC Series is a milestone in Digital Panel Meter technology. The only fully functional, factory calibrated, 3 1/2 digit, Hybrid Voltmeter available anywhere. For extreme accuracy, critical reliability, and ultra-low price in a sub-miniature, modular package, the DMS-30 is your only choice.

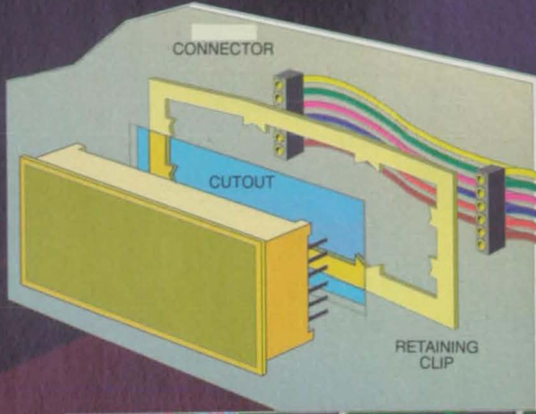

WORLD'S SMALLEST
- Low profile design
- Full size display 0.56"
- 0.94"h x 2.18"w x 0.57"d

MODULAR DESIGN
- Fully encapsulated
- Simple plug-in design
- Integrated Filter/Bezel

HIGHEST QUALITY STOCK DELIVERY
- 0.05% accuracy
- One year warranty
- Made in USA

CHOICE OF COLORS
- Red
- Green
- Yellow
- Amber
- Orange
- Blue

EVALUATION BOARD
- 4-20mA current loop with gain/offset adjust
- Battery powered (9V, 12V)
- Max. 250VDC input

CHOICE OF INPUT RANGES
- ±200mV/±2VDC/±20VDC

LOW PRICE
- As low as $29 ea. (qty. 100s)
- Quantity discounts

$29 ea.
Qty. 100s

LOW POWER DRAIN
- As low as 15mA/5VDC powered

ADVANCED TECHNOLOGY
- Laser trimmed
- Built on ceramic
- Hybrid design

RUGGED RELIABILITY
- 1 million hours MTBF
- Shock/vibration proof
- Dust/dirt proof

ACTUAL SIZE

For details call or write DATEL, Inc.
11 Cabot Boulevard, Mansfield, MA 02048
Tel (508)339-3000, FAX (508)339-6356

DATEL®

INNOVATION AND EXCELLENCE IN PRECISION DATA ACQUISITION

Circle Reader Action No. 316

Discover the one guaranteed

Stars cool. Volcanos fizzle. Even suns burn out. But the IBM RISC System/6000™ family of POWERstations and POWERservers is no flash in the pan. In the year or so since we introduced it, it's only gotten hotter—offering performance ranging from 9 to 25 MFLOPS and from 33 to 72 SPECmarks. All at prices that won't even make you break into a sweat.

An operating system that sizzles. The RISC System/6000 family operates on AIX,® IBM's enhanced version of the UNIX® operating system. AIX runs across the broadest range of platforms in the industry, and not only supports all major industry standards and programming languages, but brings you additional enhancements like enriched file system capabilities, support for advanced systems management and much more. Best of all, AIX fans the flames of the RISC System/6000 family's POWER architecture, to give you even hotter performance.

	Hardware Price	MFLOPS	SPECmarks™
POWERserver 550	$62,000	25.2	72.2
SPARCserver™ 470	$77,800	3.8	19.4
DECsystem™ 5500	$74,700	4	21.5

MFLOPS are LINPACK double-precision where n=100. AIX XL FORTRAN Version 2.1 and AIX XL C Version 1.1 compilers were used for these tests. SPECmark is a geometric mean of the ten SPECmark tests. All prices current at publication.

source of power to stay hot.

An applications platform spreading like wildfire. The RISC System/6000 family already runs over 3,000 diverse applications in mechanical design, visualization, software engineering, accounting, retail store management and on and on. But we're still feeding the fire. More and more applications are being written and ported over to run on the family every day.

IBM support: an eternal flame. There's never been anything lukewarm about IBM's commitment to its customers, and there never will be. With the RISC System/6000, you get the unparalleled worldwide support of IBM: service when you need it, 24 hours a day, 365 days a year. An IBM customer engineer can even come to your site and install your machines, configure your network and integrate all your systems, whether they're made by IBM or not. It's enough to make you feel warm all over.

To find out how you can harness the power of the RISC System/6000 family, call your IBM marketing representative or Business Partner at: 1 800 IBM-6676, ext. 845. Sorry, marshmallows not included.

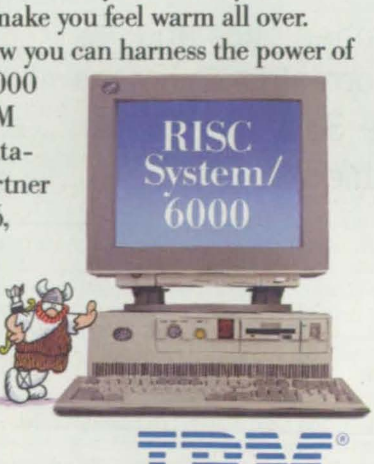

For the Power Seeker.

IBM®

NASA Tech Briefs

Transferring Technology to Industry and Government

July 1991
Volume 15 Number 7 BPA ABP

Photo courtesy Johnson Space Center

A new invention from the Johnson Space Center represents a major advance in helmet-mounted display systems. See the tech brief on page 34.

SPECIAL FEATURES

TECHNICAL SECTION

DEPARTMENTS

On The Cover: This CFD simulation created on a Personal Iris shows the position and magnitude of shock waves — regions representing sudden, dramatic changes in air flow properties — around an F-16 flying supersonically. The colors represent the Mach numbers of the shock. Reports on page 74 describe recent NASA work on shock computation which could result in more efficient aircraft designs.
(Image courtesy Fluid Dynamics International)

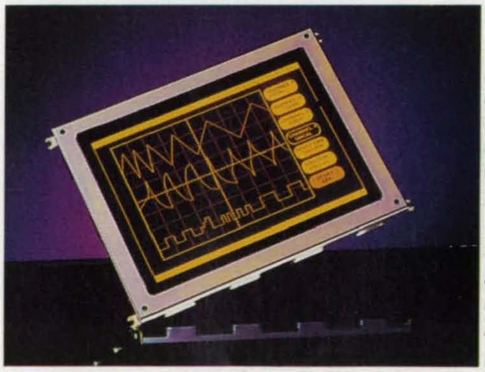

Photo courtesy Planar Systems Inc.

First developed for space and military applications, thin-film electroluminescent displays have a bright future in the commercial arena. See Mission Accomplished, page 10.

NASA Tech Briefs, ISSN 0145-319X, USPS 750-070, copyright © 1991 in U.S., is published monthly by Associated Business Publications Co., Ltd., 41 E. 42nd St., New York, NY 10017-5391. The copyrighted information does not include the individual tech briefs which are supplied by NASA. Editorial, sales, production and circulation offices at 41 East 42nd Street, New York, NY 10017-5391. Subscription for non-qualified subscribers in the U.S., Panama Canal Zone, and Puerto Rico, $75.00 for 1 year; $125.00 for 2 years; $200.00 for 3 years. Single copies $10.00. Foreign subscriptions one-year U.S. Funds $150.00. Remit by check, draft, postal, express orders or VISA, MasterCard, and American Express. Other remittances at sender's risk. Address all communications for subscriptions or circulation to NASA Tech Briefs, 41 East 42nd Street, New York, NY 10017-5391. Second-class postage paid at New York, NY and additional mailing offices. **POSTMASTER: please send address changes to NASA Tech Briefs, 41 E. 42nd Street, Suite 921, New York, NY 10017-5391.**

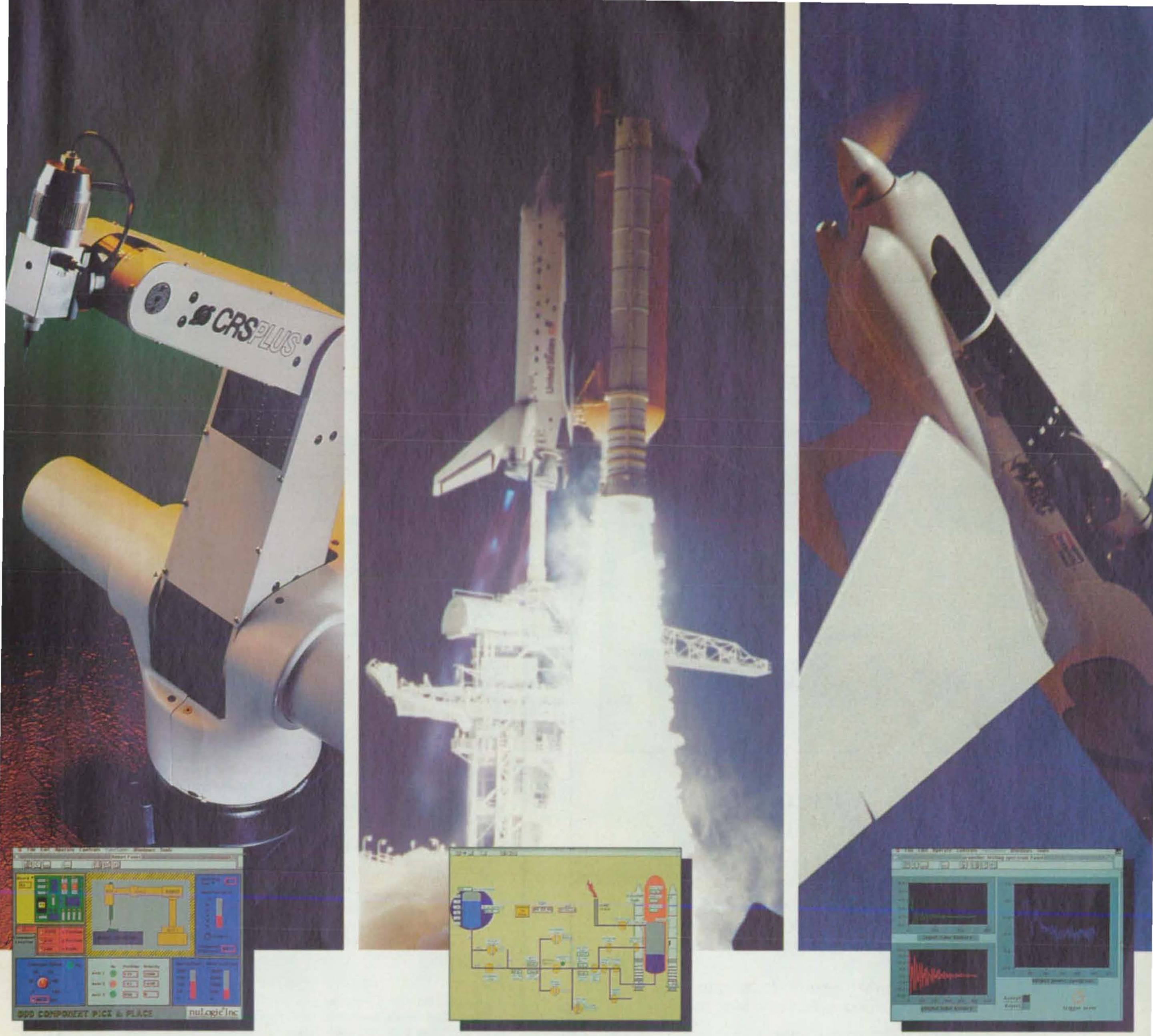

LabVIEW® 2
Where The Only Barrier Is Your Imagination.

By now, you are probably familiar with LabVIEW 2, the most celebrated application software for data acquisition and instrument control on the Macintosh. It recently won the *MacUser* magazine Editors' Choice award. Five years ago, LabVIEW introduced the combination of front panel interfaces and graphical programming. Today, engineers and scientists around the world are using LabVIEW 2 in a broad spectrum of applications.

Unlike other graphical packages, LabVIEW 2 does not sacrifice power and flexibility for ease of use. With LabVIEW 2, you quickly build block diagram programs and add your own blocks to expand upon our libraries. You also create front panel user interfaces and import pictures to customize the panels. Yet LabVIEW 2 virtual instruments run as quickly as compiled C programs.

If you thought LabVIEW 2 was just for test and measurement, call us to find out what LabVIEW 2 is really about.

For a free LabVIEW 2 Demo disk call:
(512) 794-0100 or
(800) 433-3488
(U.S. and Canada)

NATIONAL INSTRUMENTS®
The Software is the Instrument®

6504 Bridge Point Parkway
Austin, TX 78730-5039

Circle Reader Action No. 681

NASA Tech Briefs
Official Publication of National Aeronautics and Space Administration
ABP BPA

NASA Tech Briefs:

Published by ..... **Associated Business Publications**
Editor-in-Chief/Publisher ..... **Bill Schnirring**
Associate Publisher ..... **Frank Nothaft**
Editor ..... **Joseph T. Pramberger**
Managing Editor ..... **R.J Laer**
Assistant Editor ..... **Justina Cardillo**
Assistant Editor ..... **Patrick Corbett**
Technical Advisor ..... **Dr. Robert E. Waterman**
Production Manager ..... **Rita Nothaft**
Traffic Manager ..... **James E. Cobb**
Art Director ..... **Pierre Granier**
Circulation Manager ..... **Cheryl Cohen**
Advertising Coordinator ..... **Daniel Murphy**
Telecommunications Specialist ..... **Evelyn Mars**
Reader Service Manager ..... **Sylvia Valentin**

Briefs & Supporting Literature:
Provided to National Aeronautics and Space Administration by **International Computers & Telecommunications, Inc.**, NY, NY with assistance from **Logical Technical Services**, NY, NY
Technical/Managing Editor ..... **Ted Selinsky**
Art Director ..... **Luis Martinez**
Administrator ..... **Elizabeth Texeira**
Chief Copy Editor ..... **Lorne Bullen**
Staff Writers/Editors ..... **Dr. James Boyd, Dr. Larry Grunberger, Dr. Theron Cole, Jordan Randjelovich, George Watson, Oden Browne**
Graphics ..... **Zinaida Gimpeleva, Vernald Gillman, Pamela Baynham, Charles Sammartano**
Editorial & Production ..... **Bill Little, Ivonne Valdes, Susan Kyu Oh, Frank Ponce**

NASA:
NASA Tech Briefs are provided by the National Aeronautics and Space Administration, Technology Utilization Division, Washington, DC:
Administrator ..... **Richard H. Truly**
Assistant Administrator for Commercial Programs ..... **James T. Rose**
Deputy Assistant Administrator(Programs) ..... **Frank E. Penaranda**
Deputy Director TU Division(Publications Manager) ..... **Leonard A. Ault**
Manager, Technology Utilization Office, NASA Center For AeroSpace Information ..... **Walter M. Heiland**

Associated Business Publications
41 East 42nd Street, Suite 921, New York, NY 10017-5391
(212) 490-3999 FAX (212) 986-7864
President ..... **Bill Schnirring**
Executive Vice President ..... **Frank Nothaft**
Vice President ..... **Domenic A. Mucchetti**
Operations Manager ..... **Rita Nothaft**
Controller ..... **Felecia Lahey**
Systems Analyst ..... **Patrick Wolfert**

Advertising:
New York Office:(212) 490-3999 FAX (212) 986-7864
Director of Advertising Sales ..... **Domenic A. Mucchetti**
Account Executive (NY,NJ) ..... **Brian Clerkin** at (201) 366-2751
Account Executive (VA,DC,MD,DE,WV) ..... **John D. Floyd, CBC** at (215) 399-3265
Account Executive ..... **Debby Crane** at (201) 967-9838
Regional Manager (Midwest) ..... **Paul Lesher,CBC** at (312) 296-2040
Account Executive (Northwest) ..... **Bill Hague** at (206) 858-7575
Regional Sales Manager (South) ..... **Douglas Shaller** at (212) 490-3999
Account Executives (Eastern MA,NH,ME,RI) ..... **Paul Gillespie** at (508) 429-8907;**Bill Doucette** at (508) 429-9861
Account Executives (Western MA,CT,VT) ..... **George Watts** at (413) 253-9881
Account Executives (Calif.,AZ,NV,NM)
for Area Codes 714/619 **Tom Murphy**
for Area Codes 213/818/805/602/702/505 **Robert D'Alexander** at (213) 372-2744
..... for Area Codes 408/415/916/209/707 **Elizabeth Cooper** at (415) 673-5123

NTBM-Research Center
Account Supervisor ..... **Lourdes Del Valle**

PC MAGAZINE EDITORS' CHOICE
March 26, 1991
Graftool, Version 3.3

GRAFTOOL™

"extremely flexible, powerful, and easy-to-use" ..."the ultimate graphics package, fulfilling everybody's needs."

Reprinted with permission from PC Magazine, March 14th, 1989, Copyright ©1989 Ziff Communications Co. and PC Magazine, March, 26th, 1991 ©Ziff Communications Co.

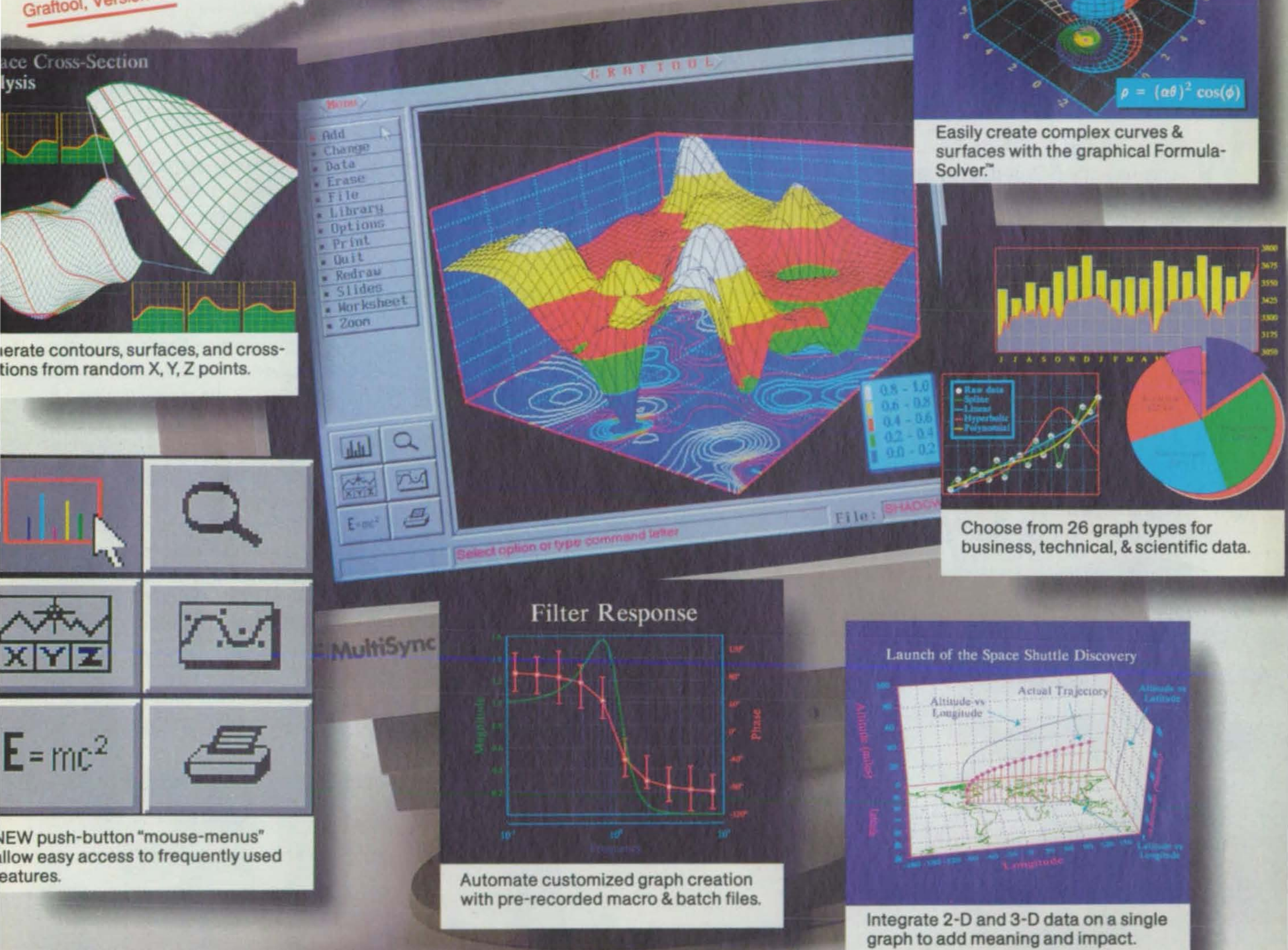

Easily create complex curves & surfaces with the graphical Formula-Solver.™

...erate contours, surfaces, and cross-...tions from random X, Y, Z points.

Choose from 26 graph types for business, technical, & scientific data.

...NEW push-button "mouse-menus" ...llow easy access to frequently used ...eatures.

Automate customized graph creation with pre-recorded macro & batch files.

Integrate 2-D and 3-D data on a single graph to add meaning and impact.

Presentation graphics and analysis for scientific users.

Your technical data requires more muscle and sophistication than basic business graphics and plotting packages can provide. It's simply a matter of using the right tool for the job. In addition to publication-quality graphics, you need powerful analysis tools and capabilities such as Graftool's ■ Intelligent Data Cursor™ to read out data points on curves & surfaces ■ Linear & non-linear curve-fitting ■ Unlimited zoom & rotation ■ Multiple axes in linear, log, or probability scales ■ Advanced data handling, allowing over 268,000,000 data points ■ Powerful scientific spreadsheet which can directly read your Lotus or ASCII files ■ Unrestricted placement of graphs & text ■ Direct compatibility with Microsoft Word & WordPerfect.

With Graftool, all this power and flexibility purr quietly under the hood, while pop-up menus and push-buttons bring an ease of use previously unheard of in scientific software. Just "point & process" with increased productivity and greater understanding.

GRAFTOOL – the right tool for your technical solutions.

GRAFTOOL $495.

- Interactive demo available
- Academic discounts.

3D 3-D VISIONS

412 S. Pacific Coast Highway, Second Floor
Redondo Beach, CA 90277
Call: 1 (800) 729-4723, 1 (213) 540-8818
FAX: 1 (213) 540-3492

Circle Reader Action No. 669

Mission Accomplished

Through the technology transfer process, many of the systems, methods, and products pioneered by NASA are reapplied in the private sector, obviating duplicate research and making a broad range of new products and services available to the public.

With the aid of NASA and the Department of Defense, a small Oregon company has emerged as a leader in the rapidly-expanding electronic display market, successfully challenging such giants as Sharp and Matsushita.

Beaverton-based Planar Systems Inc., a privately-owned firm with 150 employees, was founded in 1983 by senior managers from Tektronix and today is the world's largest producer of thin-film electroluminescent (EL) displays, one of three major flat-panel display technologies, along with liquid crystal displays (LCDs) and plasma display panels (PDPs). Offering the advantages of compactness, light weight, and low power consumption, flat-panel displays are supplanting cathode ray tubes (CRTs) in applications ranging from computers and business terminals to industrial control equipment and medical monitors, and are likely to find widespread use in future high-definition television (HDTV) systems.

EL, the newest flat-panel technology, is solid-state and therefore inherently rugged, making it particularly attractive for military and space environments. Over the last decade, the US Army and NASA have funded research and development of EL displays for application in flight simulators and aircraft and spacecraft cockpits. "The government has played a pivotal role in advancing (EL) technology," said Christopher King, Planar's executive vice president, "and has been instrumental in our company's growth."

Army/NASA support helped Planar refine its production process to achieve large-size, defect-free EL displays with high resolution. The unique fabrication process involves the vacuum deposition of a sandwich of thin films on a glass substrate patterned with transparent column electrodes. In a single step, three layers are sequentially deposited — an insulating dialectric film, a phosphor film, and another dialectric film. Aluminum row electrodes are then laid down perpendicular to the column electrodes and the display is sealed to protect it from the environment.

A circuit board, with control and drive components mounted within the same space as the viewing area on the glass panel, is connected to the back of the substrate using conductive silicone rubber interconnect technology. When AC voltage is applied between a column and row electrode, the phosphor film emits light that passes through the transparent electrode, through the glass face, and onto the viewer. The light is emitted uniformly at electrode intersections, creating precisely-defined pixels with high contrast.

In 1984, Planar became the first US manufacturer of EL displays by shipping an 80 character by 25 line monochrome product. This was followed a year later by the world's first MS-DOS-

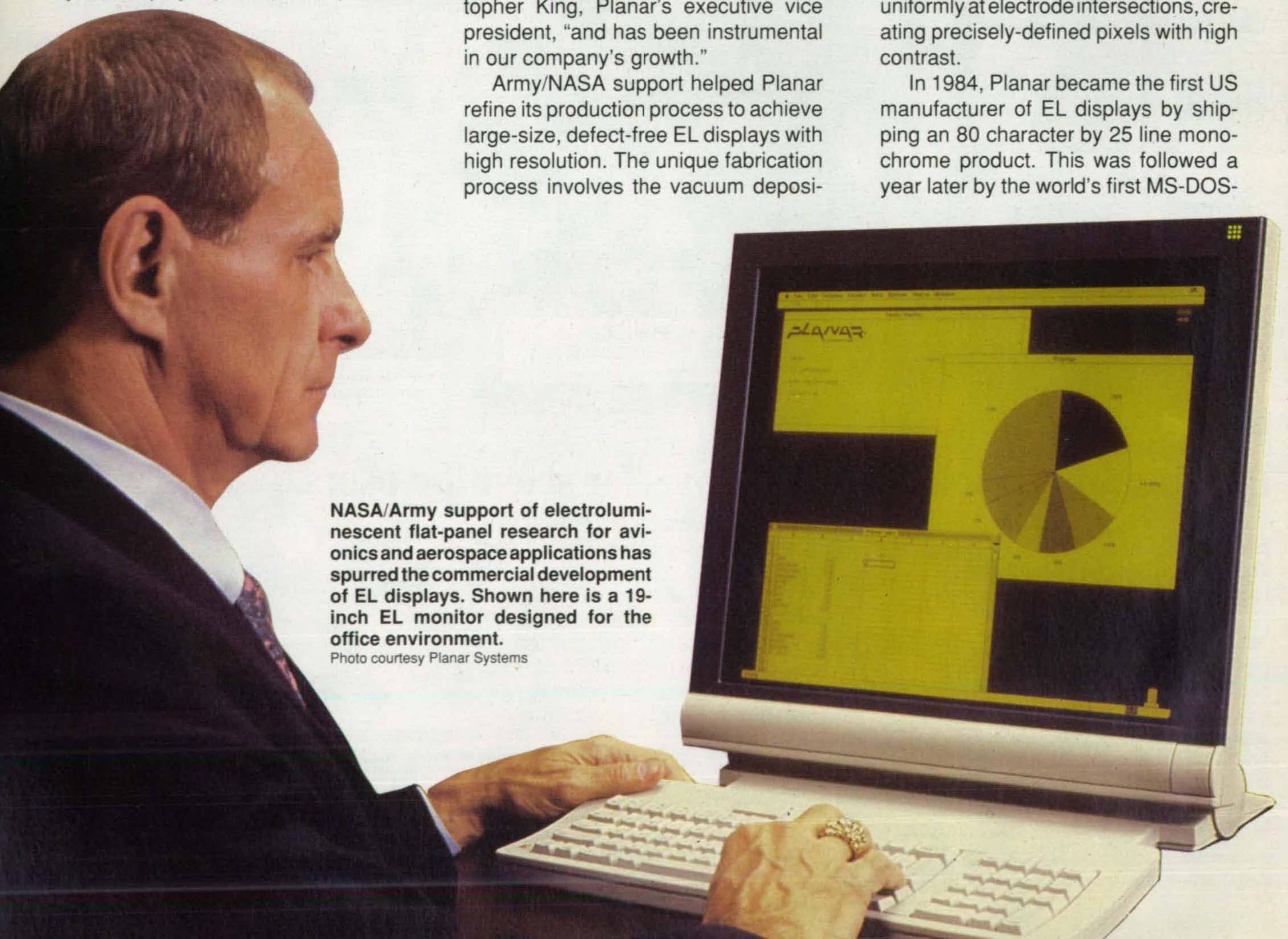

NASA/Army support of electroluminescent flat-panel research for avionics and aerospace applications has spurred the commercial development of EL displays. Shown here is a 19-inch EL monitor designed for the office environment.
Photo courtesy Planar Systems

compatible 640 by 200 pixel EL monitor. In 1988, the company introduced a 19-inch diagonal monochrome display supporting 1024 columns by 864 rows — "a major breakthrough in solid-state flat-panel fabrication," according to King. And last year, Planar produced EL displays with lower power consumption than backlit LCDs and screen brightness comparable to CRTs.

To compete with LCDs and CRTs in more than limited applications, however, EL displays must be offered in full color. This requires the use and control of phosphors in the three primary colors: red, green, and blue. Under government contract, Planar has improved the brightness of the red phosphor from 2 to 20 foot-Lamberts (fL) and introduced sputtered green phosphor into the color EL structure, doubling the luminance of the green. The company is incorporating these advances into a line of multi-color displays targeted for industrial, medical, and military applications that do not require full color but still want the extra information content available through multiple colors to highlight data or warning messages. This spring, Planar demonstrated a 9-inch diagonal CGA-format display that produces red, green, yellow, and black with CRT-like brightness. The new display, complete with CGA interface board, will be sampled for prototype development in 1992.

Research is now focused on improving the brightness of the blue phosphor, weakest of the three primary colors. "The blue has been the biggest obstacle to obtaining a full-color (EL) display," said Thomas Kelley, leader of the Display Applications Team at the Army's Technology and Devices Laboratory, "but we've begun to make some real progress in overcoming this problem. In the last year alone, we've seen the luminescence of the blue more than double."

Photo courtesy Planar Systems

Planar recently demonstrated the first commercial-quality multi-color EL display, the result of extensive research on color phosphors.

Planar has produced a saturated blue phosphor with 2.5 fL of brightness. "Our goal for a quality full-color display is 5 fL," stated King. The company is continuing development of the blue phosphor as part of DARPA's High-Definition Display program, which looks to advance HDTV technology in the US.

Full color will "open up a world of new uses," for thin-film EL displays, said Millard McDonnell, Planar's chief operating officer, and accelerate EL's already impressive growth in the electronic display market. Sales of EL products surpassed $90 million in 1990, and are expected to increase, worldwide, by 50 percent annually over the next decade. ❑

For more information about the technologies described in this article, contact:

Jeff Oromaner
Planar Systems Inc.
1400 NW Compton Drive
Beaverton, OR 97006

New Product Ideas

New Product Ideas are just a few of the many innovations described in this issue of *NASA Tech Briefs* and having promising commercial applications. Each is discussed further on the referenced page in the appropriate section in this issue. If you are interested in developing a product from these or other NASA innovations, you can receive further technical information by requesting the TSP referenced at the end of the full-length article or by writing the Technology Utilization Office of the sponsoring NASA center (see page 14). NASA's patent-licensing program to encourage commercial development is described on page 14.

Thermocouple-Signal-Conditioning Circuit

A signal-conditioning electronic circuit serves as an interface between a thermocouple and a control circuit that was designed for use with a resistance thermal device. When the signal-conditioning circuit is used, the bridge-completion network is modified in such a way that the bridge operates in a voltage mode.
(See page 20)

High-Temperature Insulating Gap Filler

A new inorganic, ceramic filler for gaps between refractory ceramic tiles offers high resistance to heat and erosion. The ceramic filler could be used as a sealing material in furnaces or as a heat shield for sensitive components in automobiles, aircraft, and home appliances.
(See page 52)

Lightweight Fibrous Ni Electrodes for Ni/H_2 Batteries

A fibrous nickel plaque electrode material reduces the weight of nickel/hydrogen batteries. The discharge voltage and discharge time of this electrode are greater than those of the equivalent standard sintered-powder electrode.
(See page 56)

Dishwasher for Earth or Outer Space

A dishwashing machine cleans eating utensils in either Earth gravity or zero gravity of outer space. A rotating tub guides used washwater to a drain, a self-cleaning filter removes food particles from the washwater without becoming clogged, and a separator extracts air from the washwater so that both air and washwater can be recycled.
(See page 78)

Imaging Microscope for "Water-Window" X Rays

A proposed microscope would operate in the "water-window" part of the x-ray spectrum, which lies at wavelengths greater than the 23.3-Å wavelength of the K absorption edge of oxygen but less than the 43.7-Å wavelength of the K absorption edge of carbon. The microscope would be well suited for making high-resolution, high-contrast images for microbiological research.
(See page 40)

Thermosyphon Suspension for Growth of Crystals

A thermosyphon apparatus uses gentle upward flow of a supersaturated solution to suspend a crystal growing from the solution. Protein crystals are so fragile that they are easily damaged by the high-shear flows produced by pumps.
(See page 82)

HOW YOU CAN BENEFIT FROM NASA's TECHNOLOGY UTILIZATION SERVICES

If you're a regular reader of TECH BRIEFS, then you're already making use of one of the low-and no-cost services provided by NASA's Technology Utilization (TU) Network. But a TECH BRIEFS subscription represents only a fraction of the technical information and applications/engineering services offered by the TU Network as a whole. In fact, when all of the components of NASA's Technology Utilization Network are considered, TECH BRIEFS represents the proverbial tip of the iceberg.

We've outlined below NASA's TU Network—named the participants, described their services, and listed the individuals you can contact for more information relating to your specific needs. We encourage you to make use of the information, access, and applications services offered by NASA's Technology Utilization Network.

How You Can Utilize **NASA's Industrial Applications Centers**—A nationwide network offering a broad range of technical services, including computerized access to over 100 million documents worldwide.

You can contact NASA's network of Industrial Applications Centers (IACs) for assistance in solving a specific technical problem or meeting your information needs. The "user friendly" IACs are staffed by technology transfer experts who provide computerized information retrieval from one of the world's largest banks of technical data. Nearly 500 computerized data bases, ranging from NASA's own data base to Chemical Abstracts and INSPEC, are accessible through the ten IACs located throughout the nation. The IACs also offer technical consultation services and/or linkage with other experts in the field. You can obtain more information about these services by calling or writing the nearest IAC. User fees are charged for IAC information services.

Aerospace Research Center (ARAC)
Indianapolis Center for Advanced Research
611 N. Capitol Avenue
Indianapolis, IN 46204
Dr. F. Timothy Janis, Director
(317) 262-5036

Central Industrial Applications Center/NASA (CIAC)
Rural Enterprises, Inc.
Post Office Box 1335
Durant, OK 74702
Dr. Dickie Deel, Director
(405) 924-5094
(800) 658-2823 (toll-free U.S.)

Science and Technology Research Center (STRC)
Post Office Box 12235
Research Triangle Park, NC 27709-2235
H.L. (Lynn) Reese, Director
(919) 549-0671

NASA Industrial Applications Ctr. 823 William Pitt Union
University of Pittsburgh
Pittsburgh, PA 15260
Lani Hummel
Executive Director
(412) 648-7000

Southern Technology Applications Center (STAC)
Post Office Box 24
Progress Ctr., One Progress Blvd.
Alachua, FL 32615
J. Ronald Thornton, Director
(904) 462-3913
(800) 354-4832 (FL only)
(800) 225-0308 (toll-free US)

NASA/UK Technology Technology Applications Center
University of Kentucky
109 Kinkead Hall
Lexington, KY 40506-0057
William R. Strong, Director
(606) 257-6322

NERAC, Inc.
One Technology Drive
Tolland, CT 06084
Dr. Daniel U. Wilde, President
(203) 872-7000

Technology Application Center (TAC)
University of New Mexico
Albuquerque, NM 87131
Dr. Stanley A. Morain, Director
(505) 277-3622

NASA Industrial Applications Center
University of Southern California
Research Annex
3716 South Hope Street
Los Angeles, CA 90007-4344
Robert Stark, Director
(213) 743-6132
(800) 642-2872 (CA only)
(800) 872-7477 (toll-free US)

NASA/SU Industrial Applications Center
Southern University Department of Computer Science
Post Office Box 9737
Baton Rouge, LA 70813-9737
Dr. John Hubbell, Director
(504) 771-6272
(504) 771-4950

If you represent a public sector organization with a particular need, you can contact NASA's Application Team for technology matching and problem solving assistance. Staffed by professional engineers from a variety of disciplines, the Application Team works with public sector organizations to identify and solve critical problems with existing NASA technology. **Technology Application Team, Research Triangle Institute, P.O. Box 12194, Research Triangle Park, NC 27709; *Dr. Doris Rouse, Director,* (919) 541-6980**

How You Can Access Technology Transfer Services At NASA Field Centers: **Technology Utilization Officers & Patent Counsels**—Each NASA Field Center has a Technology Utilization Officer (TUO) and a Patent Counsel to facilitate technology transfer between NASA and the private sector.

If you need further information about new technologies presented in NASA Tech Briefs, request the Technical Support Package (TSP). If a TSP is not available, you can contact the Technology Utilization Officer at the NASA Field Center that sponsored the research. He can arrange for assistance in applying the technology by putting you in touch with the people who developed it. If you want information about the patent status of a technology or are interested in licensing a NASA invention, contact the Patent Counsel at the NASA Field Center that sponsored the research. Refer to the NASA reference number at the end of the Tech Brief.

Ames Research Ctr.
Technology Utilization Officer:Geoffrey S. Lee
Mail Code 223-3
Moffett Field, CA 94035
(415) 604-4044
Patent Counsel:
Darrell G. Brekke
Mail Code 200-11
Moffett Field, CA 94035
(415) 604-5104

Lewis Research Center
Technology Utilization Officer: Anthony F. Ratajczak
Mail Stop 7-3
21000 Brookpark Road
Cleveland, OH 44135
(216) 433-2225
Patent Counsel:
Gene E. Shook
Mail Code LE-LAW
21000 Brookpark Road
Cleveland, OH 44135
(216) 433-5753

John C. Stennis Space Center
Technology Utilization Officer: Robert Barlow
Code HA-30
Stennis Space Center, MS 39529
(601) 688-2042

John F. Kennedy Space Center
Technology Utilization Officer: Thomas M. Hammond
Mail Stop PT-PMO-A
Kennedy Space Center, FL 32899
(407) 867-3017
Patent Counsel:
Bill Sheehan
Mail Code PT-PAT
Kennedy Space Center, FL 32899
(407) 867-2544

Langley Research Ctr.
Technology Utilization Officer: Joseph J. Mathis Jr.
Deputy Head, TU Office
Mail Stop 139A
Hampton, VA 23665
(804) 864-2484
Patent Counsel:
George F. Helfrich
Mail Code 279
Hampton, VA 23665
(804) 864-3523

Goddard Space Flight Center
Technology Utilization Officer: Donald S. Friedman
Mail Code 702.1
Greenbelt, MD 20771
(301) 286-6242
Patent Counsel:
R. Dennis Marchant
Mail Code 204
Greenbelt, MD 20771
(301) 286-7351

Jet Propulsion Lab.
NASA Resident Office
Technology Utilization Officer: Arif Husain
Mail Stop 180-801
4800 Oak Grove Drive
Pasadena, CA 91109
(818) 354-4862
Patent Counsel:
Thomas H. Jones
Mail Code 180-801
4800 Oak Grove Drive
Pasadena, CA 91109
(818) 354-5179
Technology Utilization Mgr. for JPL: Dr. Norman L. Chalfin
Mail Stop 156-211
4800 Oak Grove Drive
Pasadena, CA 91109
(818) 354-2240

George C. Marshall Space Flight Center
Technology Utilization Officer: Ismail Akbay
Code AT01
Marshall Space Flight Center,
AL 35812
(205) 544-2223
Fax (205) 544-3151
Patent Attorney:
Jerry L. Seemann
Mail Code CC01
Marshall Space Flight Center,
AL 35812
(205) 544-0021

Lyndon B. Johnson Space Center
Technology Utilization Officer: Dean C. Glenn
Mail Code IC-4
Houston, TX 77058
(713) 483-3809
Patent Counsel:
Edward K. Fein
Mail Code AL3
Houston, TX 77058
(713) 483-4871

NASA Headquarters
Technology Utilization Officer: Leonard A. Ault
Code CU
Washington, DC 20546
(703) 557-5598
Assistant General Counsel for Patent Matters: Robert F. Kempf, Code GP
Washington, DC 20546
(202) 453-2424

A Shortcut To Software: **COSMIC®**—For software developed with NASA funding, contact COSMIC, NASA's Computer Software Management and Information Center. New and updated programs are announced in the Computer Programs section. COSMIC publishes an annual software catalog. For more information call or write: **COSMIC®,** 382 East Broad Street, Athens, GA 30602 *John A. Gibson, Dir.,* (404) 542-3265.

If You Have a Question..**NASA Center For AeroSpace Information** can answer questions about NASA's Technology Utilization Network and its services and documents. The CASI staff supplies documents and provides referrals. Call, write or use the feedback card in this issue to contact: **NASA Center For AeroSpace Information,** Technology Utilization Office, P.O. Box 8757, Baltimore, MD 21240-0757. *Walter M. Heiland, Manager,* (301) 859-5300, Ext. 245.

Introducing a line of digital data recorders designed to make large volumes of information easier to digest. The Sony DIR Series.

These high-speed, high-density recorders offer a range of selectable data rates: The DIR-1000L works from 8 to 64 Mbps. The DIR-1000M from 8 to 128 Mbps. And the DIR-1000, our fastest, from 8 to 256 Mbps.

But whatever data rate suits your needs, any DIR Series recorder can store almost 100 GBytes of information on a standard cassette.

They also utilize the ANSI ID-1 rotary head recording format. So they can offer time-based data expansion and contraction, and even a bit error rate of 1×10^{-10}. Plus, they're compact and cassette-based. Which means easier data handling and storage, and better tape protection than open-reel machines.

Best of all, the DIR Series is designed and built by Sony, the acknowledged leader in digital technology.

To learn more about how the Sony DIR Series makes high-speed, high-density data recording a reality, call us at 1-800-328-SONY, ext 970. After all, we wrote the book on it.

SONY.

Sony Business and Professional Group, 3 Paragon Drive, Montvale, NJ 07645-1735.

BUSINESS AND PROFESSIONAL GROUP

Electronic Components and Circuits

Hardware, Techniques, and Processes

Stacked-Gate FET's for Analog Memory Elements

Features include nonvolatility and programmability via the application of reading and writing voltages.

NASA's Jet Propulsion Laboratory, Pasadena, California

A three-terminal, double-stacked-gate field-effect transistor (FET), has been developed as an analog memory element. It is particularly suited for use as a synapse with variable connection strength in an electronic neural network. The new FET provides a programmable, nonvolatile resistive connection, somewhat in the manner of the porous-gate FET described in "Porous-Floating-Gate Field-Effect Transistor" (NPO-17532), *NASA Tech Briefs*, Vol. 14, No. 7, page 18.

The double-stacked-gate FET resembles the commercial erasable programmable read-only memory (EPROM) device, except for the thickness of the layers of silicon dioxide that electrically isolate the gates (see Figure 1). It could be either a p-channel or an n-channel device.

The amount of electrical charge on the floating gate determines the conductance between the source and the drain. The outer gate serves as the control gate and is used to remove the charge from the inner (floating) gate. The number of electrons on the floating gate can be increased by avalanche injection of hot electrons from the junction of the drain and the substrate. This is accomplished by applying a negative potential with a magnitude of at least 10 V to the drain while the source, control gate, and substrate are held at ground potential. The injection current and the total amount of charge transferred are controlled via the amplitude and duration of the pulse. The floating gate retains more than 99 percent of the charge 11 months after it has been injected.

The charge is removed from the floating gate by Fowler-Nordheim quantum-mechanical tunneling of electrons from the floating gate to the control gate or to the substrate. This is accomplished by applying ~50 V to the control gate while the drain, source, and substrate are held at ground potential.

Figure 2 shows a double linear array of analog memory elements of the new type. One row contains p-channel transistors; the other, n-channel transistors. The n-channel transistors can function as excitatory resistive connections, with current flowing into the common output terminal (the summing point). The p-channel transistors can act as inhibitory connections, with current flowing away from the common output terminal.

This work was done by Anilkumar P. Thakoor and Alexander W. Moopenn of Caltech for **NASA's Jet Propulsion Laboratory**. *For further information, Circle 153 on the TSP Request Card.*

Inquiries concerning rights for the commercial use of this invention should be addressed to the Patent Counsel, NASA Resident Office-JPL [see page 14]. Refer to NPO-17627

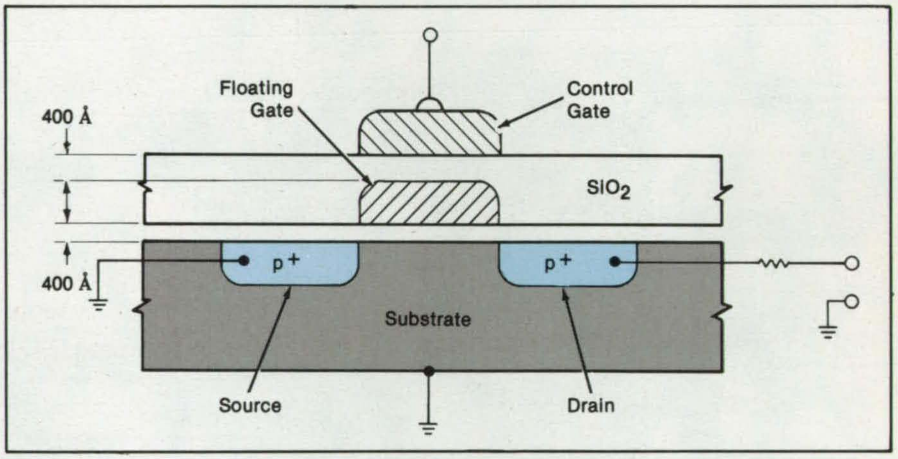

Figure 1. The **Three-Terminal, Double-Stacked-Gate, p-Channel FET** is a modified version of a commercial device of the same type. The thicknesses of the oxide layers have been changed to suit operation as an erasable, programmable analog resistive memory element. An n-channel version is also available.

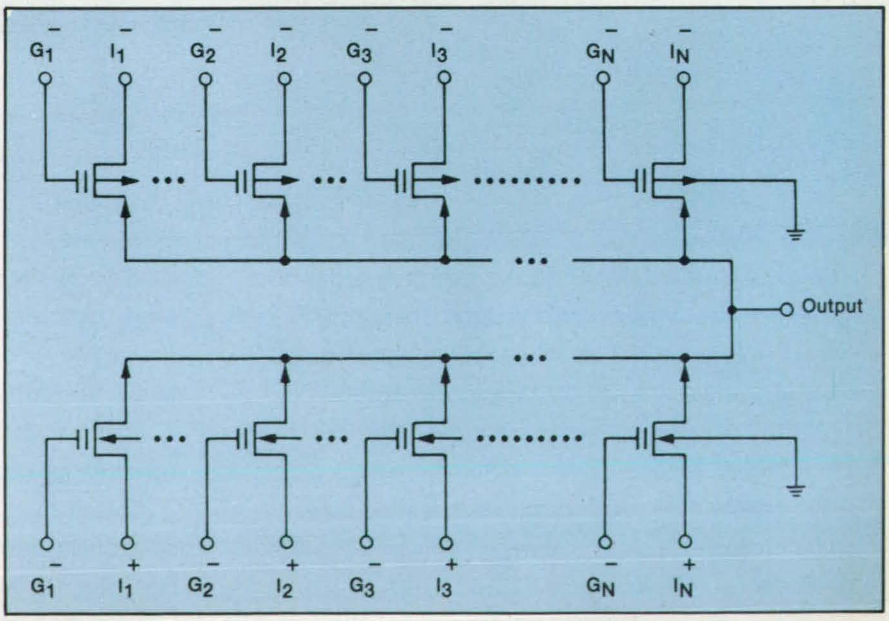

Figure 2. A **Double Linear Array** of the modified three-terminal, double-stacked-gate FET's could serve as a building block of an electronic neural network. The terminals labeled G are connected to the control gates. Those labeled I are connected to the power supply.

A Gold Mine of Technology Awaits You

U.S. government research and development programs have created a $65 billion technology storehouse that's available to you now for use in developing new products and processes. **Technology 2001** will show you how to tap into this amazing resource to improve your productivity and competitiveness, and will introduce you to America's premier researchers and technology transfer agents, including top experts from NASA, the Environmental Protection Agency, the National Science Foundation, the National Institute of Standards and Technology, and the departments of Defense, Energy, and Health and Human Services.

Technology 2001 will feature:

- Over 120 technical presentations spotlighting new advances with commercial promise in electronics, computer hardware and software, materials, manufacturing technology, and biotechnology;

- Special workshops on how to do business with government agencies, covering such areas as patent licensing, cooperative research and development agreements, and Small Business Innovation Research;

- 50,000 square feet of exhibits by federal laboratories, their prime contractors, and other high-tech firms and universities with leading-edge inventions available for license or sale;

- The second annual Technology Transfer Awards Dinner, offering a unique opportunity to network with government leaders and industry executives in an elegant setting — the grand ballroom of the San Jose Fairmont Hotel.

Show hours are 8:30 am to 6:00 pm, December 3-5. The awards dinner will be held Wednesday, Dec. 4, beginning at 7:00 pm.

Preregister And $ave

Mail the form below with check payable to the Technology Utilization Foundation, or fax the form with complete credit card information to (212)-986-7864. You may register by phone by calling (212)-490-3999 (VISA and Mastercard accepted). Government organizations may register using a purchase order. Deadline for preregistration is November 8.

	By 11/8	On-Site
Complete Registration Package	$300	$325
Symposia/Exhibits Registration	$200	$225
One-Day Symposia/Exhibits Reg.	$100	$125
One-Day Exhibits Only Reg.	$25	$30

Federal government employees are entitled to a 50% discount on above prices.

Complete Registration Package includes access to the technical sessions, workshops, and exhibits for all three days, a copy of the official **Technology 2001** proceedings, and tickets to the opening reception on Monday evening, Dec. 2 and the Technology Transfer Awards Dinner on Wednesday evening, Dec. 4. **Symposia/Exhibits Registration** includes entrance to the technical sessions, workshops, and exhibits for all three days.

Tickets to the awards dinner may be purchased separately for $150 each using the form below or by calling (212)-966-3100. Registrants may pick up their badges and reception/dinner tickets in the registration area at the San Jose Convention Center, 150 West San Carlos St; registration confirmations will be sent via mail. All registrants will automatically be mailed the **Technology 2001** Preliminary Program, available in July.

Special Rates On San Jose's Finest Hotels

Hotel space is limited, so act early to secure these special conference rates:

	single	double
Fairmont Hotel (headquarters hotel) (800)-527-4727	$105	$105
Hyatt San Jose (408)-993-1234	$85	$105
The Red Lion (408)-453-4000	$80	$80
Hotel De Anza (800)-843-3700	$115	$130

For further information about Technology 2001, or to find out how your company can exhibit at this major national event, call Justina Cardillo or Joseph Pramberger at (212)-490-3999.

Technology 2001 Registration Form

Use a separate form or photocopy for each registrant. Type or print clearly.

Name____________________

Title____________________

Company____________________

Address____________________

City/St/Zip____________________

Phone____________________

❑ check enclosed ❑ bill my: ❑ VISA ❑ Mastercard

Account No.____________________

Expiration: Mo._______ Yr._______

Signature____________________

Registration Fees:

Complete Registration	$300	$______
Symposia/Exhibits Reg.	$200	$______
One-Day Symposia/Exhibits *(circle day: Tues. Wed. Thurs.)*	$100	$______
One-Day Exhibits Only *(circle day: Tues. Wed. Thurs.)*	$25	$______
Awards Dinner Only	$150	$______
Total: (Fed govt. employees deduct 50%)		$______

Registrations and awards dinner reservations are transferable, and may be cancelled until Nov. 8, 1991 subject to a $50 cancellation fee. After that date no cancellations will be accepted and no money refunded.

Return with payment to: Technology Utilization Foundation, 41 East 42nd St., Suite 921, New York, NY 10017

Thermocouple-Signal-Conditioning Circuit

A thermocouple can be used instead of a resistance thermal device.

Marshall Space Flight Center, Alabama

A signal-conditioning electronic circuit serves as an interface between a thermocouple and a control circuit that was designed for use with a resistance thermal device. In the original design, the resistance thermal device was part of a bridge circuit that included the input portion of the controller, and the bridge circuit operated in the resistance mode. When the signal-conditioning circuit is used, the bridge-completion network is modified in such a way that the bridge operates in a voltage mode.

The signal-conditioning circuit creates a balanced bridge that minimizes common-mode noise. As "seen" by the controller at its input terminals, the combination of the thermocouple and the signal-conditioning circuit has the electrical characteristics of a voltage source in series with a resistance (see figure). An instrumentation amplifier within the signal-conditioning circuit buffers the thermocouple signal and provides gain. A small resistance-thermal-device circuit senses the temperature of the reference thermocouple junction and adjusts the input bias of the output amplifier accordingly.

The transfer function of the thermocouple and the signal-conditioning circuit approximates that of the resistance thermal device that is to be replaced. Within the control circuit, adaptation software containing thermocouple-calibration data compensates for the nonlinearities in the output of the thermocouple. The signal-conditioning circuit also includes an alarm circuit (not shown in the figure) that detects an open circuit in the thermocouple and provides off-scale output to signal malfunctions.

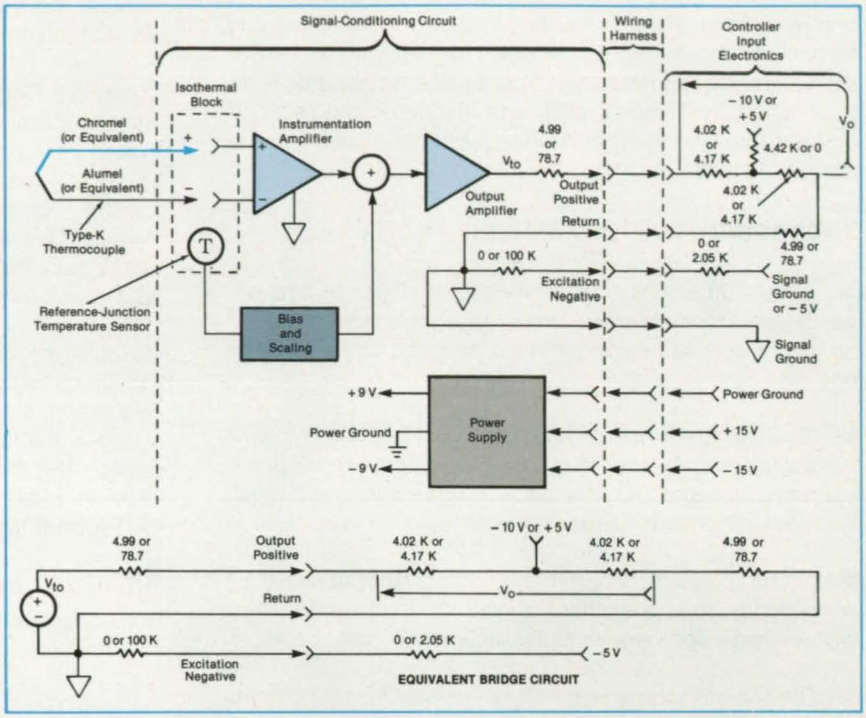

The **Thermocouple-Signal-Conditioning Circuit,** acting in conjunction with a thermocouple, exhibits the electrical behavior of a voltage in series with a resistance. The combination is part of the input bridge circuit of a controller. The circuit is configured for either of two specific applications by selection of alternative resistances and supply voltages.

This work was done by Richard A. Simon of Rockwell International Corp. for **Marshall Space Flight Center**. *For further information, Circle 116 on the TSP Request Card.*

Inquiries concerning rights for the commercial use of this invention should be addressed to the Patent Counsel, Marshall Space Flight Center [see page 14]. Refer to MFS-29695.

Calculating Scattering at Circular-Waveguide Junctions

A computer program applies to step discontinuities.

NASA's Jet Propulsion Laboratory, Pasadena, California

A computer program calculates scattering matrices for circular waveguides that include step discontinuities between collinear sections of different radii. The radius and length of each section can be specified arbitrarily. Examples of devices that can be analyzed with this program include waveguides with single step discontinuities, matching sections, corrugated straight sections, and corrugated horns (see Figure 1). In addition, sections with smooth tapers and horns with arbitrary profiles can be approximated by series of small steps.

A good computer model predicts reflec-

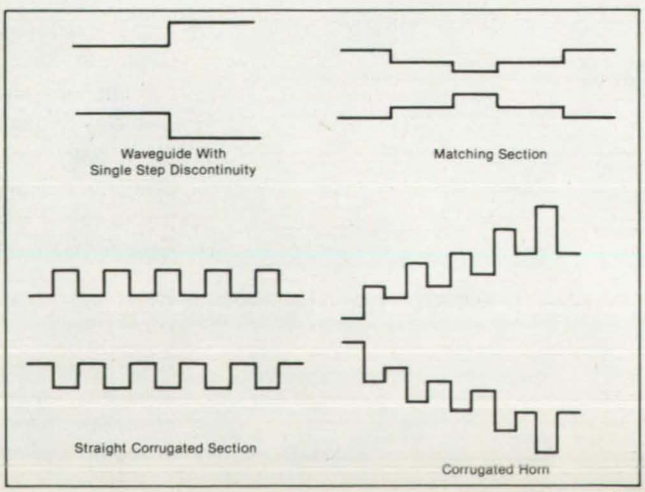

Figure 1. **Circular Waveguide Devices** with step discontinuities are accommodated by the scattering-matrix computer program.

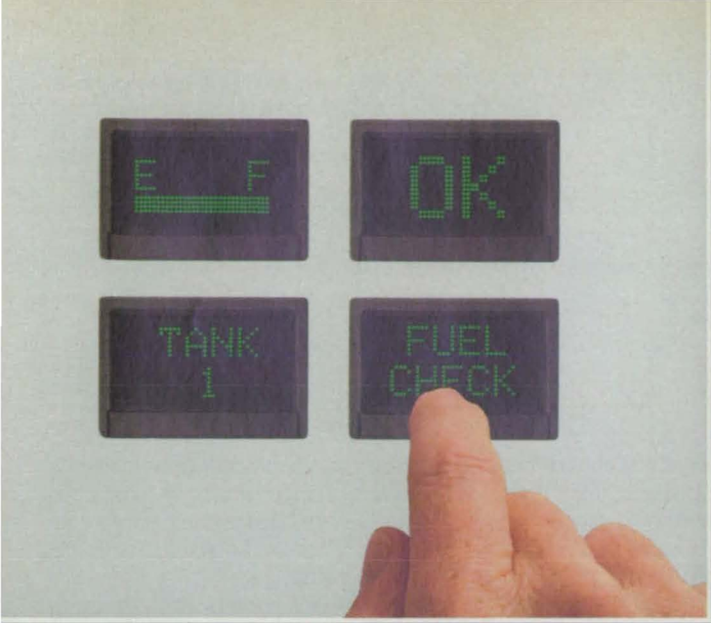

The programmable display system:

Design applications for land, sea or air.

Vivisun Series 2000, now the leading programmable display pushbutton system, interfaces the operator with the host computer. The user-friendly LED dot-matrix displays can display any graphics or alpha-numerics and are available in green, red or amber. They can efficiently guide the operator through any complex sequence with no errors and no wasted time.

They also simplify operator training as well as control panel design. One Vivisun Series 2000 programmable display system can do the work of 50 or more dedicated switches. In short, Vivisun Series 2000 gives the design engineer more control over the design.

Contact us today.

AEROSPACE OPTICS INC.
3201 Sandy Lane, Fort Worth, Texas 76112
(817) 451-1141 • Telex 75-8461 • Fax (817) 654-3405

Vivisun Series 2000 programmable displays. The intelligent communications system.

SERIES
VIVISUN 2000™

tion and transmission characteristics, taking account of excitation in modes of higher order as well as multiple reflections and energy stored at each discontinuity. Where many modes may propagate, as in a device large with respect to a wavelength, one may need to compute the reflection and transmission properties of a mode of higher order or series of modes that excite the device.

The basic building block for the mathematical model that underlies the program is the single step discontinuity. It is assumed that the discontinuity is excited only by modes of the TE_{1n} and TM_{1n} type (where "TE" and "TM" denote "transverse electric" and "transverse magnetic," respectively): therefore, because of the symmetry of the junction, only modes of the TE_{1n} and TM_{1n} type can be excited at the junction.

At the junction, one represents the electromagnetic field to the left as a sum of M normal modes of a circular waveguide of radius r_I. Similarly, the field to the right is represented as a sum of N modes for radius r_{II} (see Figure 2). M and N are chosen large enough for convergence. Next, one matches the electric and magnetic fields in the aperture at the junction. The equations that result from these matches are manipulated into a matrix• vector form in which an output vector is expressed as the product of a scattering matrix and an input vector. The matrices for the individual discontinuities are then cascaded to obtain the scattering matrix for the entire device.

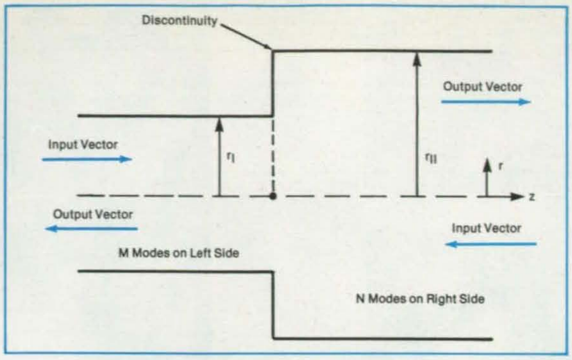

Figure 2. **Electromagnetic Modes** to the right and left of a discontinuity are matched at the discontinuity to obtain the equations that define the scattering matrix.

This work was done by D. J. Hoppe of Caltech for **NASA's Jet Propulsion Laboratory**. *For further information, Circle 142 on the TSP Request Card.*
NPO-17288

Solar-Cell Cover Glass Would Reduce Reflectance Loss

Total internal reflection at facets would trap more incident light.

Lewis Research Center, Cleveland, Ohio

A proposed faceted cover glass would take advantage of total internal reflection to increase the efficiency of a solar photovoltaic cell. As shown in the figure, the angled facets of the cover glass would refract the light as it entered. Then the portion of the light reflected at the surface of the solar cell would undergo total internal reflection at the surface of the cover glass, rather than partially escaping, and would return to the surface of the solar cell. For light incident perpendicular to the surface of the solar cell and glass with an index of refraction of 1.527, a facet with a slope $\geq 30°$ would result in total internal reflection of the rays at the surface of the cover glass. If the angle between facets A and B were 90°, total internal reflection would also occur at facets B.

One previous method that has been used to increase absorption is to "texture" the surfaces of cells, forming grooves or pyramids. Experiments show that a textured surface can reduce the reflection losses of an antireflection-coated silicon surface from 13.7 to 2.5 percent. However, for some materials and processing technologies, the texturing may be difficult or may reduce the mechanical strengths of the cells. The proposed faceted cover glass would make it unnecessary to "texture" the solar cell, yet would produce a similar improvement in efficiency.

Each pair of facets on the cover glass must be asymmetrical. If symmetrical facets are used, much of the light reflected from the surface of the solar cell would escape at the next facet. If facets B are angled as shown in the figure, that can be avoided. However, light reflected from the surface of the cell after entering through a B facet would not undergo total internal reflection at an A facet. Light incident on the B facets could be redirected to A facets by metallizing the B facets.

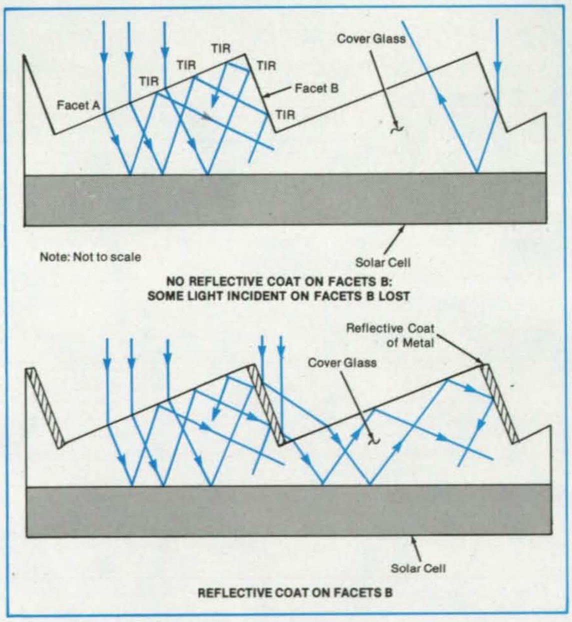

Angled Facets in the cover glass on a solar cell can increase the light-absorption efficiency of the cell by using total internal reflection (TIR) to trap more of the light. To increase absorption, facets B can be coated with metal.

If the B facets were metallized, there would be shadowed stripes running along under the B facets that would receive less illumination. If the cover glass were designed in conjunction with the metal contacts of the cell, the front contacts on the cell could be placed in the shadowed region, thereby reducing losses due to grid obscuration. For the proposed 30° slope of facets A, grid coverage of as much as 22 percent could be accommodated in the shadowed area.

This work was done by Geoffrey A. Landis of **Lewis Research Center**. *For further information, Circle 132 on the TSP Request Card.*
LEW-14942

Micro Channel/Multibus-II Interface Circuit

Independent Micro Channels can communicate over a standard bus without modification.

Lyndon B. Johnson Space Center, Houston, Texas

The Micro Channel/Multibus-II interface circuit provides the electrical interconnections that enable communications between Micro Channels of IBM Personal System/2 computers and the IEEE 1296 standard Multibus-II parallel system bus (iPSB). Made mostly of commercially available parts, the interface enables independent Micro Channels to communicate over the iPSB without modification.

The Micro Channel/Multibus-II interface (see figure) is divided into two major functional sections: the Micro Channel interface and the Multibus-II iPSB interface. The iPSB interface logic performs the following functions:

1. Access to interconnection space;
2. Arbitration of access to the bus and control of transfers;
3. Detection and correction of errors on the bus; and
4. Construction and buffering of messages.

The Micro Channel interface logic performs the following functions:

1. Direct-memory-access (DMA) transfer;
2. Input/output transfer; and
3. Programmed selection of options.

The iPSB Interface can be implemented in a single commercially available very-large-scale integrated-circuit module, the message-passing coprocessor (MPC), which directly controls the functions of the iPSB mentioned above. The MPC was chosen to implement these functions in this design because, in addition to supporting the full message-passing protocol of the parallel system bus, it provides a "back end" through which it can be connected to different local busses.

While the MPC is a common commercially available part, the Micro Channel/Multibus-II interface is the only circuit developed thus far to connect an MPC to the Micro Channel, bringing Multibus-II message passing to the IBM Personal System/2 family of computers. The Micro Channel interface logic enables the transfer of data between the MPC and the Micro Channel by use of the Micro Channel functions mentioned above. By converting Micro Channel bus operations to a form compatible with that of the MPC, the Micro Channel interface logic enables the microprocessor resident on the Micro Channel to become an agent in a Multibus-II message transaction.

The Micro Channel interface converts programmed input/output cycles on a Micro Channel to accesses to MPC registers, making it possible to gain access to such registers by "In" and "Out" instructions. The Micro Channel interface also converts Micro Channel DMA cycles into accesses to the MPC solicited-message buffer, enabling the first-in/first-out memory of this buffer to exchange data with the memory of the Micro Channel. The Micro Channel interface logic supports the selection of programmed options, allowing various parameters of the Micro Channel/Multibus-II interface to be changed in software.

This work was done by John J. D'Ambrose, Richard C. Jaworski, Nyles N. Heise, and David N. Thornton of IBM for **Johnson Space Center**. *For further information, Circle 19 on the TSP Request Card. MSC-21506*

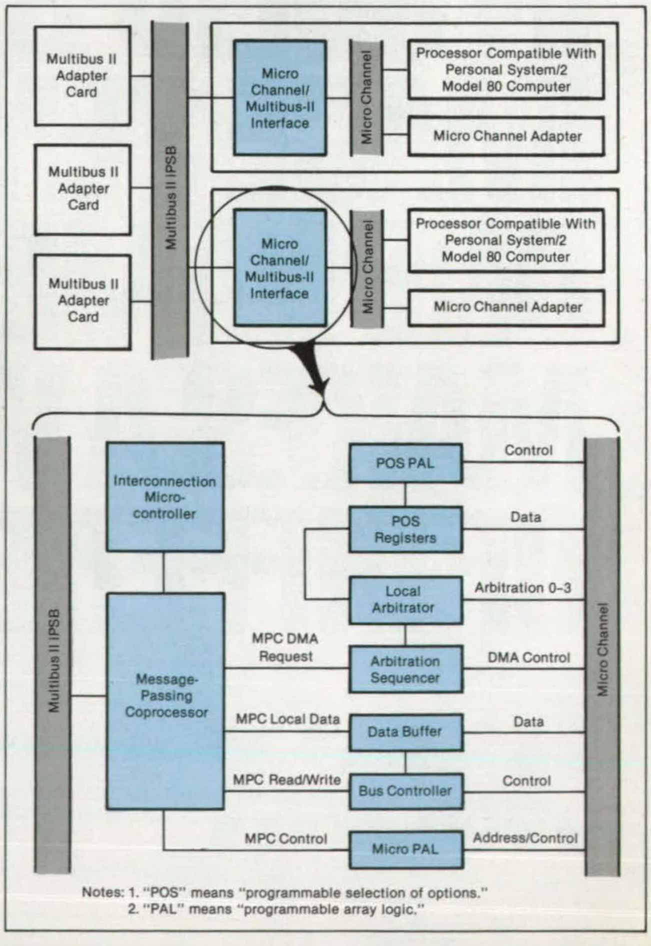

The **Micro Channel/Multibus-II Interface** enables communications between independent Micro Channels of IBM Personal System/2 computers and a Multibus-II parallel system bus.

Electronic Systems

Hardware, Techniques, and Processes

Books and Reports

Video Recording of Images in Laser Remote Sensing

The timings of the laser pulse, shutter, and video frame are synchronized.

Goddard Space Flight Center, Greenbelt, Maryland

A timing technique enables the recording of images in laser remote sensing of the environment. The technique was devised because the relatively inexpensive charge-coupled-device video cameras that are used in this application are not equipped for the input or output of the timing signals that are necessary for synchronization of the laser pulses, shutter openings, and video-recording frames. The technique can also be used in industrial or commercial processes that require clear sighting of laser beams relative to their surroundings.

The cameras of the type in question include electronic shutters that remain open down to times of less than a thousandth of a second. By synchronizing the output of a laser with the shutter opening of such a camera, one can image the laser-beam spot in the scene (e.g., a spot on the ground illuminated by a laser in an airplane and viewed by a video camera mounted with the laser). The effect of background brightness in the scene can be reduced in proportion to the shutter speed. Provided that the shutter opening lasts longer than the laser pulse does, this effect can be exploited to increase the apparent video brightness of the laser spot.

This makes it possible, for example, to use a visible-light laser in bright sunlight or other normally adverse bright background illumination, and one can view the laser spot along with the surrounding scene on a video monitor. The aperture of the camera can be adjusted to prevent saturation of the camera by the laser spot, while the shutter-speed adjustment sets the level of background illumination.

For recording the laser-spot image on a standard video-tape recorder, it is critical that the laser pulse occur during the first field of the video frame. This is because in such a recorder, only the first field is displayed during playback in the "pause" or "still frame" mode. Thus, if the laser pulse occurred during a shutter opening in the second field, the laser spot would be invisible upon playback in pause mode, even though it would be visible upon playback in the normal running mode.

During recording, the electronic shutter is opened, for whatever duration has been set, up to the end of each of the two fields. It is necessary to use the start-of-frame pulse in a camera to synchronize the laser pulse with the first field and the shutter opening. Typically, it is possible to learn from the manufacturer where the start-of-frame pulse is accessible on the circuit board of the camera. This pulse, which is often at transistor/transistor-logic level, can be used to trigger a laser directly at a pulse-repetition rate up to 30 Hz. (A laser operable at less than 30 Hz is normally triggerable only when ready, so that a train of pulses at a higher repetition rate can be sent continuously.)

Thus triggered, the laser fires during the first field as required, given the normal delay of several microseconds from triggering to discharge of light. This built-in delay, plus the time-of-flight delay to a distant target, is often sufficient to enable the use of lower shutter speeds without need for additional circuitry. Otherwise, a digital delay generator can be placed between the start-of-frame-pulse output terminal and the laser-trigger input terminal to synchronize the shutter opening with the laser signal.

This technique was used successfully to obtain data from the NASA Airborne Laser Polarimeter Sensor system during the Forest Ecosystems Dynamics Experiment near Bangor, Maine. In this experiment, a doubled neodymium:yttrium aluminum garnet (Nd:YAG) laser was used at altitudes from 100 to 300 meters. A Pulnix camera was used to obtain images of the ground where the laser was aimed. No delay generator was required for shutter speeds up to 1/1000 of a second. This shutter speed not only prevented blurring of the scene when viewed in the pause mode on video tape but sufficiently reduced the ambient light to enable recording of the approximately 15-μJ/cm^2 pulse, along with its surroundings, at the surface of the Earth on a clear day at noon.

This work was done by James E. Kalshoven, Jr., and Philip W. Dabney of **Goddard Space Flight Center**. *No further documentation is available.*
GSC-13398

Improved Remapping Processor for Digital Imagery

Features would include overlapping and variably sized preimages.

Lyndon B. Johnson Space Center, Houston, Texas

A proposed digital image processor would be an improved version of the Programmable Remapper, which performs geometric and radiometric transformations on digital images. The improved processor would overcome some of the limitations of image-warping circuit boards that can implement only those geometric transformations that are expressible in terms of polynomials of limited order. It would also overcome some of the limitations of the existing Programmable Remapper and could be made to perform the transformations at the video rate.

The existing Programmable Remapper includes two processors, each of which acts on the same input image but creates a different portion of the information in the output image, such that when the outputs of these two processors are merged, a synergistic output image is produced. One of these processors, called the "collective processor," collects or averages several input picture elements (pixels) to form each output pixel. The other processor, called the "interpolative processor," creates output pixels by interpolating between input pixels arranged in patches of 4 by 4.

The existing Programmable Remapper has several disadvantages:

- The two processors are difficult to operate in complete harmony because architectures are different.

The competition
You can call us at

It's enough to make other VME board builders call us names. Or call it quits.

A new 23 MIPS VME single board computer based on the 88100 RISC microprocessor. Or a new 20 MIPS VME board based on the 68040 CISC microprocessor.

Both are built by Motorola. And each is offered for a modest sum.

A mere $3,995 per board.

For all you multiplication buffs out there, that comes out to just $174/MIPS for the RISC board.

A far cry from the $1,000/MIPS you've been asked to pay for somebody else's board.

And it's just $200/MIPS for the

- This dual-processor approach produces a large degree of unnecessary redundancy in the design.
- The collective processor operates on the input image pixels one at a time and hence cannot use the same input pixel to contribute to any more than one output pixel.
- The total speed of the system is limited by the slower of the two processors, wasting processing power in the faster processor.

The proposed Programmable Remapper (see figure) would exhibit three major improvements over the existing version:

- The two distinct processors would be replaced by a single processor capable of performing both types of operations (collective and interpolative) without being any more complex than one of the previous processors.
- The "read–modify–write" loop involving the accumulator memory of the collective processor would be removed. This loop imposes a major limitation on speed, and so the removal of it would enable the improved processor to operate at much higher clock speeds.
- Because the pixels would be created in order of the output, multiple identical processors could be added to the system to obtain a proportional increase in processing speed. That is, each of n such processors would have to produce only $1/n$ of the total output image, so that the entire output image could be produced n times as fast.

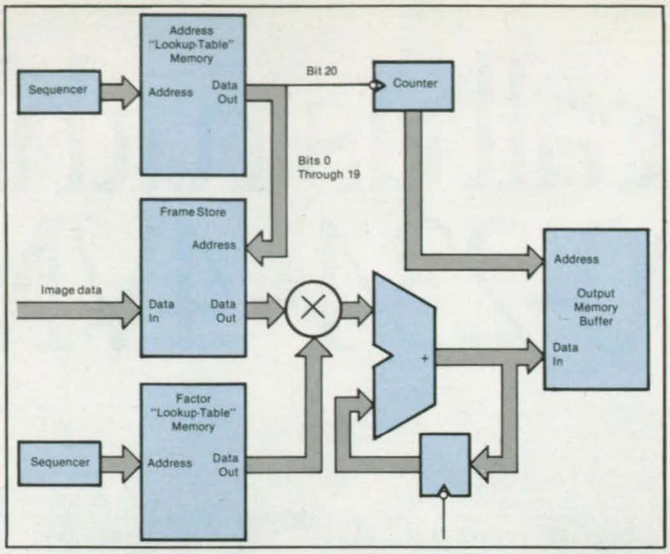

The **Improved Programmable Remapper** would include one processor that would perform operations formerly performed more slowly and less efficiently by two processors operating on the same image data.

The new Programmable Remapper would also have two features that are not found in the existing version. The first is that the pixels that used to be created with the collective processor could have overlapping preimages. This means that one input pixel could affect more than one output pixel. This feature is of paramount importance to researchers modeling the human visual system. The second new feature is variable size of the interpolation kernel. The interpolator in the existing Programmable Remapper has a fixed 4-by-4 interpolation kernel. If a smaller kernel such as a 3-by-3 kernel was desired, several machine cycles had to be wasted while the seven superfluous pixels were processed. In the proposed version, the size of the kernel would be specified in memory. Thus, no machine cycles would be wasted when a smaller kernel is desired, and a kernel larger than 4 by 4 could also be used.

This work was done by Timothy E. Fisher of **Johnson Space Center**. *For further information, Circle 29 on the TSP Request Card.*

This invention is owned by NASA, and a patent application has been filed. Inquiries concerning nonexclusive or exclusive license for its commercial development should be addressed to the Patent Counsel, Johnson Space Center [see page 14]. Refer to MSC-21481.

Resolving Phase Ambiguities in OQPSK

Performance should be enhanced while complexity is reduced.

NASA's Jet Propulsion Laboratory, Pasadena, California

An improved design for the modulator and demodulator in an offset-quaternary-phase-shift-keying (OQPSK) communication system is expected to enable the OQPSK receiver to resolve the ambiguity in the estimated phase of the received signal. Principal novel features include unique-code-word modulation and detection and the digital implementation of a Costas loop in the carrier-recovery subsystem. The improved design should enhance the performance of the carrier-recovery subsystem, reduce the complexity of the receiver by removing the redundant circuits from the previous design, and eliminate the dependence of the timing in the receiver upon a parallel-to-serial-conversion clock in the previous design.

The ambiguity in the estimated phase of the received signal ("phase ambiguity" for short) occurs because the receiver can lock onto an erroneous phase condition. Specifically, the receiver can lock onto the correct phase or inverse of the correct phase in the in-phase and/or the quadrature channel, or onto the in-phase signal

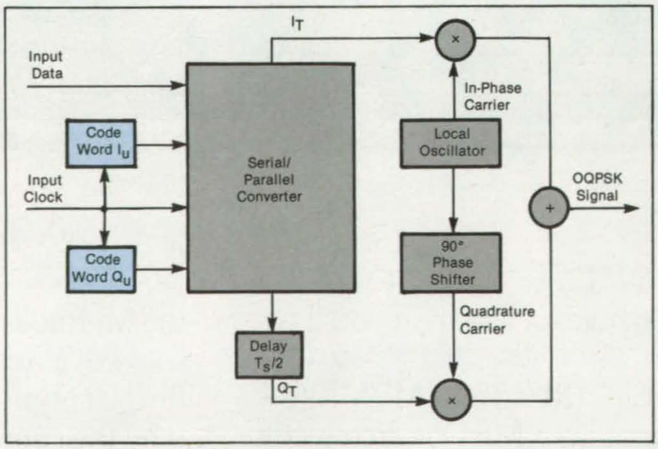

Figure 1. The **Modulator** periodically injects a unique code word into the stream of data bits to enable the demodulator to resolve three of the seven phase ambiguities.

in the quadrature channel (and, consequently, the quadrature signal in the in-phase channel) with otherwise correct or else inverse phase in either channel. Altogether, there are eight such phase-lock conditions, only one of which represents the correct reference carrier phase and phase rotation. One of the erroneous conditions represents the correct phase (0° phase error) but reverse rotation. The other erroneous conditions represent phase errors at 90°, 180°, or 270°, with normal or reverse rotation. The new design corrects all seven erroneous conditions.

The modulator (see Figure 1) resembles a conventional OQPSK modulator except that it includes circuitry that periodically inserts the unique code words I_U and Q_U in the in-phase and quadrature channels, respectively. (These code words could be

the synchronization signals.) The demodulator and carrier-recovery system (see Figure 2) incorporates the new digital Costas loop with matched arm filters in an integrated carrier/symbol-synchronizing subsystem based on digital decision feedback. This synchronizer replaces the carrier- and clock-recovery loops of the former design. Other new components in the demodulator include the analog-to-digital converters and the phase-ambiguity resolver.

The integrated carrier/symbol synchronizer corrects two of the normal-rotation and two of the reverse-rotation errors, avoiding lock at phase errors of 90° and 270°. The phase-ambiguity resolver corrects the remaining errors (0° with reverse rotation and 180° with normal or reverse rotation) by checking for I_U and Q_U in the in-phase and quadrature channels, respectively, and (1) inverting the signals in both channels if $-I_U$ and $-Q_U$, respectively, are found, (2) interchanging the signals if I_U is found in the quadrature channel and Q_U is found in the in-phase channel, or (3) both interchanging and inverting if $-Q_U$ and $-I_U$, respectively, are found.

This work was done by Tien M. Nguyen of Caltech for **NASA's Jet Propulsion Laboratory**. *For further information, Circle 34 on the TSP Request Card.*

This invention is owned by NASA, and a patent application has been filed. Inquiries concerning nonexclusive or exclusive license for its commercial development should be addressed to the Patent Counsel, NASA Resident Office-JPL [see page 14]. Refer to NPO-17853.

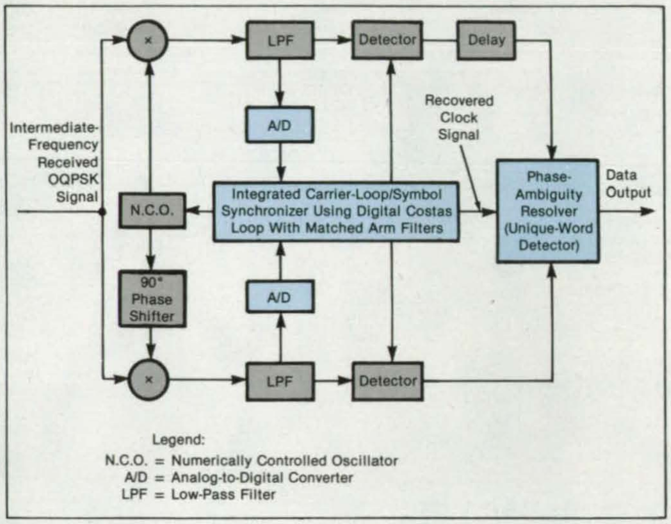

Figure 2. The **Demodulator** includes new digital circuitry to improve synchronization tracking of the carrier and to resolve the remaining four of the seven phase ambiguities.

Software Package for Real-Time Graphics

Flight data can be displayed in a variety of formats.

Ames Research Center, Moffett Field, California

The software package for the master graphics interactive console (MAGIC) at the Western Aeronautical Test Range (WATR) of NASA Ames Research Center provides a general-purpose graphical display system for real-time and post-real-time analysis of data. MAGIC is written in C language and intended for use on the workstation of an interactive raster imaging system (IRIS) equipped with the level-V Unix operating system. It enables flight researchers to create their own displays on the basis of their individual requirements. This type of software may also be applicable to the monitoring of complicated processes — for example, in the chemical industry.

Through menu options, MAGIC provides four major types of information displays: (1) time histories from a real-time data base, (2) X and Y plots from real-time data, (3) digital display of discrete or logical parameters from real-time data and messages and data written to the text ports of the IRIS, and (4) predicted data from the research vehicle in real-time applications.

MAGIC receives flight data from the aircraft radar signal and sends it to the WATR telemetry-radar acquisition and processing system (TRAPS) in the NASA WATR computer centers. The flight data are stored at the TRAPS in shared memory, passed to the mission-control centers via an Ethernet link, and displayed on an IRIS workstation (see Figure 1).

The chassis of the workstation accommodates up to 16 megabytes (MB) of the central processing unit, with 32 bit planes of display and a 170-MB disk. The workstation can display up to 4,096 colors simultaneously, from a palette of 6.7 million. The workstation includes a 19-in. (48-cm), 60-Hz noninterlaced color monitor with a resolution of 1,023 by 768 picture elements, a keyboard, an optical mouse, and a color printer.

MAGIC provides, to the user, the capabili-

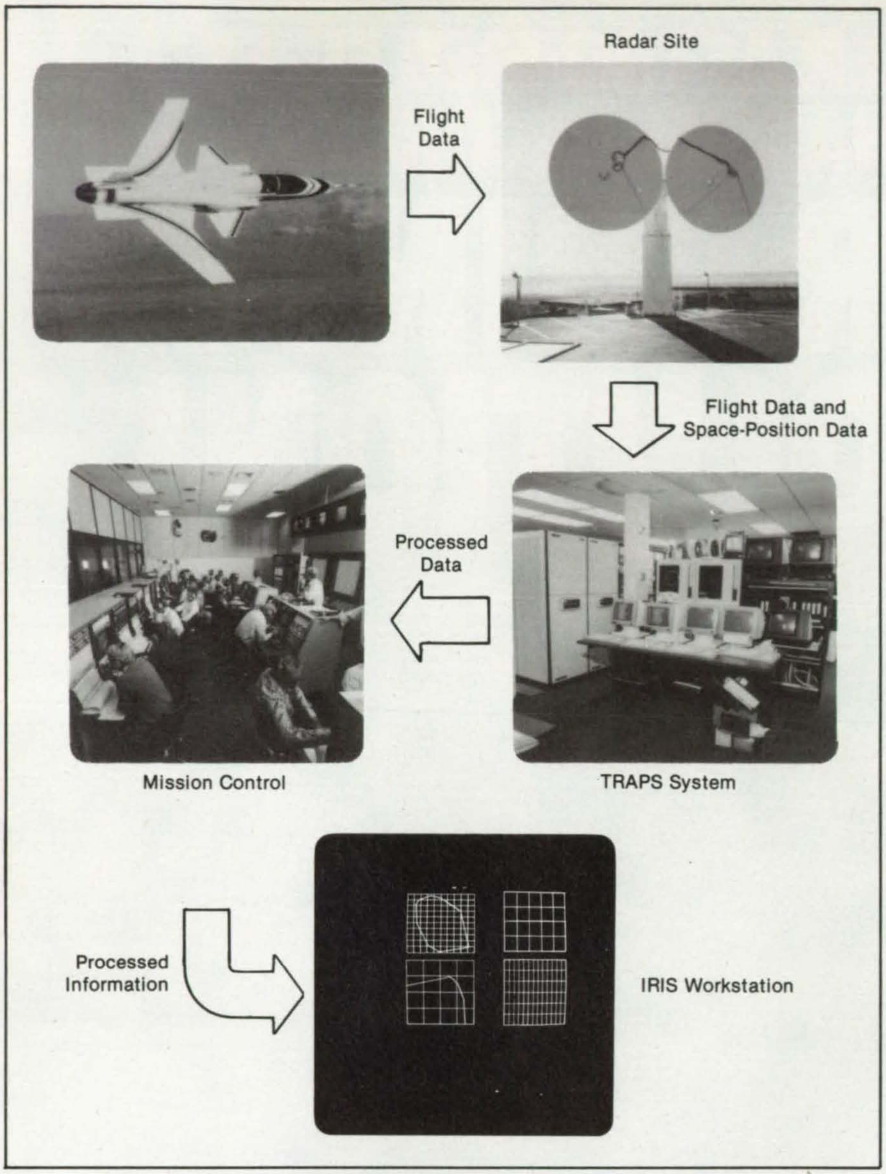

Figure 1. **Flight Data** flow from the aircraft through various systems, eventually to be displayed on an IRIS workstation in a mission-control center.

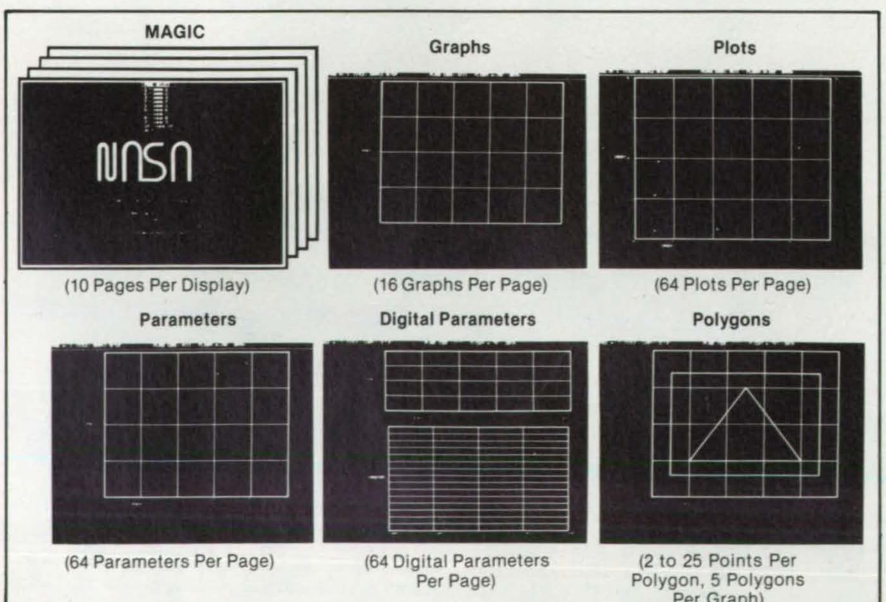

Figure 2. **MAGIC Displays Data** in a variety of formats.

ty of handling 10 pages of setups. Each page can contain up to 16 graphs, 64 plots, 64 parameters, 64 digital parameters, or 80 polygons (see Figure 2). Each graph displayed on a page is independent of all other graphs on the page and is built to specifications.

As used here, "parameters" means the various flight parameters designated by the user to be plotted during preflight, real-time, or postflight processing. "Digital parameters" denotes flight parameters that the user wants to track in their numerical state. The digital parameters can be placed anywhere on the screen, and their data processed as real, integer, or logical values. Polygons are used to prescribe limits within a graph that is to be assigned to a plot. The user can specify as many as five polygons per graph, each polygon containing 2 to 25 vertices.

This work was done by Jacqueline C. Malone and Archie L. Moore of **Ames Research Center**. *Further information may be found in NASA TM-100425 [N88-20506], "Western Aeronautical Test Range Real-Time Graphics Software Package MAGIC."*

Copies may be purchased [prepayment required] from the National Technical Information Service, Springfield, Virginia 22161, Telephone No. (703)487-4650. Rush orders may be placed for an extra fee by calling (800) 336-4700.
ARC-12357

Helmet-Mounted Liquid-Crystal Display

Eyes are directed to the position for best viewing.

Lyndon B. Johnson Space Center, Houston, Texas

A helmet-mounted binocular display provides text and images for almost any wearer; it does not require fitting for most users. Usually, a binocular display must be adjusted to the distance between pupils, which varies from person to person. The new display accommodates users from the smallest interpupillary distance (5th percentile) to the largest (95th percentile).

Two liquid-crystal display units are mounted in the helmet. The images that they generate can be seen — at least partially — from any position the head can assume inside the helmet. Once the user's eyes glimpse a part of the image, they naturally seek the region where the entire image can be seen — within a 3/4-in. (1.9-cm) square for each eye.

Liquid-crystal display units were select-

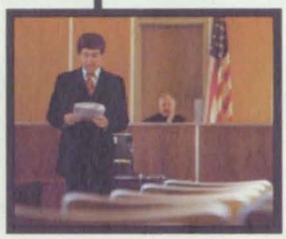

Panasonic Video. For Every Branch Of Government.

With a wide range of equipment for all your applications. From surveillance to production. Research to documentation. Training to distribution. Panasonic® has the video solution you need and the service to support it.

And when we say every branch of government, we mean it. You'll find Panasonic equipment in law enforcement agencies, hospitals, military installations, administration offices—even a few places we can't mention. All examples of the confidence Panasonic has built through years of supplying video equipment to the government.

With Panasonic, you get more than just a great product. We assist our government customers at every stage, from helping to define your needs to providing national dealer and engineering support after the sale.

So make the choice that makes sense. Panasonic has the products and the services that make us perfect for all your video applications. Whatever branch you're in.

For more information, contact your local Panasonic Professional/Industrial Video Dealer. Federal Government Agencies requesting a copy of the Authorized Communications Schedule Price List should write: Panasonic AVSG, Government Marketing Department, 52 West Gude Drive, Rockville, Maryland 20850 or call 301-738-3840.

Panasonic
Government Marketing

Circle Reader Action No. 381

ed because they consume little power. The entire display system, including its power supply, consumes only 7 W. Because the liquid-crystal display units generate no light of their own, the display is back-lit when the wearer is in darkness.

This work was done by Steve Smith, Alan Plough, Robert Clarke, William McLean, and Joseph Fournier of United Technologies Corp. and Jose A. Marmolejo of **Johnson Space Center**. *For further information, Circle 8 on the TSP Request Card.*

This invention is owned by NASA, and a patent application has been filed. Inquiries concerning nonexclusive or exclusive license for its commercial development should be addressed to the Patent Counsel, Johnson Space Center [see page 14]. Refer to MSC-21460.

Books and Reports

These reports, studies, handbooks are available from NASA as Technical Support Packages (TSP's) when a Request Card number is cited; otherwise they are available from the National Technical Information Service.

Simulation Test of Descent Advisor

Simulated times of arrival at metering fixes were within 20 s of the designated times.

A report describes a piloted-simulation test of the Descent Advisor (DA), which is a subsystem of a larger automation system that is being developed to assist human air-traffic controllers and pilots. The system has been described in previous articles in *NASA Tech Briefs*.

To recapitulate: On the basis of accurate mathematical models of the performances of airplanes and of weather conditions, the DA computes trajectories of airplanes. From these trajectories, it generates suggested clearances, including both top-of-descent-point and speed-profile data, for one or more airplanes to maintain a required separation and/or to arrive at a designated time at a metering fix or feeder fix [a point, about 30 nmi (about 56 km) from the airport, where commercial jet airplanes make the transition from en-route descent to terminal-area operation]. For airplanes not yet equipped with the avionic component of the DA subsystem, it is desired that the actual time of arrival at metering fixes be within ±20 s of the designated times.

The DA algorithm resides in a microprocessor-based workstation that interacts with, and receives aircraft-surveillance data from, the National Airspace Host Computer. As an unequipped airplane approaches the descent area, the algorithm

predicts its time of arrival. The predicted time of arrival is presented to the human air-traffic controllers, along with predictions for all other aircraft in their sector, by use of several graphical techniques. The controller chooses an optimum time of arrival for an airplane by adjusting its descent-speed profile, using a mouse-based, menu-driven interface with the DA algorithm. When the controller accepts a descent-speed profile that will enable the aircraft to arrive at the desired time, the controller issues the speed-profile advisory notice to the aircraft in the form of a clearance.

The DA was tested at the Man-Vehicle Systems Research Facility at Ames Research Center with a view toward evaluating it in terms of both the performances of pilots and the acceptance of DA clearances. The piloted simulation was conducted jointly with a simulation of the DA/controller-interface subsystem to study the acceptability and accuracy of the DA automation from both the pilots' and the air-traffic controllers' perspectives. To generate a substantial and representative data base, 42 pilots from 4 major airlines and 9 air-traffic controllers participated. The simulation scenario was based on the northwest arrival sectors of the Denver Air Route Traffic Control Center.

This study focuses on the results of the piloted simulation, in which the airline crews executed controller-issued descent advisories along standard curved-path arrival routes. The crews were able to achieve an arrival-time precision of ±20 s at the metering fix. An analysis of errors generated in turns resulted in further enhancements of the algorithm to increase the accuracies of its predicted trajectories. Evaluations by pilots indicate general support for the DA concept and provide specific recommendations for improvement.

This work was done by Thomas J. Davis and Steven M. Green of **Ames Research Center**. *Further information may be found in NASA TM-101086 [N90-17376], "Piloted Simulation of a Ground-Based Time-Control Concept for Air Traffic Control."*

Copies may be purchased [prepayment required] from the National Technical Information Service, Springfield, Virginia 22161, Telephone No. (703) 487-4650. Rush orders may be placed for an extra fee by calling (800) 336-4700.
ARC-12626

Multiple-Bit Errors Caused by Single Ions

Experiments and simulations complement each other.

A report describes an experimental and computer-simulation study of multiple-bit errors caused by the impingement of single energetic ions on a 256-Kb dynamic random-access memory (DRAM) integrated circuit. These studies illustrate the effects of different mechanisms for the transport of charge from ion tracks to various elements of integrated circuits. It is shown that multiple-bit errors occur in two different types of clusters about the ion tracks that cause them.

In both the experiments and the simulations, the ion tracks were perpendicular to the memory planes. The critical charge, Q_C, required to cause a bit error in one memory cell is given by $Q_C = C_S(V_{DD} - V_B)$, where C_S is the data-storage capacitance of the cell, V_{DD} is the supply voltage, and V_B is the bias voltage of the bit-sensing amplifier. In the experiments, V_{DD} was varied to vary the critical charge to observe the consequent expansion and contraction of the error clusters for each combination of ion species and energy.

The computer simulations were conducted with a two-dimensional simulation program, PISCES, that had been converted from Cartesian to cylindrical coordinates to simulate the three-dimensional normal-incidence ion-track events. The geometric parameters used in the simulation differed slightly from those of the real integrated circuit because the radii and thickness of annular rings in the cylindrical coordinates were chosen to optimize the overlay of these rings on the data-storage capacitors, which were rectangular. For each simulated ion impact, the data-storage capacitors were assumed to be charged to V_{DD} and the transient response of the data-storage nodes was computed.

When the data from the experiments and the simulations are plotted in histograms that show the relative frequencies of various numbers of bit errors per ion, it becomes apparent that there are two classes of events: (1) those with a small number of bit errors, the number being essentially insensitive to V_{DD}, and (2) those with a substantially larger number of bit errors, the number being very sensitive to V_{DD}. From an intuitive correlation of the results of the experiment and the simulation, it appears that the events of the first and second types are caused, respectively, by ion tracks that intersect or do not intersect charge-collecting junctions.

The simulation also shows that the charge-collecting junction that an ion most probably hits to produce an event of the first kind or misses to produce an event of the second kind is a bit-line buried contact. Charge collected by a junction under a storage capacitor is too small for lateral transport of charge to depend on whether an ion hits or misses this junction. The charge from an ion track that does not touch a junction diffuses laterally over a wide area, thereby affecting a greater number of junctions and tending to cause more bit errors.

This work was done by John A. Zoutendyk, Larry D. Edmonds, and Laurence S. Smith of Caltech for **NASA's Jet Propulsion Laboratory**. *To obtain a copy of the report "Characterization of Multiple-Bit Errors from Single-Ion Tracks in Integrated Circuits," Circle 88 on the TSP Request Card.*

This invention is owned by NASA, and a patent application has been filed. Inquiries concerning nonexclusive or exclusive license for its commercial development should be addressed to the Patent Counsel, NASA Resident Office-JPL [see page 14]. Refer to NPO-18075.

Analysis of Lock Detection in Costas Loops

Phase jitter in the tracking loop degrades performance.

A report presents an analysis of the detection of phase lock in Costas loops, which are used in coherent binary-phase-shift-keying communication systems to track both subcarrier and suppressed carrier signals. The detection of phase lock ("lock detection" for short) is an important part of the operation and monitoring of the operation of a Costas or other tracking loop because it provides insight into the behavior of the loop in real time. This analysis focuses on the effects of phase jitter and the correlation between samples of the phase error in an all-digital Costas loop, in which lock detection is implemented via an algorithm. Previous analyses have not taken account of these effects.

Lock detectors (including lock-detecting algorithms) for Costas loops fall into two main categories: square-law and absolute-value detectors. A square-law detector operates on samples of $I^2 - Q^2$ (where I and Q denote the instantaneous in-phase and quadrature signals, respectively). An absolute-value detector operates on samples of $|I| - |Q|$. Previous analyses of lock detectors of both types were performed for high signal-to-noise ratios, at which phase-tracking errors approach zero and phase jitter can be ignored. At low signal-to-noise ratios, the assumption of zero phase jitter leads to inaccurate predictions of performance.

The new analysis, which is applicable to both sinusoidal and square-law carrier signals, incorporates new mathematical models of the square-law and absolute-value detectors. The models include both additive zero-mean white Gaussian noise components in the samples of I and Q and the effects of a zero-mean white Gaussian phase noise (phase jitter) upon the signal components of these samples. Computer simulations were performed to verify these models, and the report presents the numerical results in the form of probabilities of true lock detection as functions of signal-to-noise ratios for given probabilities of false lock detection.

The results show that at low signal-to-noise ratios, the probability of true lock detection is degraded by phase jitter. The degradation is greater in an absolute-value detector than in a square-law detector, and it is more pronounced for a square-wave signal than for a sine-wave signal. The degradation can be reduced by appropriate readjustment of the design parameters.

This work was done by Alexander Mileant and Sami M. Hinedi of Caltech for **NASA's Jet Propulsion Laboratory**. *To obtain a copy of the report, "Lock Detection in Costas Loops," Circle 86 on the TSP Request Card.*
NPO-18102

Back Azimuth Guidance in Departures and Missed Approaches

Tests in flight simulators help in the development of procedures and specifications.

A report describes studies conducted with pilots in a flight simulator to examine the use of the front azimuth and, more importantly, the back azimuth functions of the microwave landing system (MLS) during precise departures immediately after takeoffs and during missed approaches. These studies provided data to determine the optimum back azimuth signal sensitivity (that is, the angular range of the back azimuth display), to establish operationally acceptable limits and procedures for the use of back azimuth guidance, and to determine the optimum technique for switching from front azimuth to back azimuth guidance.

The studies were conducted at the Man-Vehicle Systems Research Facility at Ames Research Center in a Singer-Link Boeing 727 advanced-technology simulator with a six-degrees-of-freedom motion system and a Singer-Link-Miles Image II three-channel, four-window, dusk/night visual system. The airport simulated for these studies was Los Angeles International runway 24R. The MLS simulation was added to the facility specifically for use in MLS research. Whereas most previous MLS research was concerned with "advanced" MLS capabilities, such as the curved-path guidance best able to take advantage of the large coverage volume, this study addressed the use of the MLS in the "basic" mode and considered minimum additional airborne equipment.

To facilitate testing and allow a certain amount of flexibility to the researcher, a matrix of test conditions was prepared. It included a takeoff initial condition, an approach initial condition, a variety of headwind and crosswind cases, and several visibility conditions. A typical session in the simulator lasted 1 h. During a session, the subject pilots either did a series of takeoffs or a series of missed approaches. They were told that the missed-approach and departure altitude was 3,000 ft (914 m).

Altogether, over 500 simulated flights were conducted by 18 pilots. Fifty-seven continuous measures and 17 discrete events were sampled at a 1-Hz sampling rate during all evaluation flights. Video and audio recordings of all cockpit activity were also made. Subjective questionnaires were filled out by each pilot after the completion of a data session.

The following conclusions were drawn from the accumulated data:

1. The MLS back azimuth signal can support up to a ±30° offset radial departure during takeoffs and missed approaches using "basic"-mode avionics.
2. The switch from front azimuth guidance to back azimuth guidance during a missed-approach procedure should be accomplished automatically, but a manual-override capability should be provided.
3. A switching logic based on the loss of the front azimuth signal is recommended.
4. A ±6° full-scale back azimuth display sensitivity value is recommended for "basic"-mode departures and missed approaches.
5. While a flight director can provide useful guidance during takeoffs and missed approaches using back azimuth radials, it is not required.
6. The acceptability of a particular signal sensitivity is dependent on the operational procedures used. The proposed ±6° sensitivity is tolerant of variations in operational procedures. However, it is recommended that intercept angles be limited to 10° for capturing back azimuth radials up to ±15° offset angles, and limited to 20° when capturing back azimuth radials greater than ±15°. These limitations should be incorporated in the published departure and missed-approach procedures.
7. MLS back azimuth status information should be presented within the pilot's scan pattern and should indicate whether the back azimuth is available, whether the aircraft is within back azimuth coverage, and whether the back azimuth signal is being used for guidance.
8. The back azimuth value that is set in the control display unit should be visible at all times as a reminder of what the missed-approach maneuver or departure procedure will be.

This work was done by Barry C. Scott of **Ames Research Center** *and Tsuyoshi Goka of T. Goka Avionics. To obtain a copy of the report, "Simulator Evaluation of 'Basic' Mode Back Azimuth Issues in Departure and Missed Approach Usage," Circle 17 on the TSP Request Card.*
ARC-12611

Physical Sciences

Hardware, Techniques, and Processes

Books and Reports

Computer Programs

Imaging Microscope for "Water-Window" X Rays

Images would be formed at wavelengths that enhance visibility of biological structures.

Marshall Space Flight Center, Alabama

A proposed microscope would operate in the "water-window" part of the x-ray spectrum, which lies at wavelengths greater than the 23.3-Å wavelength of the K absorption edge of oxygen but less than the 43.7-Å wavelength of the K absorption edge of carbon. The "water window" is so named because water is quite transparent to x rays at these wavelengths. On the other hand, carbon is highly absorptive at wavelengths just below the 43.7-Å absorption edge. Because of these spectral features and because biological specimens contain carbon-based structures immersed in water, the proposed microscope would be well suited for making high-resolution, high-contrast images for microbiological research.

The microscope and ancillary equipment would be operated in a vacuum. The microscope (see figure) would contain two concentric spherical mirrors — a concave primary and a convex secondary. Typically, the radii of curvature and the positions of the object and image planes are chosen to produce a magnification of 25. The mirror substrates could be made of sapphire; they would have to be ground to surface figures within 1/20 visible-light wavelength of sphericity and polished to a surface smoothness of 3 Å root mean square or better. The polished surfaces of the mirror substrates would be coated with alternating diffracting layers of tungsten and spacing layers of silicon with a thickness spatial period of 18 Å. These layers would act as normal- and near-normal-incidence Bragg reflectors with peak reflectivity at a wavelength of 36 Å. Other Bragg-reflector materials and specimens could also be used as long as they yielded sufficiently high reflectivity (of the order of 10 percent) at a wavelength in the water window and low reflectivity at other x-ray wavelengths.

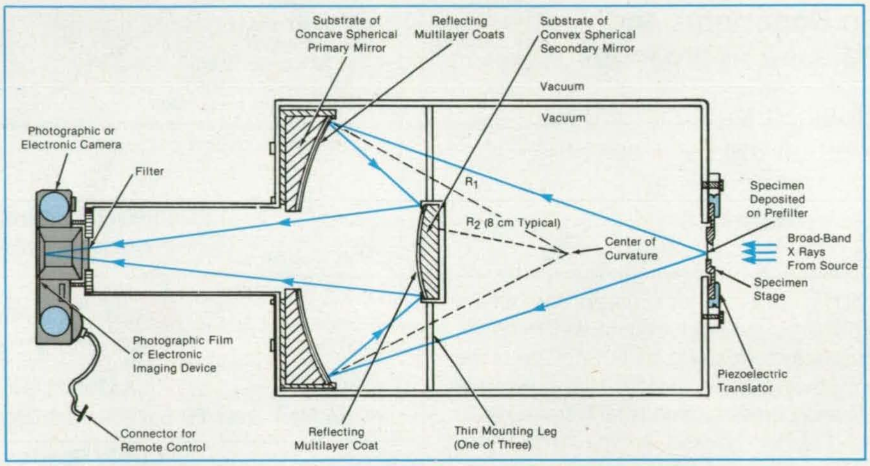

The **"Water-Window" X-Ray Camera** would contain spherical-mirror substrates coated with multiple thin layers of material that exhibit Bragg reflection at a wavelength at which water is transparent.

The specimen would be illuminated by broadband x rays from a pulsed (e.g., plasma) or steady (e.g., conventional x-ray tube) source. The specimen would be mounted on a prefilter, which would suppress both visible light and x rays outside the water window. A similar filter would be placed near the image plane at the entrance to the camera or other imaging device. Typically, this prefilter and specimen holder would be a titanium foil 1,500 Å thick supported by a nickel mesh. The prefilter and specimen would be mounted on a holder on a piezoelectrically driven translation stage, which would be used to bring the specimen to focus in the microscope and to scan across the specimen.

Although an electronic imaging device could be used, to obtain the highest resolution, it would be necessary to form the x-ray image on photographic film. For example, one film that is sensitive to water-window x rays has a resolution of 2,000 line pairs per millimeter. Such high-resolution images could be enlarged further by photographic or other conventional means to obtain effective magnifications of several thousand. If an intense source of x rays could be pulsed at regular intervals while the film was advanced, one could then make a high-resolution x-ray motion picture of processes in a living cell.

This work was done by Richard B. Hoover of **Marshall Space Flight Center**. *For further information, Circle 104 on the TSP Request Card.*

Inquiries concerning rights for the commercial use of this invention should be addressed to the Patent Counsel, Marshall Space Flight Center [see page 14]. Refer to MFS-28485.

Laser Velocimeter for Outdoor or Wind-Tunnel Measurements

Range is increased from 10 to 20 m.

Ames Research Center, Moffett Field, California

A laser velocimeter has been developed for remotely controlled operation in a large wind tunnel or at an outdoor aircraft-testing site. The instrument, called the Long Range Laser Velocimeter (LRLV) (see figure), represents the upgrading of a prior dual-beam, single-color laser velocimeter that had a maximum focal distance of 10 m to a double-dual-beam, two-color laser velocimeter that has a focal range of 2.6 to 20 m.

Because the laser-backscatter measurements on which a laser velocimeter depends become impractical at longer ranges, the LRLV is typically placed on the floor inside the wind tunnel. A streamlined housing minimizes the perturbation of the wind-tunnel flow. The two-color, double-dual-beam configuration enables the LRLV to measure two orthogonal components of velocity simultaneously. Stepping motors and position encoders under computer control position the test point within the flow field.

An argon-ion laser head operating in the broad-band mode generates an output beam of nominally 18 W maximum continuous power. This beam enters a three-prism assembly, which disperses the colors of the broad-band beam, yielding a blue beam (wavelength 488.0 nm) and a green beam (wavelength 514.5 nm). The diverging beams are separated farther by mirrors, then expanded in a pair of telescopes. Each beam is then split into two beams of equal intensity by two beam splitters located downbeam of the beam-expanding telescopes.

Each of the four beams is then shifted in frequency by four acousto-optical cells, driven at frequencies of 44.0 and 52.0 MHz, before passing through the final focusing optics. This eliminates directional ambiguity by creating an 8-MHz zero-offset frequency, and increases the number of cycles per Doppler burst for a given particle velocity. The dual-cell configuration is used to facilitate filtering of the Doppler signal by ensuring separation of the signal frequency from any radio-frequency radiation generated by the cell-driving electronics.

The frequency-shifted beams are then focused to a point in the flow field by one of two interchangeable, three-module zoom lens systems. Focal distances ranging from 2.6 to 10 m and from 10 to 20 m can be reached by selecting the appropriate set. A large folding mirror reflects the beams into the flow field.

Light is scattered in all directions when particles moving with the flow field pass through the measuring volume illuminated by the transmitted beams. But only the rays that fall within an imaginary cone formed by rotation of the transmitted pairs of beams about the optical axis are collected. These rays pass back in through the same lens system that is used for transmission at the focal range of 2.6 to 10 m and are then reflected out of the main optical path by an elliptical dielectric mirror. A dichroic mirror separates the colors, and each color is imaged at a 0.5-mm pinhole and filtered by a narrow band-pass interference filter at the photomultiplier tubes. No translation of the photomultiplier tubes is necessary to maintain foci of the images over the focal range.

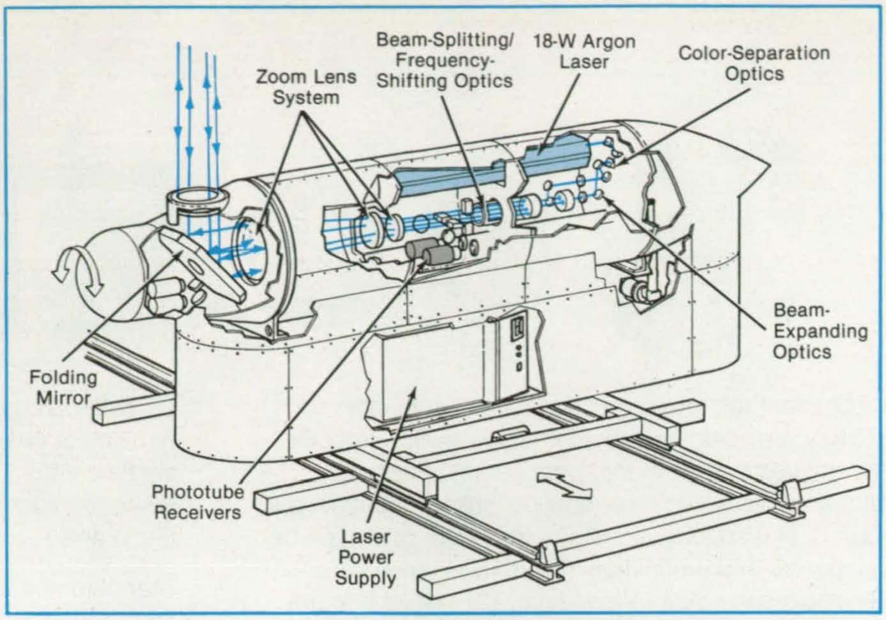

The **Long-Range Laser Velocimeter** has an expanded focal range and the ability to measure two perpendicular components of velocity simultaneously. It also includes electronic subystems for control and the acquisition of data.

A different set of receiving optics is used in the focal range of 10 to 20 m. In this range, an isolated collection lens is used to improve the immunity to noise. A dichroic mirror separates the two colors ahead of the photomultiplier tubes. The collected light is imaged at 0.5-mm-diameter pinholes and transmitted through band-pass interference filters before entering the photomultiplier tubes. To maintain the foci of the images at the pinholes over the zoom range, the photomultipliers are positioned by a stepping-motor-driven translation stage with absolute-position-encoder readback. The position is slaved through software to the zoom position of the transmitting optics.

Four stepping motors and electronic drivers position the test point within the flow field. Two are dedicated to generating the displacements required for optical zoom of the transmission and collection optics. The third is dedicated to translating the system laterally along support rails mounted on the floor. The fourth is dedicated to rotation of the beam-scanning assembly that contains the folding mirror. An onboard controller is linked through an interface circuit to a main computer.

Data are acquired via the peripheral electronics within the LRLV housing and supplied to the main computer from either signal processors or a high-speed correlator. When data are acquired with the shorter-focal-range receiving optics, signals are photon-saturated, and the counter-type signal processors are used. The high-speed correlator is required when the longer-focal-range receiving optics are used; signals acquired over these focal distances are composed of photon-resolved pulses and cannot be processed by use of counters.

This work was done by Michael S. Reinath of **Ames Research Center**. *Further information may be found in NASA TM-101081 [N89-26207], "A Long-Range Laser Velocimeter for the National Full-Scale Aerodynamics Complex: New Developments and Experimental Application."*

Copies may be purchased [prepayment required] from the National Technical Information Service, Springfield, Virginia 22161, Telephone No. (703) 487-4650. Rush orders may be placed for an extra fee by calling (800) 336-4700.
ARC-12592

Transformations for Atmospheric-Radiation Calculations

The number of data that have to be stored is reduced greatly.

NASA's Jet Propulsion Laboratory, Pasadena, California

Atmospheric radiation calculations are an essential part of climate models and inversion techniques for analyzing remote sensing observations. Both absorbing gases and scattering particles contribute to the radiation field. Rigorous methods for computing the radiation field exist but often require far too much computer time because the gas absorption coefficients vary rapidly with wavelength. Two spectral mapping transformation methods were developed to reduce the computing time and storage requirements greatly while preserving the accuracy achievable with rigorous methods.

It is possible, of course, to calculate scattering properties accurately by the "line-by-line" (LBL) method, which is the straightforward "brute-force" method in which the radiation field is computed by use of absorption coefficients (k) as functions of wavelength (λ) or wave number (ν) on a computational grid fine enough to resolve the spectral peaks. The LBL method is computationally expensive, requiring the storage of complete spectral data and a radiation-transport calculation for every wave-number interval in the spectral grid (there could be several thousand intervals in a typical calculation).

One transformation method developed previously to reduce the burden of computation and storage is called the "correlated-k" (c-k) method. It involves a mapping in which spectral intervals that have nearly the same k are grouped together and the radiation field is calculated for each group as a whole rather than for each spectral interval. In the c-k method, the grouping is performed according to the cumulative frequency (in the statistical sense) distribution

$$g(k) = \int_0^k f(k')dk'$$

where $f(k')$ is the distribution function. This mapping can be inverted to yield k as a function of g, k increases monotonically with g (see figure), and g replaces ν or λ in the radiation-transport calculations.

The two new methods evolved from the c-k method. They were developed because the c-k method entails the assumption that the mapping is the same in all layers of the atmosphere — an assumption that is not always true for an inhomogeneous atmosphere and that leads to errors in the radiation-transport calculation. In the first method, k is first segmented according to g for one layer of the atmosphere as in the c-k method. Then the effect of the initial segmentation on the second layer is determined, and the segmentation is refined by remapping onto smaller intervals and reshuffling as necessary. The additional segmentation and reshuffling are also imposed on the first layer.

Next, one proceeds to the third layer, refining and reshuffling for the first two layers as necessary, and so on throughout all the layers. At the end of this refinement-and-reshuffling procedure, all layers have the same number of intervals, and the segmentation and mapping of the final layer is imposed on all the previous layers. To reduce the number of data to be stored, the k's for all ν's in a given segment of g in a given layer are averaged and the average used as the k for all ν's in the given segment of g in that layer.

In the second method, all the ν intervals of the LBL representation that have nearly the same k at all levels of the atmosphere are grouped together in a simple "binning" scheme. If, for any, tentative bin and layer, any k differs from the average k in that tentative bin by more than a specified amount, then the bin is split into two bins. The computation proceeds quickly because it involves only differences, comparisons, and averages. It also requires very little storage because it operates on only one ν interval at a time.

This work was done by Robert A. West, David Crisp, and Luke Chen of Caltech for **NASA's Jet Propulsion Laboratory**. *For further information, Circle 124 on the TSP Request Card.* *NPO-18026*

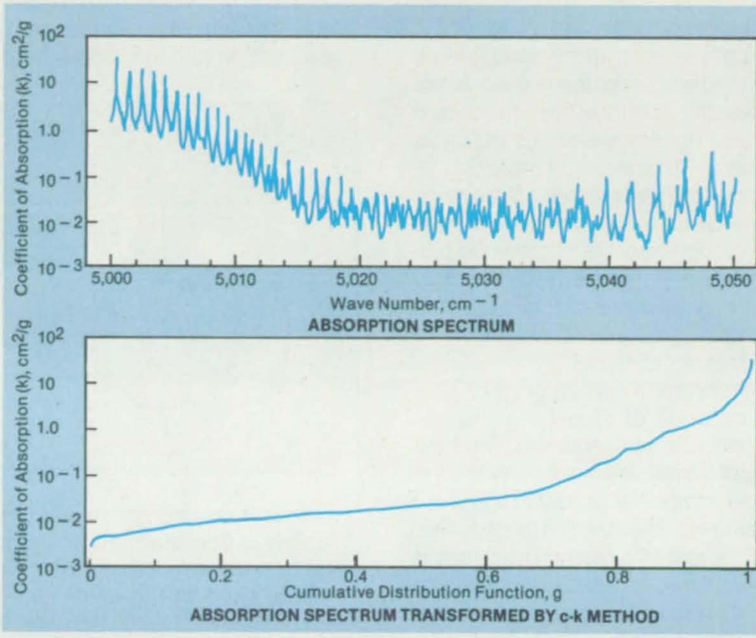

The **Comblike Absorption Spectrum** of CO_2 in one layer of a model atmosphere is transformed into a smooth plot by the c-k method. The new methods, which are based on the c-k method, effect similar transformations applicable to all layers to reduce the number of data that have to be retained in radiation-transport computations.

Garment Would Provide Variable Cooling

The cooling medium would have a variable coefficient of heat transfer.

Lyndon B. Johnson Space Center, Houston, Texas

A conceptual protective garment would include tubes containing a pumped cooling slurry. Unlike other, more-complicated liquid-cooled garments, this one would not have an active control system that would require sensing of temperatures and metabolic rates and processing of these data into flow-control signals. Instead, the cooling slurry would be circulated steadily, and the thermal properties of the slurry would provide the required thermal regulation. This concept may be applicable to suits worn when cleaning up spilled chemicals or fighting fires, for example.

The slurry would consist of water containing capsules of waxes that melt at several different temperatures. The heat capacity of a small volume of slurry and the coefficient of transfer of heat into and out of the slurry would depend on the temperature and the rate of transfer of heat into and out of the slurry. As each wax melted or froze at its unique melting temperature, it would absorb or emit its latent heat of fusion, transferring that heat to or from the water.

The cooling system would be designed so that the melting temperatures would act as "switches" to turn the various heat-transfer coefficients on and off in a way that yields the required overall heat-transfer coefficient as a function of the rate of input of heat from the wearer's body. This design would involve the iterative consideration of several different heat-transfer coefficients (see figure); the temperatures of the environment, the wearer's body, the slurry, and the heat sink; the areas of contact between the tubes and the wearer's body and between the tubes and the heat sink; the heat stored in the wearer's body; and the wearer's metabolic rates. The product of this analysis would be a specification for a slurry that has the appropriate upper and lower heat-transfer coefficients. Preliminary theoretical and experimental work have been done to test the slurry concept, but further research would be necessary to demonstrate the feasibility of the overall cooling-garment concept.

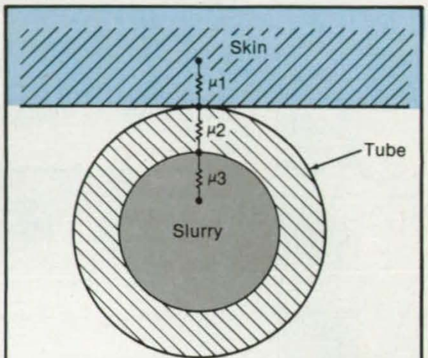

Overall Heat-Transfer Coefficient

$\mu = 1/[1/\mu_1 + 1/\mu_2 + 1/\mu_3]$

The **Overall Coefficient for the Transfer of Heat** from the wearer to the slurry depends on the tube-to-skin, through-the-wall-of-the-tube, and tube-to-slurry coefficients. The biggest problem in the design is to specify a slurry that has the proper range of tube-to-slurry coefficients.

This work was done by Theresa M. Buckley of **Johnson Space Center**. *For further information, Circle 20 on the TSP Request Card.*

MSC-21531

Variable-Vision Sun Visor

A polarized sheet can be rotated to adjust the attenuation of direct sunlight and glare.

Langley Research Center, Hampton, Virginia

Conventional Sun visors in automobiles or other vehicles are usually opaque, and the areas of the windshields in which they can be used are limited. Such a visor can obscure or block out a portion of a wind-

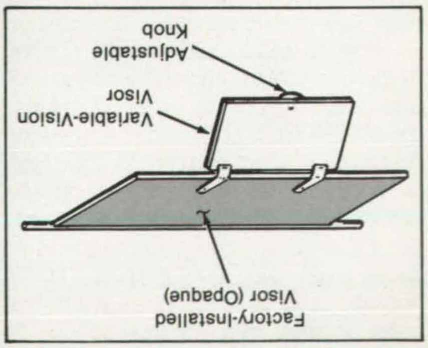

The **Variable-Vision Visor** installed in an automobile enables a driver to attenuate sunlight and glare selectively without obscuring vision.

shield and prevent a driver from seeing traffic signals, stop signs, other vehicular traffic, or pedestrians. A newly developed visor can be adjusted manually to reduce glare and to attenuate variably the sunlight headed toward the eyes of the operator of a car, bus, boat, train, aircraft, balloon, or helicopter.

The variable-vision visor (see figure) includes a frame that holds a sheet of polarized, optically transparent material. A second, smaller sheet of similar material is overlaid in such a way that it can be rotated manually in its plane from 45° to 90° with respect to the polarization of the larger sheet, thereby varying the reduction in the amount of sunlight and glare impinging on the driver's eyes from 75 percent to 99.9 percent. The operator can also adjust the angular orientation of the rotatable sheet to any angle between 45° and 90° to select any desired reduction between the two extremes.

The frame of the device is provided with spring clips so that the variable-vision visor can be readily attached to the factory-installed visor in an automobile. It is also hinged to enable it to fold up behind the regular visor when it is not in use.

In addition to obvious applications for the operators of automobiles and other vehicles, variable-vision visors can be adapted for use in passenger cabin windows in airplanes, buses, trains, and boats. They could also be used as adjustable glare shields for cathode-ray-tube displays.

This work was done by Lester J. Rose and John M. Franke of **Langley Research Center**. *No further documentation is available.*

This invention is owned by NASA, and a patent application has been filed. Inquiries concerning nonexclusive or exclusive license for its commercial development should be addressed to the Patent Counsel, Langley Research Center [see page 14]. Refer to LAR-14147.

Estimating Atmospheric Turbulence From Flight Records

Reconstructed wind fields can be used to predict and avoid future hazards.

Ames Research Center, Moffett Field, California

A method for the estimation of the atmospheric turbulence encountered by airplanes utilizes the wealth of data captured by multichannel digital flight-data recorders and air-traffic-control radar. The method was developed as part of a continuing effort to understand how airplanes respond to such potentially hazardous phenomena as (1) clear-air turbulence generated by destabilized wind-shear layers above mountains and thunderstorms and (2) microbursts (intense downdrafts that strike the ground), which are associated with thunderstorms. With the help of data produced by this method, mathematical models of the wind phenomena can be formulated for use in predicting and avoiding dangerous winds.

Figure 1 illustrates the method for estimating the wind field penetrated by an airplane along its flightpath. A digital flight-data recorder collects measurements of the three components of acceleration, the three angles of orientation, the angle of attack, the pressure altitude, the indicated airspeed, the deflections of the elevators and the rudder, the thrust generated by the engine, and the temperature of the air. Every variable is sampled at least once per second; some are sampled twice or four times per second. In the first step of the analysis, the accelerations measured aboard the airplane are converted to accelerations in the terrestrial frame of reference via a straightforward transformation based on the measured angles of orientation.

The accelerations in the terrestrial frame are integrated to obtain a history of the velocity and then integrated again to obtain the flightpath. This flightpath is then upgraded by forming a best match among it, the tracking data from the air-traffic-control radar, and the pressure-altitude data. Next, the velocity of the airmass with respect to the airplane is computed from the indicated airspeed and the other measurements. Finally, the wind vector in the terrestrial reference frame is computed by vectorial addition of this wind velocity to the velocity of the airplane in the terrestrial frame.

This type of analysis has been applied to several cases of severe turbulence at altitudes above 30,000 ft (9.1 km). The resulting wind-vector data showed that the airplanes had encountered arrays of vortexes generated by wind-shear layers associated with strong temperature inversions near the tropopause. The destabilization of the wind-shear layers was caused by such barriers as mountain ranges and lines of thunderstorms below and upstream of the encounters. The wind patterns in these encounters have been identified via mathematical models that include arrays of horizontal vortexes.

The analysis has also been applied to the highly publicized microburst that caused Delta Airlines flight 191 to crash while attempting to land at Dallas/Forth

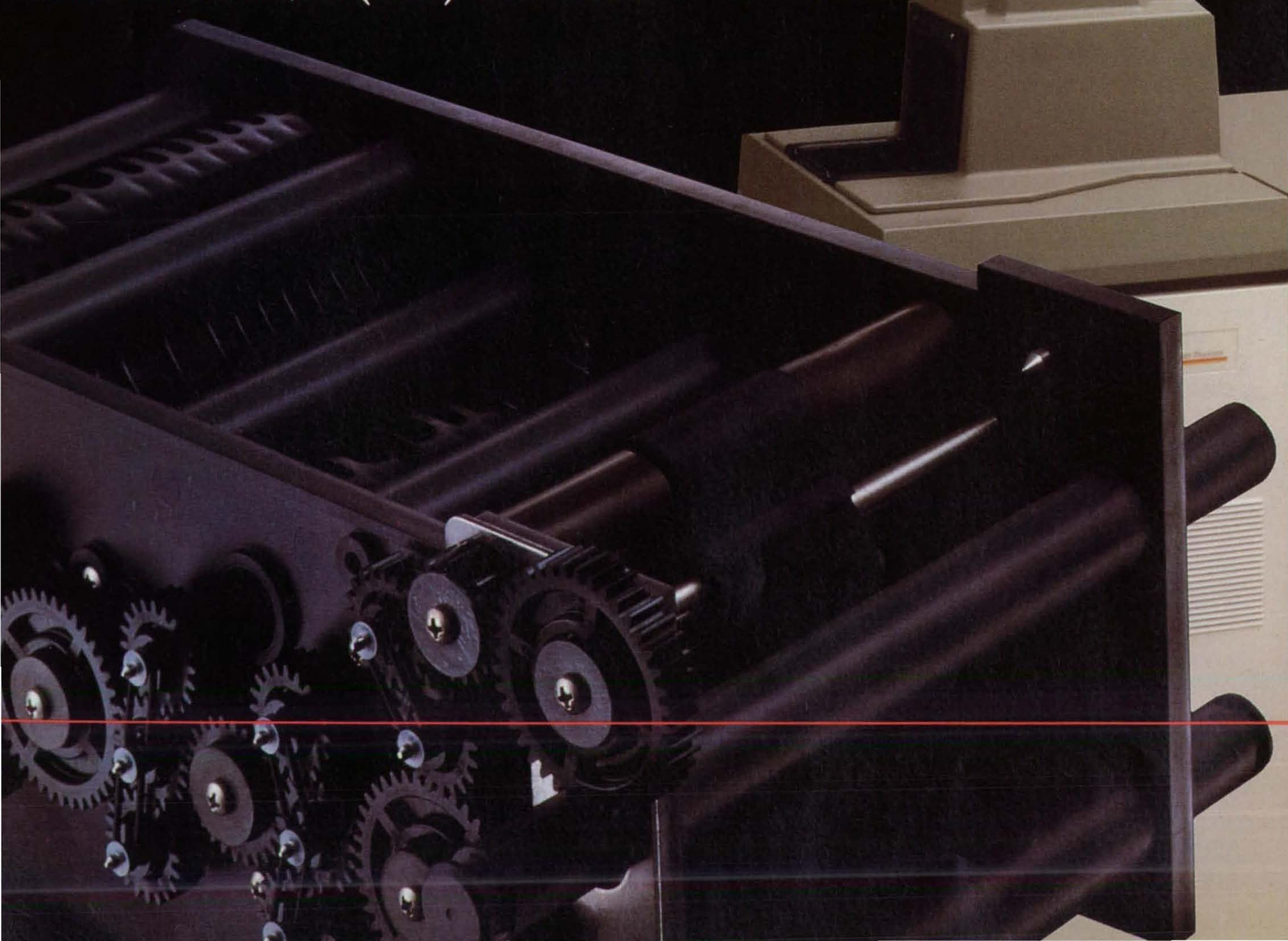

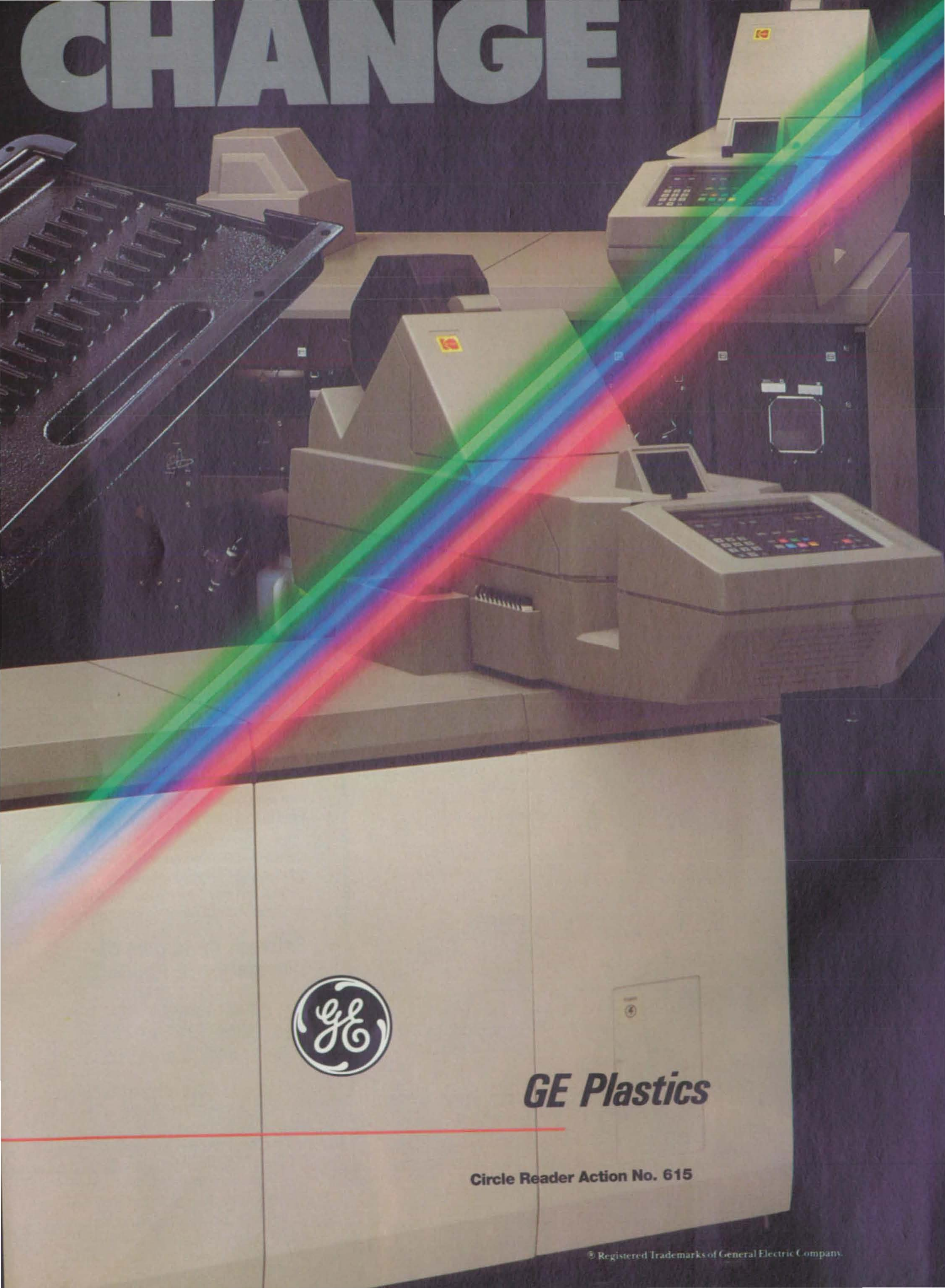
CHANGE
GE Plastics
Circle Reader Action No. 615
® Registered Trademarks of General Electric Company.

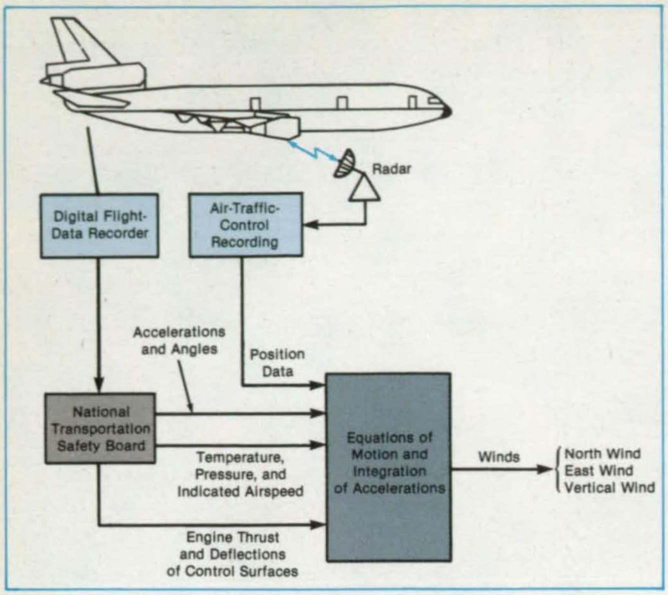

Figure 1. **Flight Data Recorded Aboard the Airplane** and on the ground are used to deduce the wind vector at each point along the flightpath.

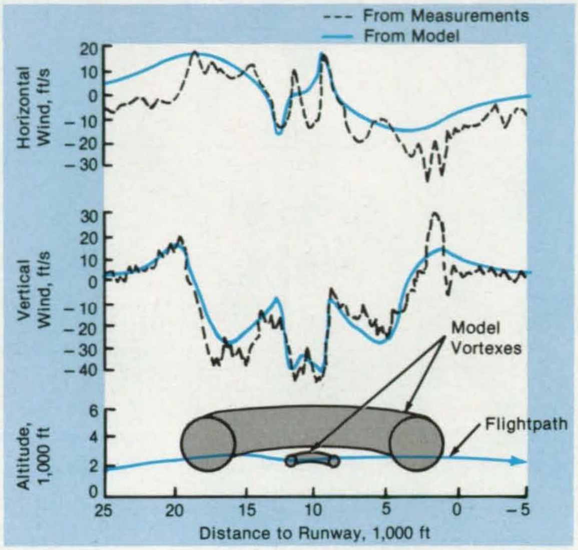

Figure 2. **Horizontal and Vertical Winds** encountered by an airplane in a real microburst (as computed in an analysis of flight data) are compared with those that would be encountered by an airplane flying along the same path through two vortexes in a microburst represented by a simple mathematical model.

Worth airport in 1985. Data from the accident aircraft showed that it encountered a strong microburst downflow followed by a strong outflow accompanied by large and rapid changes in vertical wind. Data from American Airlines flight 539, which arrived shortly afterward and had to go around before attempting to land again, indicated a broad pattern of downflow in the microburst, with regions of upflow at the extreme edges. The combined results indicate a microburst that was increasing in size with vortex-induced velocity fluctuations embedded in a strong outflow near the ground. The wind pattern in the microburst was identified through a mathematical model that included a large vortex ring at the leading edge of the microburst and a smaller vortex ring embedded in the downflow (see Figure 2). This analysis provides a realistic model of the wind field that can be used in flight simulators to understand better the problems of controlling airplanes in severe microbursts.

This work was done by R. C. Wingrove, R. E. Bach, Jr., and T. A. Schultz of **Ames Research Center**. *Further information may be found in NASA TM-102186 [N89-25977], "Analysis of Severe Atmospheric Disturbances From Airline Flight Records."*

Copies may be purchased [prepayment required] from the National Technical Information Service, Springfield, Virginia 22161, Telephone No. (703) 487-4650. Rush orders may be placed for an extra fee by calling (800) 336-4700. ARC-12589

Books and Reports

These reports, studies, handbooks are available from NASA as Technical Support Packages (TSP's) when a Request Card number is cited; otherwise they are available from the National Technical Information Service.

Extrema Principles of Dissipation in Fluids

Issues of stability, dissipation, and the principle of least action are discussed.

A report discusses the application of the principle of least action and other variational or extrema principles to the dissipation of energy and the production of entropy in fluids. The principle of least action has been applied successfully to the dynamics of particles and to quantum mechanics, but it is not universally accepted that variational principles are applicable to thermodynamics and hydrodynamics, and research in this field continues. This report argues for the applicability of some extrema principles to some simple flows.

Section I of the report is an introduction that summarizes previous analyses that involved the application of extrema principles to turbulence, heating, and other phenomena related to dissipation in flows. Section II presents the derivation of an exact equation for the dissipation function of a homogeneous, isotropic, Newtonian fluid. This function includes terms that account for three important mechanisms of dissipation in real flows: irreversible compression or expansion, the generation and radiation of pressure/density (i.e., sound or shock) waves, and the generation of vorticity.

Section III discusses considerations of entropy in slow parallel and cylindrical shear flows. The dissipation function is applied, and it is shown, by use of entropy-extrema principles, that simple flows like incompressible flow in a channel and a cylindrical vortex are characterized by distributions that have minimal dissipation.

Section IV discusses consideration of dissipation in unsteady, two-dimensional flows. The application of extremum conditions of the production or dissipation of entropy is facilitated by the consideration of the mean and fluctuating components of the dissipation function. This section concludes with a description of an experiment in which measurements of pressure and velocity in a typical periodic shear flow — a jet that flows along a wall and off the wall at a sharp edge. The measurements were processed to obtain estimates of the mean and fluctuating components of the dissipation field.

The authors conclude that the steady motion of a viscous fluid may be described as a near-equilibrium process and is compatible with a condition of minimum dissipation. In contrast, the principal notions of the stability of parallel shear flows concerning the maximum growth rate of vortical disturbances appear to be consistent with a maximum dissipation condition. These observations are consistent with Prigogine's distinction between stable thermodynamic states or processes that are either linear and near equilibrium, or nonlinear and far from equilibrium. In this context, vortexes and acoustic wave sources appear to be examples of dissipative structures.

This work was done by W. Clifton Horne of **Ames Research Center** *and Krishnamurty Karamcheti of Florida State University. To obtain a copy of the report, "Extrema Principles of Entropy Production and Energy Dissipation in Fluid Mechanics," Circle 10 on the TSP Request Card.*
ARC-12318

Experiments on Rotating, Charged Liquid Drops

Results have implications for containerless processing and modeling of atomic nuclei.

A report describes experiments in which electrically charged drops of liquid were levitated electrostatically and rotated and vibrated acoustically. The physics of rotating drops has been studied for many years: Lord Rayleigh calculated the axisymmetric shapes of rotating drops in 1914. The topic continues to have theoretical importance because it relates to phenomena over a large range of sizes — from rotating heavenly bodies to liquid-drop models of atomic nuclei. It also has practical importance for the emerging field of containerless processing, with potential applications in the manufacture of drugs and highly pure materials and in ultraclean chemical experiments.

The experimental apparatus was a hybrid electrostatic/acoustic levitation chamber. The drop was suspended electrostatically in air along the vertical axis between two electrodes. A video camera monitored the vertical position of the drop, and the measured position was processed into a feedback signal to control the voltage on the electrodes to keep the position constant. The acoustic torques and forces that rotated and vibrated the drops about the vertical axis were applied by two perpendicular horizontal acoustic transducers locked to each other at the same frequency and at selected differences in phase.

Drops of water (low viscosity) and anhydrous glycerol (high viscosity) having diameters of about 3 mm and electrically charged to various degrees were suspended. Vibrations and rotations of the drops were induced by modulating the acoustic pressure and torque. Pulsation and toroidal oscillation modes were identified and discussed on the basis of theories developed previously. As the speed of rotation was increased from zero, families of axisymmetric, triaxial, peanut, and dumbbell shapes and eventual fission were observed.

When the surface electrical charge on the drop was treated mathematically as giving rise to an effective surface tension that modifies the surface tension of the natural liquid, the results of the experiments on drops carrying low charges were found to agree well with the prediction of a 1980 study on the shapes and stabilities of rotating liquid drops. It is especially noteworthy that, at the bifurcation point, the ratio of the speed of rotation to the characteristic frequency of the toroidal mode of the uncharged drop was found to agree within 3 percent with the predicted value of 0.559. However, as the charge on the drop approached the Rayleigh limit, dumbbell and peanut shapes and direct breakup from axisymmetric shapes were observed. These results agree only qualitatively with existing theories, which do not apply in the high-charge limit.

The report discusses the possibility of measuring the charges of drops of low-viscosity liquids by the drop-oscillation method. It also discusses the measurement of the surface tensions of highly viscous liquids by the drop-rotation method.

This work was done by Won-Kyu Rhim, Sang Kun Chung, and Daniel D. Elleman of **NASA's Jet Propulsion Laboratory**. *To obtain a copy of the report, "Electrostatic Containerless Processing Technology: Experiments on Rotating Charged Liquid Drops," Circle 61 on the TSP Request Card. NPO-17893*

Effects of Multiple Ion Species on Plasma Instabilities

Effects depend on both ion masses and types of waves.

A report presents the results of a theoretical study of the effects of cometary newborn O^+, H_3O^+, and H_2O^+ ions on wave instabilities in the solar-wind magnetoplasma. The report adds to the body of knowledge of plasma instabilities caused by streaming ions. The information is important for understanding the solar wind and may be useful in studies of thermonuclearfusion plasmas in which instabilities of this type could be present.

The solar-wind magnetoplasma is represented by an idealized mathematical model consisting of isotropic Maxwellian electron and proton populations with temperatures of 17.2 and 6.9 eV, respectively, and equal number densities of 4.95 cm^{-3}. The interplanetary magnetic field is taken to equal 8 nT and to define the z axis of the coordinate system. In the spacecraft and cometary coordinate systems used, the solar wind flows with a speed of 400 km/s at an angle α with the magnetic field. Each species of newborn ion is added to the background at a number density of 0.05 cm^{-3}, to be neutralized by a simultaneously created population of photoelectrons, and to have zero initial average velocity in the spacecraft and cometary coordinate systems.

The evolution of velocity distributions of the various ion species is represented by the linearized Maxwell–Vlasov equations. These equations are solved numerically at $\alpha = 71.57°$ ($\sin^2\alpha = 0.9$) and at $\alpha = 18.43°$ ($\sin^2\alpha = 0.1$). The results are plotted as complex dispersion relations for the various wave modes, with frequencies expressed in units of the solar-wind proton cyclotron frequency of 0.122 Hz and wave numbers (reciprocal distances) normalized by multiplication by the proton gyroradius of 47.4 km.

An analysis of the stability of the low-frequency electromagnetic modes excited by the coexisting newborn ion species shows that the effects of these species on the growth of waves depend not only on the masses of these ions but also on the physical nature of the wave modes. Whereas each of the coexisting ion beams tends to stimulate instabilities without undue influence from the other species that have different masses, newborn ions that have similar masses can strongly catalyze the growth of fluidlike, nonresonant wave modes. However, newborn ions that have similar masses can cause only weak enhancements of growth in cyclotron resonant instabilities. The authors observe that the implications of this dissimilar dependence of the resonant and fluid-mode instabilities on the coexistence of newborn species may be particularly relevant in the interpretation of wave activity close to the nuclei of comets. The increase in the variety and density of newborn ions suggests a likely gradual prominence of the fluid modes, although the concomitant deceleration of the solar wind would reduce the available free energy of the cometary particles.

This work was done by Bruce T. Tsurutani and Armando L. Brinca of Caltech for **NASA's Jet Propulsion Laboratory**. *To obtain a copy of the report, "Influence of Multiple Ion Species on Low Frequency Electromagetic Wave Instabilities," Circle 25 on the TSP Request Card.*
NPO-17771

Overview of Aerothermodynamics of Hypersonic Flight

Research and development challenges posed by new programs are examined.

A paper reviews recent developments in the technology of hypersonic flight. The paper notes the renewed interest in hypersonic flight, including proposals for a commercial hypersonic transport (the "Orient Express") and atmospheric-braking orbital-transfer vehicles. The paper considers the flight environments in which such aircraft will operate, the fluid-dynamic and chemical phenomena of hypersonic flight, the computational challenges to designers and developers of aircraft and powerplants, and the difficulties of validating computer models of hypersonic phenomena.

The new aircraft will need air-breathing propulsion systems well beyond the current technological base. Supersonic combustion ram (scram) jets are likely candidates. Integration of the engine with the airframe will be a major issue; nearly the entire underside of an aircraft will be considered part of the powerplant.

Among the fluid-dynamical phenomena to be studied are strong shock waves, interactions between viscous and inviscid flows, interactions between shock waves and boundary layers, boundary-layer-transition and turbulent flows, and separation and vortex flows. Chemical effects in real gases — which may be combined with fluid-dynamical phenomena — include equilibrium chemistry, nonequilibrium chemistry, combustion, and radiation.

Computational fluid dynamics (CFD) has made great strides and will help greatly in studies of the phenomena. Nevertheless, CFD programs must be validated, and experimental facilities on the ground will not be adequate for this purpose. The solution is to validate the programs for individual phenomena and to combine the programs for multiple phenomena as carefully as possible. Well-instrumented flight tests will contribute to validation.

This work was done by Gary T. Chapman of **Ames Research Center**. *To obtain a copy of the report, "An Overview of Hypersonic Aerothermodynamics," Circle 7 on the TSP Request Card.* *ARC-12217*

Materials

High-Temperature Insulating Gap Filler

Lifetime and maximum operating temperature are increased.

Lyndon B. Johnson Space Center, Houston, Texas

A new inorganic, ceramic filler for gaps between refractory ceramic tiles offers high resistance to heat and erosion. In tests (see figure), the gap filler between tiles withstood supersonic blasts of air as hot as 2,300 °F (1,260 °C) for as long as 12½ min with no significant degradation. The all-ceramic filler was developed as a replacement for an organic filler used on the thermal-protection system of the Space Shuttle. The organic filler deteriorates and erodes during reentry and often must be replaced after a single mission. The new inorganic filler promises to serve for many missions and to reduce greatly the cost and delay of refurbishing the aerospace craft. The ceramic filler also could be used as a sealing material in furnaces or as a heat shield for sensitive components in automobiles, aircraft, and home appliances.

The filler consists of a ceramic-fiber fabric precoated with silica and further coated with silica containing a small amount of silicon carbide powder to increase its thermal emittance. The fabric can be coated before or after it has been installed in a gap.

The precoat is applied as a slurry of 80 percent (by weight) colloidal silica and 20 percent isopropyl alcohol. The slurry is brushed on the fabric and dried in air for 4 h. The topcoat is applied as a slurry composed of 47 percent colloidal silica, 50 percent ground silica powder, and 3 percent silicon carbide powder. It, too, is brushed evenly on the fabric, then allowed to dry for 24 h.

This work was done by Gordon R. Toombs, Kevin K. O'Young, and Everett G. Stevens of Rockwell International Corp. for **Johnson Space Center**. *For further information, Circle 2 on the TSP Request Card.*

Inquiries concerning rights for the commercial use of this invention should be addressed to the Patent Counsel, Johnson Space Center [see page 14]. Refer to MSC-21644.

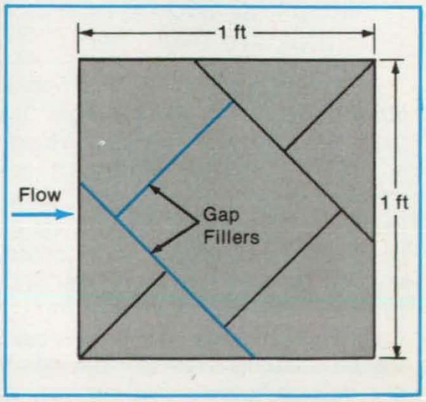

Test Specimens consisted of panels of ceramic tiles with ceramic-fabric-based filler in the gaps between the tiles. Gaps of 0.07 and 0.1 in. (1.8 and 2.5 mm) were evaluated.


MONEL alloys
Machining
Joining
Inco Alloys International
Resistance to Corrosion
Inco Alloys International
NIMONIC alloy 75
INCONEL alloy 625
Alloys International
800HT
alloy 825
718

New Synthesis of High-Performance Bismaleimides

A general synthesis scheme produces tough, easy-to-process, high-performance thermoplastics.

Langley Research Center, Hampton, Virginia

In the last few years, many toughened bismaleimides (BMI's) have been developed in response to growing interest in BMI's as high-performance matrix resins and adhesives. Almost invariably, however, increased toughness has been achieved at a considerable loss of performance at high temperature. Consequently, a new general synthesis of tough and easy-to-process high-performance BMI's has been developed. The synthesis involves the reaction of acetylene-terminated compounds with BMI's or biscitraconimides.

The synthesis offers matrix resins and adhesives that have combined advantages of the toughness characteristic of thermoplastics and the easy processability characteristic of thermosetting materials. To demonstrate the concept of the synthesis, LaRC-RP80—a new BMI—was prepared from the reaction of a commercially available acetylene-terminated compound with a new biscitraconimide that contains a flexibilizing hexafluoroisopropylidene linking group.

In comparison with other state-of-the-art BMI's, LaRC-RP80 exhibited significant increases in fracture toughness (324 J/m^2), resistance to moisture (2.4 percent equilibrium uptake of moisture), thermo-oxidative stability (5 percent loss of weight at 514 °C by thermogravimetric analysis in air), and lap shear strength under hot and wet conditions [lap shear strength of 2,963 psi (20.43 MPa) when tested wet at 232 °C].

Preliminary results support the concept of the formation of addition-type thermoplastic polymers through the Diels-Alder reaction of acetylenes with maleimides. The figure shows that any of three reaction routes is plausible for the reaction of an acetylene with a maleimide. They are (a) the homopolymerization of the individual reacting components, (b) the Diels-Alder reaction, and (c) the "ene" addition of the acetylene across the double bond of the maleimide. Of these three possibilities, only the Diels-Alder reaction leads to a tough linear thermoplastic material.

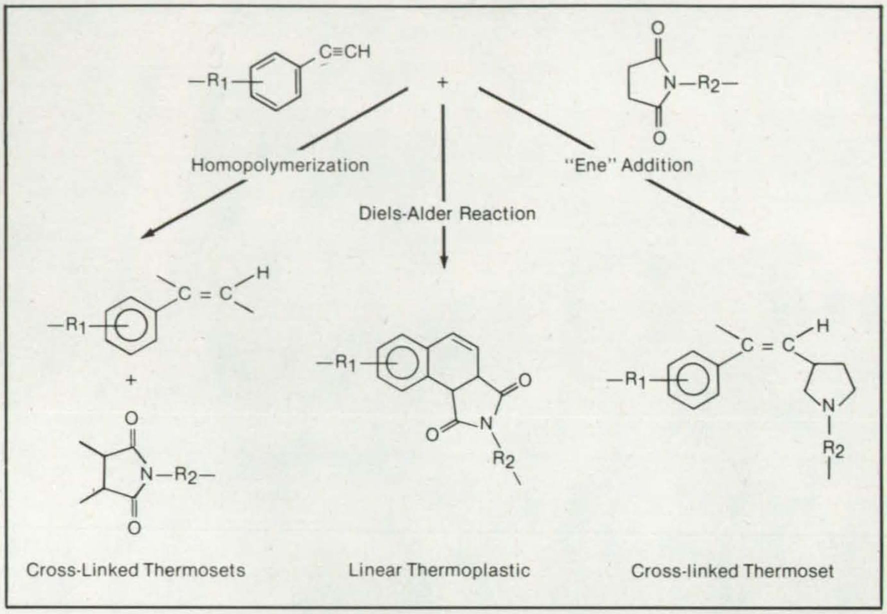

Of the **Three Plausible Reactions** for this synthesis, the Diels-Alder reaction is the only one that can produce a tough linear thermoplastic material.

The LaRC-RP80 thus produced shows considerable promise as a high-temperature matrix resin and adhesive. However, the concept of this synthesis has general applicability and potential for development of tough and easy-to-process addition-type thermoplastics. This synthesis scheme has the potential for providing high-performance matrix resins that survive well at high temperatures and absorb little moisture.

This work was done by Ruth H. Pater, Sharon Lowther, Michelle Cannon, Janice Smith, and Karen Whitely of **Langley Research Center**. *For further information, Circle 66 on the TSP Request Card.*

This invention is owned by NASA, and a patent application has been filed. Inquiries concerning nonexclusive or exclusive license for its commercial development should be addressed to the Patent Counsel, Langley Research Center [see page 14]. Refer to LAR-13958.

Iridium/Rhenium Parts for Rocket Engines

Maximum operating temperature is increased to 2,200 °C from 1,400 °C.

Lewis Research Center, Cleveland, Ohio

Oxidation/corrosion of metals at high temperatures is the primary life-limiting mechanism of parts in rocket engines. A combination of metals greatly increases the operating temperature and longevity of these parts. The combination consists of two transition-element metals — iridium and rhenium — that melt at extremely high temperatures. These materials have previously been very difficult to fabricate into parts.

Structural rhenium can be formed into the complex geometry of a small rocket engine chamber by chemical-vapor deposition of rhenium onto a mold. A coating of iridium is applied to the rhenium, also by chemical-vapor deposition, for oxidation protection of the rhenium at high temperatures. The combination of materials raises the operating temperature of small rocket-engines to 2,220 °C, 800 °C higher than that of the best material previously available; i.e., silicide-coated niobium. Already, the iridium/rhenium combination has increased the operating lifetimes of small rocket engines by more than a factor of 10 at the conventional operating temperature of 1,400 °C. The lifetime of this material combination at the elevated temperature of 2,200 °C is at least comparable to the lifetimes of the existing materials at 1,400 °C. The lifetime is limited by the oxidation rate/thickness of the iridium coat and by differences in the diffusion rates of the two materials at their interface resulting in the formation of Kirkendall voids and delamination of the iridium. Once the technique for fabrication is improved, it should be possible to make hotter-operating, longer-lasting components for turbines and other heat engines.

This work was done by Steven J. Schneider of **Lewis Research Center**, *John T. Harding of Ultramet, and John R. Wooten of Aerojet TechSystems Co. For further information, Circle 84 on the TSP Request Card. LEW-14924*

Lightweight Fibrous Ni Electrodes for Ni/H_2 Batteries

Weight is reduced by 40 percent.

Lewis Research Center, Cleveland, Ohio

A fibrous nickel plaque electrode material reduces the weight of nickel/hydrogen batteries. The weight of an electrode made of the new material is 40 percent less than that of an equivalent electrode made of the previous material, which was a porous nickel plaque made by sintering fine nickel powder onto a wire screen. The new lightweight fibrous plaque is also expected to lead to improvements in performances, increases in energy densities, and decreases in the costs of nickel electrodes.

The fabrication of the electrode material begins with the extrusion of a mixture of nickel oxide and binding agents into fibers. The fibers are sintered into mats, which are layered with nickel and cobalt powders. Cobalt is included because electrodes made from porous lightweight mats commonly exhibit low initial utilization that increases gradually with charge/discharge cycling and because the addition of $Co(OH)_2$ was previously found to help achieve full utilization of the $Ni(OH)_2$ active material earlier during cycling. The composition of the electrode material immediately after fabrication and before electrochemical impregnation is 50 percent nickel fiber, 35 percent nickel powder, and 15 percent cobalt powder.

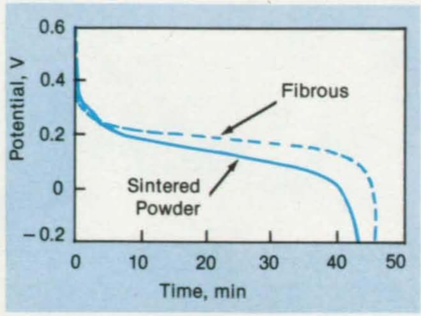

The **Discharge Voltage and Discharge Time** of a fibrous electrode are greater than those of the equivalent standard sintered-powder electrode.

The electrode plaques are impregnated electrochemically in an aqueous bath containing 1.5M $Ni(NO_3)_2$, 0.175M $Co(NO_3)_2$, and 0.075M $NaNO_2$ made acidic by the addition of 50-percent nitric acid. The bath is maintained at a temperature of 95 to 100 °C and a pH of 3 to 4. After impregnation, the elements are formed further by subjecting them to charge/discharge cycles.

Tests show that the performance of an electrode of the new type compares favorably with that of a sintered electrode (see figure). The major disadvantage of the new electrode material appears to be that the charge capacity decreases with the number of charge/discharge cycles at high rates of discharge. However, this does not signify a decrease in total capacity, inasmuch as the capacity at low rates of discharge does not seem to deteriorate.

This work was done by Doris L. Britton of **Lewis Research Center**. *Further information may be found in NASA TM-101997 [N89-22710], "Lightweight Fibrous Nickel Electrodes for Nickel-Hydrogen Batteries."*

Copies may be purchased [prepayment required] from the National Technical Information Service, Springfield, Virginia 22161, Telephone No. (703) 487-4650. Rush orders may be placed for an extra fee by calling (800) 336-4700.

LEW-14955

Improved microstructural homogeneity.
AMS 4225 cylinder head.
Hot isostatically pressed (HIPed).
Microporosity eliminated.

Books and Reports

These reports, studies, handbooks are available from NASA as Technical Support Packages (TSP's) when a Request Card number is cited; otherwise they are available from the National Technical Information Service.

Tests of Flexible Multilayer Insulations

Composite blankets containing reflective layers are compared with fibrous silica insulation.

A report describes a comparative experimental and theoretical study of 11 flexible insulating blankets that ranged in thickness from 1.0 to 2.5 in. (2.5 to 6.4 cm). Two of these blankets, constituting the baseline materials for comparison, were made of the silica felt, advanced flexible reusable surface insulation (AFRSI) that is used in the thermal-protection system on the Space Shuttle. The other nine blankets — candidate thermal shields for the proposed Aeroassisted Orbital Transfer vehicle — consisted of various combinations of multiple reflecting layers of stainless steel, aluminum foil, or aluminized polyimide film interspersed with spacing and/or insulating layers of aluminoborosilicate scrim or mat, silica felt or mat, and/or alumina mat; all sandwiched between aluminoborosilicate outer fabrics and quilted together with ceramic thread.

The multilayer insulations are intended for use in the partial vacuums of outer planetary atmospheres, where the mean free paths of gas molecules are much less than the characteristic lengths of cells in the insulation and consequently the conductive and convective effects of the gas are minimal. Accordingly, the blankets were tested in partial vacuums. In each test, thermocouples were mounted on the front and rear faces of each blanket, the front face was heated to ~1,050 °C for ~21/2 minutes, and the resulting increase in temperature on the rear face was measured for 20 minutes. The experimental data were also compared with the predictions of a mathematical model developed for analyzing the heat-transfer properties of these and similar multilayer composite insulating blankets.

The data showed that the multilayer blankets that contained aluminum foils were the most effective in that they reduced the increase in rear-face temperatures by as much as 50 percent below those of the baseline AFRSI. However, these blankets were slightly heavier than the baseline blankets were. The blanket that contained the aluminized polyimide also maintained a lower rear-face temperature, yet had weight and thickness equal to those of one of the baseline blankets. The spectral reflectance of the aluminum foil and the aluminum deposited on polyimide was found not to deteriorate significantly as a function of temperature. The effectiveness of the multilayer insulation was found to increase with thickness, as one would expect intuitively. The predictions of the mathematical model indicated that lower thermal conductivity can be achieved in the composite insulation containing aluminum layers than in the AFRSI, and that a composite insulation containing aluminized film could be used to reduce the weight of the thermal-protection system of the Aeroassist Orbital Transfer Vehicle.

This work was done by D. A. Kourtides of **Ames Research Center** *and W. C. Pitts of Eloret Institute. To obtain a copy of the report, "Composite Multilayer Insulations for Thermal Protection of Aerospace Vehicles," Circle 117 on the TSP Request Card.*

This invention is owned by NASA, and a patent application has been filed. Inquiries concerning nonexclusive or exclusive license for its commercial development should be addressed to the Patent Counsel, Ames Research Center [see page 14]. Refer to ARC-12405.

Computer Programs

COSMIC: Transferring NASA Software

COSMIC, NASA's Computer Software Management and information Center, distributes software developed with NASA funding to industry, other government agencies and academia.

COSMIC's inventory is updated regularly; new programs are reported in *Tech Briefs*. For additional information on any of the programs described here, circle the appropriate TSP number.

If you don't find a program in this issue that meets your needs, call COSMIC directly for a free review of programs in your area of interest. You can also purchase the annual *COSMIC Software Catalog*, containing descriptions and ordering information for available software.

COSMIC is part of NASA's Technology Utilization Network

COSMIC® — *John A. Gibson, Director,*
(404) 542-3265
The University of Georgia, 382 East Broad Street, Athens, Georgia 30602

Computer Programs

These programs may be obtained at a very reasonable cost from COSMIC, a facility sponsored by NASA to make computer programs available to the public. For information on program price, size, and availability, circle the reference number on the TSP and COSMIC Request Card in this issue.

Physical Sciences

Computing Performance of an Optical System

A collection of programs performs complicated ray-tracing and diffraction calculations.

The Optical Surface Analysis Code (OSAC) is designed to provide a comprehensive analysis of the performance of an optical system. OSAC can analyze both conventional systems and x-ray systems. The program is composed of nine compatible programs that are executed in a sequence defined by the user.

GEOSAC reads a file of data, entered by the user, that contains all the parameters necessary to define an optical system. It performs all the necessary geometric calculations, such as finding the distances between the foci of the various conical optical elements and finding the location of the geometrical or Gaussian focal plane of the system.

NABRAT traces an input bundle of collimated rays through a two-element optical system in order to verify that the parameters of the system are reasonable and to provide a feel for the performance of the system. NABRAT traces the entire optical system in one run and puts out three files containing ray-intersection information — one for each of the surfaces and one for the focal plane.

DRAT traces a bundle of rays through a single element of an optical system. The element can be conical or folded flat. Surfaces traced by DRAT can have polynomial deformations. If the surface is the first surface in the system, the input bundle of rays is collimated. If not, the input-ray information is taken from the output of a previous DRAT run.

SUSEQ provides a mapping from scatter angles at the optical surfaces to displacements of rays at the focal plane. DEDRIQ enables the user to specify high-spatial-frequency deformations (roughness). Roughness can be specified in terms of a surface-height-autocovariance function, a roughness power spectral-density function, or a one-or two-dimensional grating profile. Part of the output of DEDRIQ is a file on an array of picture elements in the focal plane specifying how much diffusely scattered energy is contained in each picture element. The remaining output is a file containing information on the intersections of rays in the focal plane, identical to the file produced by NABRAT or DRAT except that the intensity of each ray is attenuated by the amount of diffuse scatter. SUSEQ and DEDRIQ work together to calculate scale factors for the intersections of each ray with each optical surface. If the system is an x-ray system, an additional set of scale factors is calculated to address the change in grazing angle of the ray at each succeeding surface.

OPD provides a map of optical-path differences in the pupil plane of the system. PSF uses the OPD and ray-intensity information to calculate a pupil function, then Fourier-transforms that function to calculate the energy distribution or point-spread function in the focal plane due to diffraction. The output of PSF is a file that tells how much diffracted energy is contained in each picture element of the focal plane.

FPLOOK combines specular-ray files and files on arrays of picture elements in

the focal plane into a single focal-plane-picture-element-array file in order to show the energy contained in a set of picture elements specified by the user. COGEN fits a set of polynomials to a set of actual mirror-deformation data so that the resulting polynomial coefficients can later be used by DRAT in tracing rays through the deformed system. The polynomials are Zernike polynomials for conventional systems and Legendre-Fourier polynomials for an x-ray system.

The integrated OSAC system employs a standard coordinate system within which each optical surface and the focal planes are defined. Upon entering the optical system, each ray is assigned an intensity or "weight" of unity. This weight is subsequently attenuated by reflections and scattering by the mirror surfaces. OSAC allows for four types of surfaces: on-axis conical surfaces, off-axis conical surfaces, flat surfaces, and on-axis conical surfaces for x-ray systems. The system takes into account the effects of misalignments of optical surfaces, deformations of low and high spatial frequencies, and diffraction.

OSAC is written in FORTRAN IV and has been implemented on the IBM 360/75 and the DEC VAX computers. The double-precision IMSL Subroutine Libraries are required. The VAX version requires 118K of 8-bit bytes, not including the IMSL routines. This program was released in 1988.

This program was written by P. Glenn and R. Noll of Perkin-Elmer Corp. for **Goddard Space Flight Center**. *For further information, Circle 37 on the TSP Request Card.*
GSC-13128

Program Computes Universal Transverse Mercator Projection

The spheroid is projected by use of transformations of the elliptic integral.

A computer program produces the Gauss–Kruger (constant meridional scale) transverse Mercator projection, which is used to construct the U.S. Army's universal transverse Mercator (UTM) grid system. The program is capable of mapping the entire Northern Hemisphere of the Earth (and, by symmetry of the projection, the entire Earth) accurately with respect to a single principal meridian and is, therefore, mathematically insensitive to proximity to the pole or the equator and insensitive to the departure of the meridian from the central meridian. This program could be useful to any mapmaking agency.

The program overcomes the limitations of the "series" method (Thomas, 1952) presently used to compute the UTM grid: specifically, its complicated derivation, nonconvergence near the pole, lack of rigorous error analysis, and difficulty of obtaining increased accuracy. The method is based on the principle that the parametric colatitude of a point is the amplitude of the elliptic integral of the second kind, and this (irreducible) integral is the desired projection. Thus, a specification of the colatitude leads most directly (and with strongest motivation) to a formulation in terms of amplitude. The most difficult problem to be solved was setting up the method so that the elliptic integral of the second kind could be used elsewhere than on the principal meridian.

The point to be mapped is specified in conventional geographic coordinates (geodetic latitude and longitudinal departure from the principal meridian). Using the colatitude (complement of latitude) and the longitude (departure), the initial step is to map the point to the north polar stereographic projection. The closed-form, analytic function that coincides with the north polar stereographic projection of the spheroid along the principal meridian is put into a Newton–Raphson iteration that solves for the tangent of one-half the parametric colatitude, generalized to the complex plane. Because the parametric colatitude is the amplitude of the (irreducible) incomplete elliptic integral of the second kind, the value for the tangent of one-half the amplitude of the elliptic integral of the second kind is now known.

The elliptic integral can then be computed by any desired method, and the result is the Gauss–Kruger transverse Mercator projection. This result is a consequence of the fact that these steps produce a computation of real distance along the image (in the plane) of the principal meridian and an analytic continuation of the distance at points that do not lie on the principal meridian. The elliptic-integral method used by this program is one of the "transformations of the elliptic integral" (similar to Landen's transformation) that appear in standard handbooks of mathematical functions. Only elementary transcendental functions are used. The output of the program is the conventional (as used by the mapping agencies) cartesian coordinates, in meters, of the transverse Mercator projection. The origin is at the intersection of the principal meridian and the equator.

This FORTRAN77 program was developed on an IBM PC-series computer equipped with an Intel Math Coprocessor. Double-precision complex arithmetic and transcendental functions are needed to support a projection accuracy of 1 mm. Because such functions are not usually part of the FORTRAN library, the needed functions have been explicitly programmed and included in the source code. The program was developed in 1989 and is copyrighted.

This program was written by David E. Wallis of Caltech for **NASA's Jet Propulsion Laboratory**. *For further information, Circle 103 on the TSP Request Card.*
NPO-18086

Computing Temperatures in Optically Pumped Laser Rods

Radial and axial distributions are calculated for rods of finite length.

Managing the heat that accumulates within solid-state laser materials under active pumping is of critical importance in the design of laser systems. Earlier mathematical models that calculated the temperature distributions in laser rods were one-dimensional and included laser rods of infinite length. A computer program presents a new model that solves the temperature-distribution problem for laser rods of finite length and calculates both the radial and axial components of temperature distributions in these rods.

The rod in the mathematical model is pumped from either the end or the side by a continuous or a single-pulse pump beam. (At present, the model gives average values for pump sources that provide multiple pulses.) The optical axis is assumed to coincide with the axis of the rod. It is also assumed that it is possible to cool different surfaces of the rod at different rates.

The user defines the characteristics of the laser rod material, determines the types of cooling and pumping to be modeled, and selects the desired time frame via the input file. The program contains several self-checking schemes to prevent the overwriting of memory blocks and to provide simple tracing of information in case of trouble. Output from the program consists of (1) an echo of the input file; (2) diffusion properties, radius, length, and time for each data block; (3) the radial increments from the center to the outer edge of the laser rod; and (4) the axial increments from the front of the laser rod to the other end of the rod.

This program was written in Microsoft FORTRAN77 and implemented on a Tandon AT computer with a 287 math coprocessor. The program can also run on a VAX 750 minicomputer. It has a memory requirement of about 147 KB and was developed in 1989.

This program was written by Usamah O. Farrukh of Hampton University for **Langley Research Center**. *For further information, Circle 67 on the TSP Request Card.*
LAR-14209

Mathematics and Information Sciences

Graphics Software for VT Terminals

The software is transportable to many different computers.

VTGRAPH is a graphics software tool for the DEC/VT computer terminal or terminals compatible with it, which are widely used by government and industry. VTGRAPH, which is callable in FORTRAN or C language, is a library program that enables the user to cope with many computer environments in which VT terminals are used for window management and graphic systems. It also provides a PLOT10-like package plus color or shade capability for VT240, VT241, and VT300 terminals. The program is transportable to many different computers with which VT terminals are used. With this graphics package, the user can easily design more-friendly user-interface programs and design PLOT10 programs on VT terminals with different computer systems.

VTGRAPH was developed by use of the ReGis Graphics set, which provides a full range of graphics capabilities. The basic VTGRAPH capabilities are the following: window management, PLOT10-compatible drawing, generic program routines for two- and three-dimensional plotting, and color graphics or shaded graphics.

The program was developed in VAX FORTRAN in 1988. VTGRAPH requires a ReGis graphics set terminal and a FORTRAN compiler. The program has been run on a DEC MicroVAX 3600-series computer operating under VMS 5.0 and has a virtual-memory requirement of 5 KB.

This program was written by Caroline Wang of **Marshall Space Flight Center**. *For further information, Circle 146 on the TSP Request Card.* *MFS-27214*

Program for Generating Interactive Displays

The user can construct custom software interfaces.

The Sun/Unix version of the Transportable Applications Environment Plus (TAE+) computer program provides an integrated, portable software environment for developing and running interactive window, text, and graphical-object-based application software systems. The program enables a programmer or nonprogrammer to construct easily a custom software interface between a user and an application program and to move the resulting interface program and its application program to different computers. The Plus can be viewed as a productivity tool — both for the application developers and the application end users, who benefit from the resultant consistent and well-designed user interface that shelters them from the intricacies of the computer.

The main components of TAE+ are (1) the WorkBench, a "what you see is what you get" (WYSIWYG) software tool for the design and layout of a software interface between the user and the application program ("user interface," for short); (2) the WPT's (Window Programming Tools) software package, which is a set of callable subroutines that control the user interface; and (3) TAE Command Language (TCL), an easy-to-learn command language that provides an easy way to develop an executable prototype application program with a language that is interpreted at run time.

The WorkBench enables the person developing the application program to construct the layout of the display screen of the application program interactively by manipulating a set of interaction objects, including such input items as buttons, icons, and scrolling lists. Also included are such data-driven graphical objects as dials, thermometers, and strip charts, which TAE+ updates as the values of the data change. The user specifies the windows and interaction objects that will be included in the user interface, then specifies the sequence of the dialogue between the user interface and the user. The description of the user interface thus designed is then saved in resource files. Once the user interface has been designed, the WorkBench has the option to generate a source-code-program (C, Ada, FORTRAN and TCL), which fully controls the user interface through runtime functions (WPT's), and is ready for the application-specific code to be integrated.

The WPT's provide the services used at run time by application programs to display and control the user interfaces. Because the WPT's gain access to the WorkBench-generated resource files during each execution, such details as color, font, location, and object type remain independent from the application code, allowing changes to the user interface without recompiling and relinking.

In addition to WPT's, TAE+ offers control of interaction objects from the interpreted TAE Command Language. TCL provides an extremely powerful means for the more experienced developer to quickly prototype an application program's use of the interaction objects in TAE+ and to add programming logic without the overhead of compiling or linking.

TAE+ uses the MIT X-Window software system as the underlying windowing standard software. The WorkBench and WPT's are written in C++, and the remaining code is written in C. TAE+ is available by license for an unlimited time. The licensed program product includes the TAE source code and one set of supporting documentation. Additional documentation may be purchased separately. Recommended minimum memory is 8 MB, and 60 MB are required in disk space to load the TAE+ TAR tape. This tape includes a public domain C++ compiler (GNU's C++). TAE+ was developed in 1989.

TAE+ is available in a form suitable for the following six different groups of computers: (1) DEC VAX station and other VMS VAX computers (specify TK50 or 9-track VMS Backup format), (2) Macintosh II computers running AUX [on 1/4-in. (6.35-mm) mini tape cartridge in Unix TAR format], (3) Apollo Domain Series 3000 [on 1/4-in. (6.35-mm) cartridge in TAR format], (4) DEC VAX and reduced-instruction-set-computer workstations running Ultrix (TK-50 in TAR format), (5) Sun 3- and 4-series workstations running Sun OS and IBM RT/PC and PS/2 computers running AIX [on 1/4-in. (6.35-mm) Sun cartridge in TAR format], and (6) HP 9000 Series-800 workstations (HP preformatted, 16-track cartridge tape in TAR format).

This program was developed by Jay Costenbader, Walt Moleski, Martha Szczur, and David Howell of **Goddard Space Flight Center**; *Norm Engelberg, Tin P. Li, Dharitri Misra, Philip Miller, Leif Neve, Karl Wolf, Ken Sall, Nick Ide, Ted Pang, Deborah Budacz, Donald Link, Ross Sugar, and Terry Bleser of Century Computing; Tom Seamster of Carlow Associates; Richard Gemoets of Appaloasa Systems; and Elfrieda Harris and Arleen Yeager of RMS. For further information, Circle 65 on the TSP Request Card. GSC-13275*

Another Program for Generating Interactive Graphics

The user can construct custom software interfaces.

The VAX/Ultrix version of the Transportable Applications Environment Plus (TAE+) computer program provides an integrated, portable software environment for developing and running interactive window, text, and graphical-object-based application software systems. The program enables a programmer or nonprogrammer to construct easily a custom software interface between a user and an application program and to move the resulting interface program and its application program to different computers. When used throughout a company for a wide range of applications, TAE+ makes both the application program and the computer seem transparent, with noticeable improvements in the learning curve.

The main components of TAE+ are (1)

the WorkBench, a "what you see is what you get" (WYSIWYG) software tool for the design and layout of a software interface between the user and the application program ("user interface," for short); (2) the WPT's (Window Programming Tools) software package, which is a set of callable subroutines that control the user interface; and (3) TAE Command Language (TCL), an easy-to-learn command language that provides an easy way to develop an executable prototype application program with a language that is interpreted at run time.

The WorkBench enables the person developing the application program to construct the layout of the display screen of the application program interactively by manipulating a set of interaction objects, including such input items as buttons, icons, and scrolling lists. Also included are such data-driven graphical objects as dials, thermometers, and strip charts, which TAE+ updates as the values of the data change. The user specifies the windows and interaction objects that will be included in the user interface, then specifies the sequence of the dialogue between the user interface and the user. The description of the user interface thus designed is then saved in resource files. For one who desires to develop the program that governs the user interface thus designed into an operational application program, the WorkBench software also generates source code (C, Ada, FORTRAN, and TCL), which fully controls the user interface through function calls to the WPT's.

The WPT's provide the services used at run time by application programs to display and control the user interfaces. Because the WPT's gain access to the WorkBench-generated resource files during each execution, such details as color, font, location, and object type remain independent from the application code, allowing changes to the user interface without recompiling and relinking.

In addition to WPT's, TAE+ offers control of interaction objects from the interpreted TAE Command Language. TCL provides an extremely powerful means for the more experienced developer to quickly prototype an application program's use of the interaction objects in TAE+ and to add programming logic without the overhead of compiling or linking.

TAE+ uses the MIT X-Window software system as the underlying windowing standard software. The WorkBench and WPT's are written in C++, and the remaining code is written in C. TAE+ is available by license for an unlimited time. The licensed program product includes the TAE source code and one set of supporting documentation. Additional documentation may be purchased separately. Recommended minimum memory is 8 MB, and 60 MB are required in disk space to load the TAE+ TAR tape. This tape includes a public domain C++ compiler (GNU'S C++). TAE+ was developed in 1989.

TAE+ is available in a form suitable for the following six different groups of computers: (1) DEC VAX station and other VMS VAX computers (specify TK50 or 9-track VMS Backup format), (2) Macintosh II computers running AUX [on 1/4-in. (6.35-mm) mini tape cartridge in Unix TAR format], (3) Apollo Domain Series 3000 [on 1/4-in. (6.35-mm) cartridge in TAR format], (4) DEC VAX and reduced-instruction-set-computer workstations running Ultrix (TK-50 in TAR format), (5) Sun 3- and 4-series workstations running Sun OS and IBM RT/PC's and PS/2 computers running AIX [on 1/4-in. (6.35-mm) Sun cartridge in TAR format], and (6) HP 9000 Series 800 workstations (HP preformatted, 16-track cartridge tape in TAR format).

This program was developed by Jay Costenbader, Walt Moleski, Martha Szczur, and David Howell of **Goddard Space Flight Center**; *Norm Engelberg, Tin P. Li, Dharitri Misra, Philip Miller, Leif Neve, Karl Wolf, Ken Sall, Nick Ide, Ted Pang, Deborah Budacz, Donald Link, Ross Sugar, and Terry Bleser of Century Computing; Tom Seamster of Carlow Associates; Richard Gemoets of Appaloasa Systems; and Elfrieda Harris and Arleen Yeager of RMS. For further information, Circle 81 on the TSP Request Card.*
GSC-13276

...ONE GIANT STEP FOR ENGINEERING

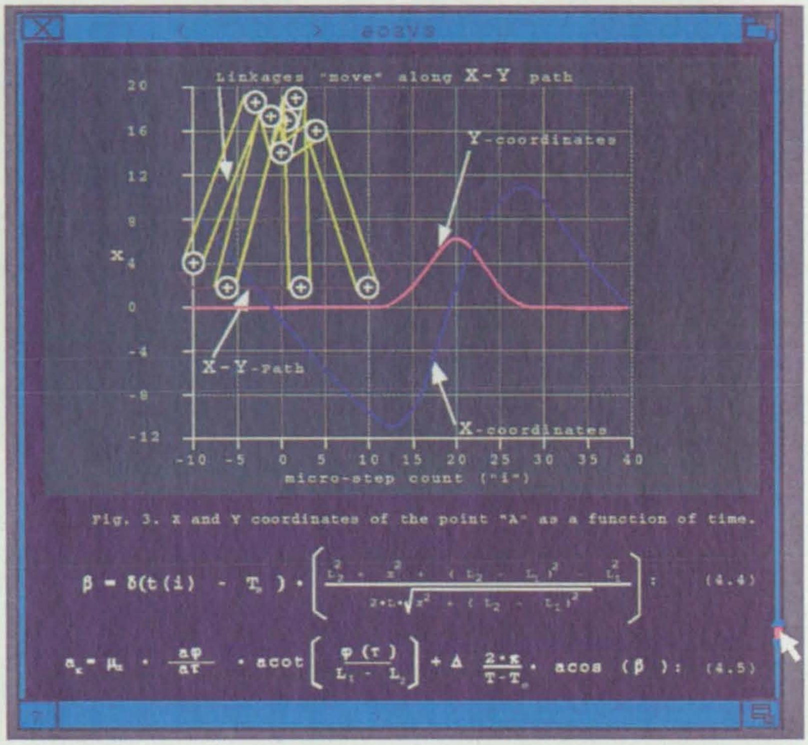

A revolutionary PC based software so advanced, it will change the way you solve day to day engineering problems.

POWERFUL COMBINATION UNDER "ONE ROOF"

EOSys is a new engineering language and application package...but EOSys is more...the combination of E-Language with its applications and utilities is synergistic. The result is a powerful combination of capabilities assembled in one easy to use package. Its integrated design uniquely combines vivid graphics, mathematical capabilities, full scope editor and recalculation capabilities by use of E-Language.

EASY TO LEARN AND USE

This powerful, easy to learn and use language is modeled after the human thought process. EOSys is based on English and math, so if you can read and write in English, you can understand and use EOSys.

ONE GIANT STEP FOR ENGINEERS AND SCIENTISTS

E-Language allows you to write applications and support many of your technical needs. With EOSys you don't have to be an expert programmer. The only thing required is creativity. The power and expressiveness of E-Language allows you to attack problems you would not have dreamed of solving with Computer Aided Engineering programs currently on the market.

ADVANCED COMPONENTS

EOSys is state of the art, featuring a windowing WYSIWYG environment, parametric modeling, on the fly reconfigurable keymap, mouse interface and on line help. Plus, EOSys provides important basic facilities such as natural user interface, 350 commonly used functions, and solving equations including the creation, editing, and solving of complex formulas and graphics. EOSys will print all analysis in presentation quality documents using regular laser printers.

Call us for a free EOSys interactive demo disk, available in 5-1/4 and 3-1/2 inch diskettes.
Dial 1-800-EOSys-21, that's 1-800-367-9721.
Available for IBM/AT™ and compatibles.
Thirty day unconditional money back guarantee.

1333 Blue Hills Avenue
Bloomfield, CT. 06002

Mechanics

Hardware, Techniques, and Processes

Books and Reports

Triangular Element for Analyzing Elasticity of Laminates

The element has properties that are desirable in the analysis of laminated composites.

Ames Research Center, Moffett Field, California

A flat triangular element has been developed for use in finite-element analyses of stress and strain in laminated plates made of such materials as plywood or advanced fiber/epoxy composite materials. The element may consist of any number of orthotropic layers, each layer having different material properties and angular orientation. The formulation includes coupling between bending and extension, which is essential for analysis of unsymmetric laminates. Shearing deflections are included because laminated and sandwich construction frequently results in shear stiffness much smaller than bending stiffness. The formulation of the element is straightforward, and the calculation of its stiffness matrix is simple and fast. A typical finite-element solution converges at about the same rate for thick or thin plates, regardless of the shape of the element. The element appears to be mathematically quite robust and capable of correctly modeling behavior of general, unsymmetric, sandwich, laminated composite shells. Convergence is slower than that of some other three-node elements that do not include shearing deflections.

The equations of the triangular element are derived in a local coordinate system with origin at the centroid of its middle layer. The nodes of the element are the corners of the triangle. The x axis is parallel to the edge between nodes 1 and 2, as shown in the figure. The z axis is perpendicular to the plane of the element. In the computer implementation of the element, properties of the material of a layer are defined with respect to a material coordinate axis, which may be oriented at an angle α measured from the x axis to the 1 axis of the material. The 3 axis of the material coincides with the z axis of the element.

Displacements in the x, y, and z directions are denoted by u, v, and w, respectively. The usual right-hand vector convention is used for directions of rotations, which are denoted by θ_x, θ_y, and θ_z. The rotations θ_x and θ_y are rotations of lines originally perpendicular to the middle surface of the undeformed element. The total

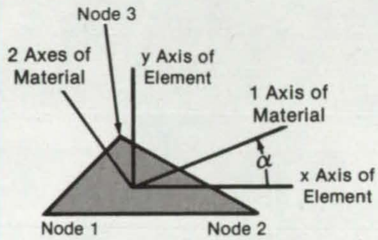

Note: The z axis of the element and the 3 axes of the material are perpendicular to the page.

COORDINATE SYSTEM

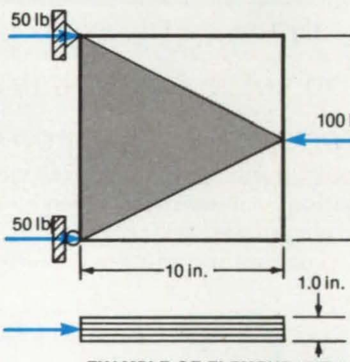

EXAMPLE OF ELEMENT WITH IN-PLANE LOADS

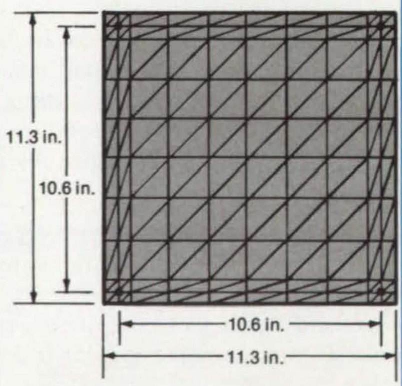

EXAMPLE OF FINITE-ELEMENT MESH USED TO CALCULATE STIFFNESS OF A LAMINATED COMPOSITE PLATE

The **Triangular Plate Element** has multiple layers, each of which can have different isotropic or orthotropic elastic properties. Many such elements are used in a finite-element mesh to calculate the stiffness of a plate.

deflection w is in the z direction and is further decomposed via

$$w = w' + w^*$$

where w' is the Kirchhoffian part of the deflection and w^* is the part due to out-of-plane shear. In this formulation, a straight line perpendicular to the middle surface before loading remains straight, but not perpendicular to the deformed middle surface, after loading. The slopes of the middle surface are $w_{,x}$ and $w_{,y}$, whereas the slopes of the line that was originally perpendicular to the middle surface become

$$-\theta_y = w_{,x} - w^*_{,x} \text{ and } \theta_x = w_{,y} - w^*_{,y}$$

and

$$\theta_x = -v_{,z} \text{ and } \theta_y = u_{,z}.$$

The strains in the element are related to nodal displacements, e.g.,

$$\bar{u} = \begin{bmatrix} u_1 \\ u_2 \\ u_3 \end{bmatrix}$$

where the subscripts denote the nodes and the same convention is used to represent the other components of nodal displacement. The displacements u, v, θ_x, θ_y, and w^* in the interior of the element are each interpolated from their nodal values by the same linear function. The result is that the strains ϵ_o on the middle surface are

$$\epsilon_o = \frac{1}{2A}[MN]\begin{bmatrix} \bar{u} \\ \bar{v} \end{bmatrix}$$

and the curvatures X are given by

$$X = \frac{1}{2A}[N-M]\begin{bmatrix} \bar{\theta}_x \\ \bar{\theta}_y \end{bmatrix}$$

where

$$N = \begin{bmatrix} 0 & 0 & 0 \\ x_3-x_2 & x_1-x_3 & x_2-x_1 \\ y_2-y_3 & y_3-y_1 & y_1-y_2 \end{bmatrix}$$

$$M = \begin{bmatrix} y_2-y_3 & y_3-y_1 & y_1-y_2 \\ 0 & 0 & 0 \\ x_3-x_2 & x_1-x_3 & x_2-x_1 \end{bmatrix}$$

and A is the area of the element. The out-of-plane shear strain γ is given by

$$\gamma = \begin{bmatrix} \gamma_{xz} \\ \gamma_{yz} \end{bmatrix} = \frac{1}{4A}\left(\begin{bmatrix} y_2-y_3 & y_3-y_1 & y_1-y_2 \\ x_3-x_2 & x_1-x_3 & x_2-x_1 \end{bmatrix}\right.$$

$$\begin{bmatrix} 1 & 0 & 0 & -y_1 & 0 & 0 & x_1 & 0 & 0 \\ 0 & 1 & 0 & 0 & -y_2 & 0 & 0 & x_2 & 0 \\ 0 & 0 & 1 & 0 & 0 & -y_3 & 0 & 0 & x_3 \end{bmatrix} +$$

$$\left.\begin{bmatrix} y_2-y_3 & y_3-y_1 & y_1-y_2 & 0 & 0 & 0 & \frac{2A}{3} & \frac{2A}{3} & \frac{2A}{3} \\ x_3-x_2 & x_1-x_3 & x_2-x_1 & \frac{-2A}{3} & \frac{-2A}{3} & \frac{-2A}{3} & 0 & 0 & 0 \end{bmatrix}\right)$$

$$\begin{bmatrix} \bar{w} \\ \bar{\theta}_x \\ \bar{\theta}_y \end{bmatrix}$$

or

$$\gamma = \frac{1}{4A}[H]\begin{bmatrix} \bar{w} \\ \bar{\theta}_y \\ \bar{\theta}_y \end{bmatrix}$$

In the computer implementation of this element, the matrices that relate strains to nodal displacements are calculated from the aforementioned algebraic expressions. The remaining calculations are performed numerically, layer by layer. The strain-energy integrals are processed to yield the corresponding submatrix of the stiffness matrix of the element, and the results are added into the proper location in the stiffness matrix of the element. The program then goes on to process the next layer, and so forth, until all the layers of the element have been processed and the stiffness matrix of the element is complete.

This work was done by C. Wayne Martin, S. F. Lung, and K. K. Gupta of **Ames Research Center**. *Further information may be found in NASA TM-4125 [N89-27213], "A Three-Node C° Element for Analysis of Laminated Composite Sandwich Shells."*

Copies may be purchased [prepayment required] from the National Technical Information Service, Springfield, Virginia 22161, Telephone No. (703) 487-4650. Rush orders may be placed for an extra fee by calling (800) 336-4700.
ARC-12534

Lightweight Memory-Metal Pin Puller

The device is adaptable to cryogenic and vacuum environments.

NASA's Jet Propulsion Laboratory, Pasadena, California

A memory-metal pin puller designed for use in the aperture-cover mechanism of a camera aboard a spacecraft could be adapted to small-volume instrument environments that must be kept free of contamination. Small and light in weight, the device uses relatively simple electronic drive circuitry that consists of a timed source of current.

The pin puller (see figure) includes a freely sliding pin that engages a slot in a mating part. A compression spring presses against a spring retainer that pushes the pin, preloading the pin into the slot. Looping through passages in the pin are two memory-metal wires that occupy orthogonal planes. Shims can be used to adjust the tension in each wire, to set the extension of the pin, and to adjust the preload of the compression spring. In operation, when the memory-metal wires are heated by electrical current, they contract, pulling the pin. When the current is turned off, the wires cool and relax to their original length. In repeated tests, the wire pulled against a 5-lb (22-N) load.

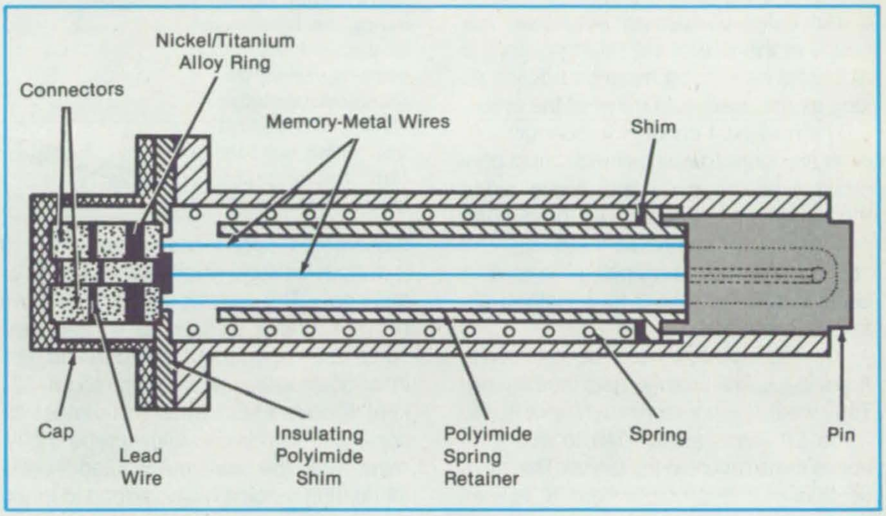

The **Lightweight Pin Puller** includes memory-metal wires that pull the pin when heated.

Special beryllium/copper connectors provide for the electrical contact and mechanical retention of the memory-metal wire. Each such connector consists of a beryllium copper socket that is slit, forming tangs that are bent outward. A nickel/titanium-alloy ring, which is expanded by the tangs when cooled and shrinks as it warms, is used to squeeze the tangs to grip one end of a memory-metal wire. During assembly, the connector is dipped into liquid nitrogen, and the wire is slipped into the connector; then, as the connector warms up to room temperature, the wire is squeezed and retained.

Because the failure modes of the device are benign — the wire might break or anneal but would still be captured — the device does not pose a risk of contamination of its environment. The pin puller can be adapted to operate at cryogenic temperatures and in vacuum as well as in a normal-temperature environment, and it can be cycled a large number of times without degradation of performance.

This work was done by Virginia G. Ford and Michael R. Johnson of Caltech and A. David Johnson of TiNi Alloy Co. for **NASA's Jet Propulsion Laboratory**. *For further information, Circle 100 on the TSP Request Card.*
NPO-18131

Stress Stiffening of STARDYNE Plate Elements

A FORTRAN program calculates additions to a stiffness matrix.

Marshall Space Flight Center, Alabama

A computer program modifies the STARDYNE general-purpose finite-element stress-and-dynamics computer code by providing for the calculation of stress stiffening. STARDYNE, which has been used to analyze the dynamics of the Space Shuttle main engine, can be used to perform analyses of a linear nature but has no capability to account for stress stiffening.

The stress-stiffening program, written in the FORTRAN language, calculates the geometric stiffness matrix, which is the stiffness matrix that results from a stressed condition. Then the program creates a file that can be appended to the STARDYNE bulk data deck that contains entries that are to be added to the STARDYNE stiffness matrix. The format of this file is compatible with STARDYNE.

This work was done by Dennis C. Philpot of Rockwell International Corp. for **Marshall Space Flight Center**. *For further information, Circle 111 on the TSP Request Card.* *MFS-29738*

Penetrable Linear-Gap Pressure Seal

Lips would accommodate the movement of a penetrating object.

Lewis Research Center, Cleveland, Ohio

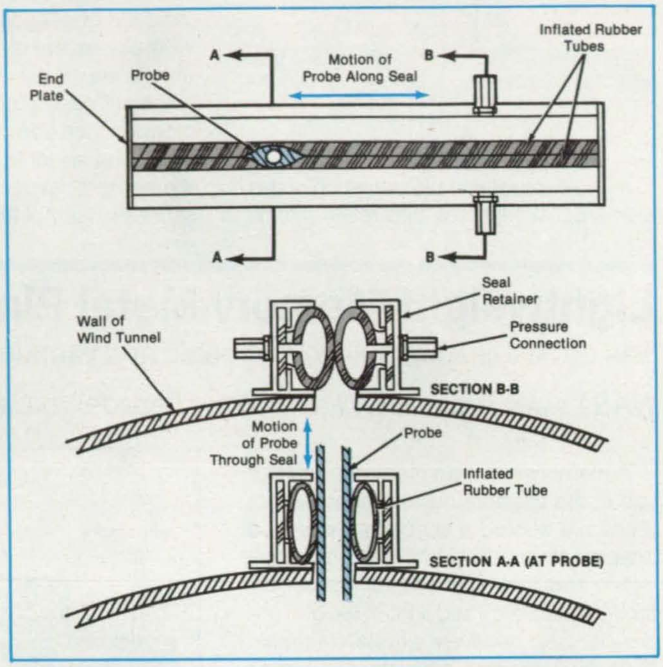

The **Probe Would Move Longitudinally and Transversely** between opposing tubes of a pressure seal. The probe would be shaped like a double teardrop in cross section to enhance the tightness of the seal. As the sectional views show, the pressurized tubes would press against each other but conform to the probe where it intrudes.

A pair of opposed inflatable rubber tubes would allow an object to be moved between them while maintaining a pressure seal. The seal was conceived for a pressurized wind tunnel into which sensor probes are to be inserted and positioned from outside. With the proposed seal, a probe could be moved along the seal gap, pushed inward, and/or pulled outward while different pressures are maintained inside and outside the tunnel.

The proposed seal would replace a bulky sealing unit that includes a bottom face seal and a top sliding plate and that requires bulky positioning actuators. Because of the size of the sliding plate, the actuators have to be more than twice as long as the maximum travel of the probe.

The new seal concept is adaptable to other situations in which objects must penetrate pressure walls and move along them. It should work as well for vacuum chambers and for pressure vessels. The concept may also be applicable to dust seals that do not have to withstand differential pressures.

The sealing tubes would be mounted in a slot in a liplike arrangement (see figure). They would be pressurized individually to 20 to 30 lb/in.^{2} (about 140 to 200 kPa) above the pressure in the tunnel. The cross section of the probe, where it passes through the seal, would be shaped with a gradual transition so that the sealing tubes could deform easily to conform to it without leakage, whether it is moving or stationary. The prototype seal has shown no measurable leakage at vessel pressures of 30 psig (about 329 kPa) and seal inflation pressure of 50 psig (about 467 kPa). Frequent lubrication is of utmost importance, however, to allow probe movement while the seals are inflated. A self-lubricating system will be added to bleed silicone grease out of the probe teardrop segment.

This work was done by Paul Trimarchi of ***Lewis Research Center****. For further information, Circle 9 on the TSP Request Card.*

This invention is owned by NASA, and a patent application has been filed. Inquiries concerning nonexclusive or exclusive license for its commercial development should be addressed to the Patent Counsel, Lewis Research Center [see page 14]. Refer to LEW-14965.

Streamwise Algorithm for Simulation of Flow

Applications include analyses of flutter of wings.

Ames Research Center, Moffett Field, California

An algorithm for the numerical solution of the Euler and Navier–Stokes equations of unsteady flow incorporates upwind differencing based on the streamwise direction. The algorithm has been generalized to calculate unsteady transonic flows over wings; as such, it is suitable for analyses of flutter of wings affected by such flows.

The algorithm is derived from the thin-layer, Reynolds-averaged Navier–Stokes equations in curvilinear coordinates. The coordinate system is rotated locally to align one of its axes with the streamwise direction. For differencing, in the streamwise direction, of the terms that represent convection, there is devised a form of flux-vector splitting in which the local flux-vector bias is switched between a subsonic and a supersonic value, depending on whether the local mach number is less than or greater than 1, respectively. The new flux splitting takes advantage of the fact that there is no flow in the local plane perpendicular to the streamwise direction. The formulas for differencing in this rotated coordinate system are transformed back to the original coordinate grid, where the numerical calculations are performed.

The use of the locally rotated coordinate system in this formulation allows the bias of the convective-flux vectors to depend on the total mach number. This confers the advantage that the flux-vector bias is switched as the flow crosses a shock wave or a sonic surface, and the proper domain of dependence is used in regions of supersonic flow. In comparison, many other upwind-differencing algorithms involve switching based on components of mach-number vectors along coordinate lines; such switching criteria allow downstream phenomena to influence flows unrealistically at upstream locations in supersonic flows and allow unrealistic switching up-

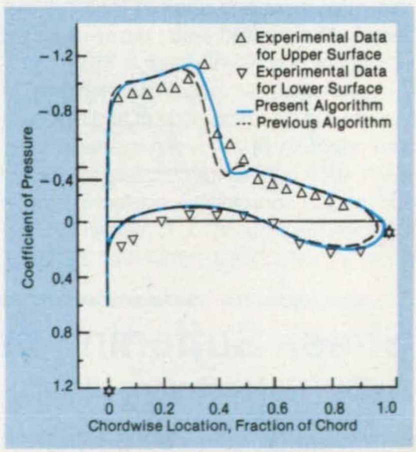

The **Pressure as a Function of Position** on the upper and lower surface of a wing with a small region of separated flow was calculated by the present and previous algorithms and measured in an experiment. The locations of the shock and the suction peak along a span station in the region of separated flow as computed by the present algorithm agree slightly more closely with the experimental data.

stream of shock waves and downstream of sonic surfaces in multidirectional flows. Another advantage of the new algorithm is that the formulas for the differencing of the convective-flux vectors do not contain any parameters that have to be specified by the user. Consequently, the amount of numerical dissipation is determined automatically.

The present algorithm has been used to compute unsteady and steady flows at mach 0.85 over an airfoil. Also, computations using this algorithm were found to agree slightly better with measurements of the flow and also to give fuller boundary layer profiles than did the results of a computation with a previous algorithm that incorporated central differencing and fourth-order numerical dissipation (see figure), for steady flow over a wing with a small region of separation.

This work was done by Peter M. Goorjian of **Ames Research Center**. *Further information may be found in NASA TM-101019 [N88-29751], "A Streamwise Upwind Algorithm for the Euler and Navier–Stokes Equations Applied to Transonic Flows."*

Copies may be purchased [prepayment required] from the National Technical Information Service, Springfield, Virginia 22161, Telephone No. (703) 487-4650. Rush orders may be placed for an extra fee by calling (800) 336-4700.
ARC-12718

Placing Control Surfaces To Suppress Aeroelastic Flutter

Control should be exerted where the transfer of energy is maximum.

Ames Research Center, Moffett Field, California

A method for assigning the positions of control surfaces to suppress aeroelastic flutter involves analysis of the transfer of energy. The method neither depends on nor prescribes the specific form of the control law. Rather, assuming that a suitable control law is available by whatever means, the method shows how to determine where on an aircraft or airfoil the control surface(s) would be maximally effective in suppressing flutter.

The figure illustrates the application of the method to determine the spanwise location of trailing-edge control surfaces on a swept wing. The surface of the wing is divided into boxes arranged in strips along its span. Using each strip as an element, a finite-element modal aeroelasticity analysis is performed. The best spanwise position of an active control surface is then found by the following steps:

1. Determine the flutter dynamic pressure Q_F of the system.
2. Increase Q_F to bring it within the unstable region, and obtain the eigenvector of the unstable mode.
3. Compute the aerodynamical matrices for all the strips, at the reduced frequency appropriate for the unstable mode.
4. Since the fluttering wing is unstable, the work W_A done by the wing on the environment during one cycle should assume a negative value. Compute the energy ratios $\overline{W}^r_A = W^r_A / W_A$ and the specific energy ratios $\overline{\overline{W}}{}^r_A = W^r_A / s_r$, where W^r_A denotes the work done by the rth strip on the environment during one cycle and s_r denotes the span of boxes at the rth strip. Negative values of $\overline{W}^r_A$ and $\overline{\overline{W}}{}^r_A$ indicate that the rth strip is absorbing energy from its surroundings (and thus contributing towards instability).
5. Determine the location of the strip $r = r_0$ where $\overline{\overline{W}}{}^r_A$ assumes the largest negative value. This strip absorbs most energy per unit span and, therefore, would be the location where an active control surface would be most effective in suppressing flutter.

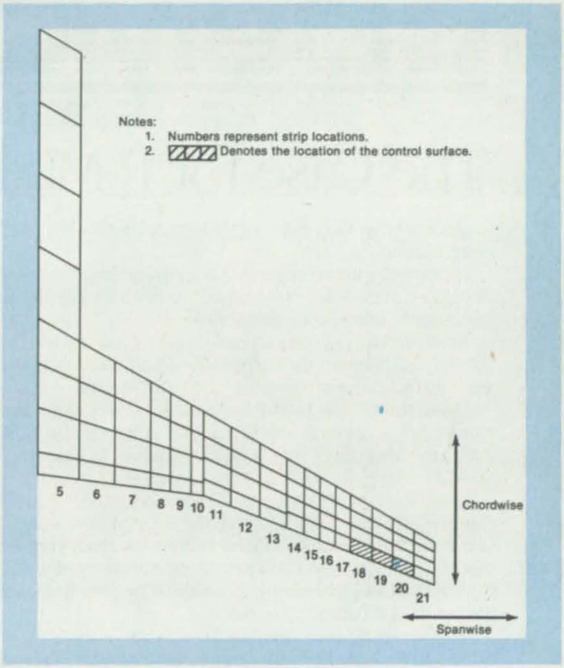

Half of the Fuselage and One Wing are represented in a simplified finite-element model. The wing is divided along its span into strips, each of which is divided further along the chordwise direction into boxes. An aeroelasticity analysis is performed to find the strips in which the maximum amount of energy is locally transferred from the flow of air into flutter of the wing. The control surface is placed there to suppress flutter.

In a case in which more than one critical flutter mode exists, this procedure can be repeated for each flutter mode, and the optimum locations of the control surfaces can be determined. If a compromise single location for one control surface cannot be found, then a multiplicity of active control surfaces should be seriously considered.

This work was done by E. Nissim and John J. Burken of **Ames Research Center**. *Further information may be found in NASA TP-2873 [N89-16196], "Control Surface Spanwise Placement in Active Flutter Suppression Systems."*

Copies may be purchased [prepayment required] from the National Technical Information Service, Springfield, Virginia 22161, Telephone No. (703)487-4650. Rush orders may be placed for an extra fee by calling (800) 336-4700. *ARC-12411*

Computing the No-Escape Envelope of a Short-Range Missile

Strategies for attack or avoidance can be evaluated.

Ames Research Center, Moffett Field, California

A method for computing the no-escape envelope of a short-range air-to-air missile has been devised. The "no-escape envelope" is the range of initial conditions (e.g., positions and velocities of the attacking and attacked aircraft at the moment the missile is fired) within which the missile will strike the attacked aircraft, no matter what evasive maneuvers it performs. The method is useful for the analysis of both strategies for avoidance and strategies for attack. With modifications, the method may also be useful in the analysis of control strategies for one-on-one air-to-air combat, or wherever multiple control strategies are considered.

The first step of the method is to select realistic mathematical models to simulate the combat—including models for the motor, control laws, and failure modes of the missile and models for the thrust and drag characteristics, maneuvering capabilities, and acceleration limits of the attacking and attacked aircraft. The next step is to find candidate control laws or strategies for the avoidance of missiles. This can be done, for example, by asking pilots about the missile-avoiding techniques they use and/or by solving simplified optimal-control problems.

Another important step is the selection of the space of initial conditions over which the problem is to be solved. The space must be discretized. The discrete step sizes must be small and numerous enough to enable determination of the regions within which various control laws or strategies are effective, but not so small and numerous that the computational load becomes excessive. For example, in the test case (two F-15 airplanes and a "fire-and-forget" missile), the discretized variables were all combinations of three initial speeds for each aircraft at the moment of firing (from mach 0.48 to mach 0.98), two initial track angles at 15° intervals, and the initial range at 1,000-ft (305-m) intervals up to the maximum effective range of the missile.

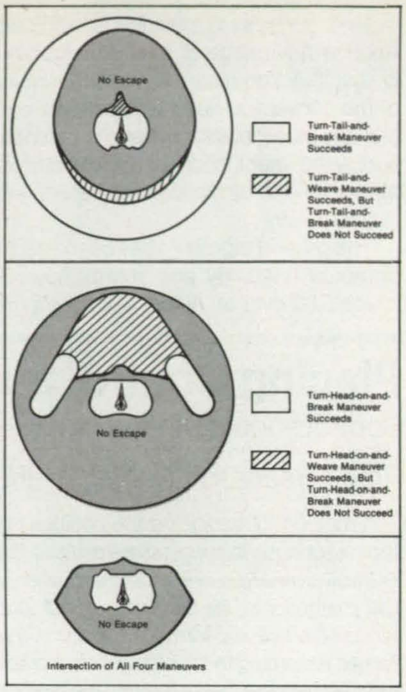

These **No-Escape Envelopes** show positions, with respect to a target airplane, from which a missile can be launched and various maneuvers will succeed or fail in avoiding the missile.

For each suggested control law and each initial condition, the system is simulated to optimize the control parameters. For the missile-avoidance problem, four separate control laws were identified: turning toward the missile (turn head-on) or turning away from the missile (turn-tail) followed by either a single sharp bank maneuver (break-turn) at the appropriate time or a series of bank reversals (weave-maneuver). The parameters optimized in each case included the ranges to the missile at which the transient maneuver should be initiated, and, in the case of the weave-maneuver, also the rates at which the weaves should occur. Once the data are obtained from the simulation, they are stored in tabular form for the best control strategy and the corresponding best control parameters as functions of initial conditions.

The data are then plotted in various ways to gain insight into the problem. For example, this includes plotting the range of missile-launching positions centered on the target aircraft (see figure). The data are used to make decisions about the choice of control law — first in a simulation, then in the fully implemented system. For the missile-avoidance problem, the data are used in two ways: First, they are used by the attacking aircraft, assuming that the attacked aircraft is aware of the attacker, to determine whether the missile should be launched. (If the attacked aircraft is not aware of the attacker, a much larger kinematic launch envelope can be used.) Second, the data are used by the target aircraft to determine the optimal avoidance maneuver. This requires interpolation of data for the selection of control laws and the optimal parameters of those laws.

This work was done by Frank Neuman of **Ames Research Center**. *For further information, Circle 3 on the TSP Request Card.*
ARC-12404

Push-to-Lock, Push-to-Release Mechanism

A single movement of one hand locks or unlocks a latch.

Lyndon B. Johnson Space Center, Houston, Texas

A latch can be locked or unlocked with a single motion of the hand. No tools are needed to operate it, and a user can easily open or close it with a heavily glooved hand. A pushbutton in the mechanism rests flush with the surface of a plate when it is locked and projects when it is unlocked so that its state is obvious.

To lock the latch, the user presses the projecting pushbutton cap (see figure). This action drives the stem on which the pushbutton is mounted into the body, where dowel pins engage a groove in the stem. A helical retaining spring and guide ring hold the pins in the groove, thereby locking the pushbutton to the main body.

To unlock the latch, the user presses the pushbutton, which is now flat against the surrounding round plate (which is, in effect, a larger pushbutton). This action drives the ring surrounding the stem against the sleeve in the main body. The sleeve forces the guide ring against the retaining spring, compressing it and releasing the dowel pins from the groove. A helical ejection spring, which had been compressed by the pushbutton stem in the locked position, expands and forces the stem away from the main body. The latch is now unlocked.

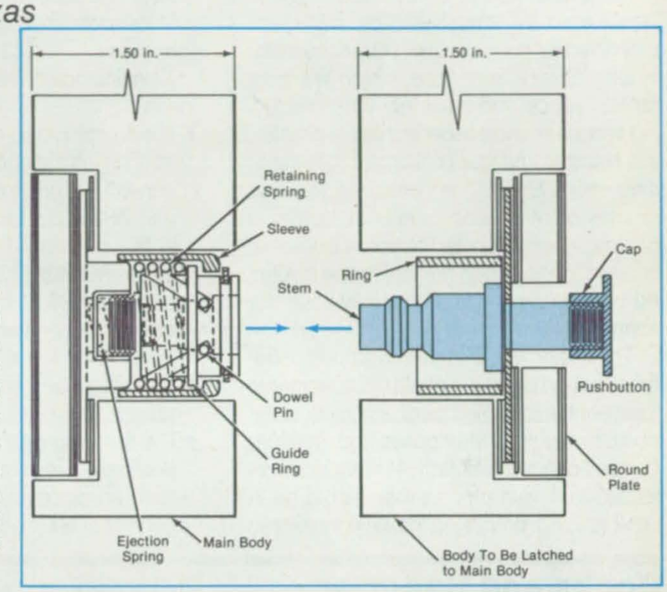

When the Latch is Unlocked, the stem is free of the main body. In the locked state, indicated by dashed lines, dowel pins in the main body hold the stem. The latch can be equipped with a lock and key so that only authorized users can operate it.

This work was done by Anselmo Lozano, Jr., of Rockwell International Corp. for **Johnson Space Center**. *For further information, Circle 18 on the TSP Request Card.*
MSC-21520

Test Adapter for Infrared Detectors

A fixture mounts the detector on a cryogenic finger for testing the optical and electrical characteristics.

Ames Research Center, Moffett Field, California

A convenient fixture for testing infrared-detector integrated circuits includes the electrical connections for the 42-pin dual-in-line package (DIP), thermal connection to a cryogenic probe, and an optical filter. Using the fixture, the electrical and optical properties of the detector can be measured at 4 K.

As the figure shows, the cold finger is a block of copper with a heavy screw connection for thermal coupling to the cryogenic probe. Strip connectors for the pins of the DIP are fastened to the sides of the copper block, with a sapphire slab in between them to give good thermal transfer and electrical isolation. A hole is drilled into the copper underneath the sapphire to allow the installation of a thermistor for temperature measurement.

When the detector package has been plugged into the connectors on the cold finger, an opaque cover (the radiation shield) is screwed down over it. A hole in the center of the cover holds a filter that passes only the 3.39-micron laser light for optical testing.

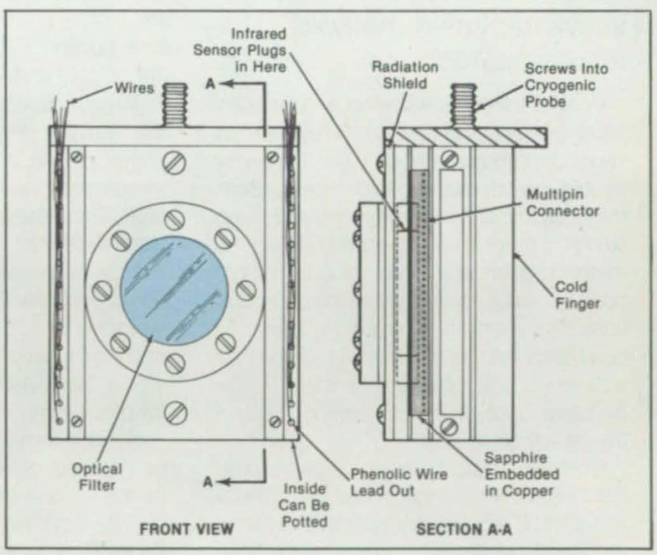

This **Test Fixture** is convenient for testing the electrical and optical characteristics of solid-state infrared detectors, such as those used in surveying sensors, optical communications, receivers, optical power meters, and noncontacting thermometers.

The connector pins are on 50-mil (1.27-mm) centers, so packages with pins on 50-, 100-, or 150-mil (1.27-, 2.54-, or 3.81-mm) centers can be accommodated. The cryogenic application and the low background radiation occurring at the test wavelength make this unit ideal for spot scanning and detector characterization.

This work was done by Albert G. Campbell and A. L. Gable of Rockwell International Corp. for **Ames Research Center**. *No further documentation is available.*
ARC-11389

Damping of Vibrations in Graphite/Epoxy Structures

Outgassing in vacuum decreases damping effects hardly at all.

Marshall Space Flight Center, Alabama

A report describes a study of the vibration-damping properties, in air and vacuum, of graphite/epoxy composite structural members joined by adhesives. The study was prompted by concern over vibrations in the Hubble Space Telescope, which will peer far into space and back into time, producing images of unprecedented clarity of galaxies, planets, and stars billions of light-years away from Earth. The telescope requires precise pointing, and its optical system is held together by a graphite/epoxy truss with bonded joints. When the telescope is rotated, vibrations in the truss and joints can blur images.

The study was conducted to determine the vibration-damping effects of specimens representative of members and joints of the truss, particularly after gases and moisture trapped during manufacture have been released in a vacuum, as they would be in outer space. Damping ratios were measured under free and forced vibrations and before and after outgassing in a vacuum. The effects of end-support conditions and high and low temperatures on damping were also measured.

The findings of the study include the following:
- The damping ratio of a specimen depends strongly on the end-support conditions. In general, the end fixtures contribute a large part of the damping.
- In the particular tube specimens tested (outer diameter 6.17 cm, wall thickness 0.16 cm, length 95.5 cm), the damping ratio increased with frequency, ranging from about 0.1 percent at 500 Hz to 0.36 percent at 2,840 Hz under normal Earth atmosphere.
- The damping ratio of the tube specimens decreased after prolonged exposure to vacuum, dropping to 0.06 percent and 0.11 percent at 500 and 2,840 Hz, respectively.
- The removal of the atmosphere accounts for most of the decrease in the damping ratio. Outgassing and the desorption of moisture seemed to affect the damping ratio by only about 0.016 percent.
- The damping ratio increased with temperature, rising to about 3 percent near the glass-transition temperature of the material. There was also a small decrease in the damping ratio below the normal atmospheric temperature.
- Bonded joints did not increase the damping ratio significantly.

This work was done by Malcolm J. Crocker, Mohan D. Rao, P. K. Raju, and Xinche Yan of Auburn University for **Marshall Space Flight Center**. *To obtain a copy of the report, "Measurement of Damping of Graphite Epoxy Materials & Structural Joints," Circle 82 on the TSP Request Card.*
MFS-27228

Books and Reports

These reports, studies, handbooks are available from NASA as Technical Support Packages (TSP's) when a Request Card number is cited; otherwise they are available from the National Technical Information Service.

High-Resolution Numerical Simulation of Shock Waves

Upwind and symmetric shock-capturing methods are compared.

A NASA technical memorandum compares the results of upwind and symmetric shock-capturing methods in the numerical simulation of gas-dynamic flows. Both methods find shocks as sharp variations in fluid properties over a few grid points. The methods differ in the type of artificial viscosity introduced to stabilize the computations. The symmetric method is shown to be as accurate as the upwind method, but with fewer and simpler time steps in the transient case or fewer iteration steps in the steady-state case.

The symmetric method is a generalization of a previous implicit total-variation-diminishing (TVD) scheme for the simulation of two-dimensional compressible flow based on the Euler equations. Starting with a one-dimensional system of hyperbolic conservation laws, the author describes the extension of the TVD scheme to two dimensions. Various "limiter" functions (artificial viscosity) are listed. Steady-state solutions are independent of the time steps.

Numerical simulations were performed for one-dimensional shock-tube problems and for two-dimensional problems involving either of two standard airfoils. In problems containing shocks only, the implicit symmetric TVD schemes proved as accurate as an implicit upwind TVD scheme that had previously been modified by the author, even though it required less computational effort. In problems that contained both shocks and contact discontinuities, the explicit symmetric TVD schemes are slightly more diffusive than is the explicit upwind TVD scheme, especially at the contact surfaces.

Various steady-state airfoil calculations indicate the degree of sensitivity to the shape of the coordinate grid, the free-stream mach number, and the angle of attack. The effects of boundary conditions were also noted — proper boundary conditions are essential to the numerical simulation of fluid flow. The improper treatment of boundary conditions can lead to instability and inaccuracy, even if one starts with a stable, high-resolution scheme designed for problems with shocks. For certain flow regimes, alternative linearization or relaxation procedures may improve the convergence rates of steady-state calculations.

This work was done by H. C. Yee of **Ames Research Center**. *Further information may be found in NASA TM-88325, [N88-12332], "Numerical Experiments with a Symmetric High-Resolution Shock-Capturing Scheme."*

Copies may be purchased [prepayment required] from the National Technical Information Service, Springfield, Virginia 22161, Telephone No. (703) 487-4650. Rush orders may be placed for an additional fee by calling (800) 336-4700.
ARC-11730

Overview of Methods for Computation of Shocks

A unified and generalized formulation for one class of methods is presented.

A NASA technical memorandum provides a systematic overview of a class of conservative finite-difference shock-capturing numerical-integration methods for the solution of hyperbolic conservation laws. More specifically, the document (1) presents a unified and generalized formulation of the total-variation-diminishing class of high-resolution (with respect to space), explicit and implicit (with respect to time) numerical-integration methods that capture the essential features of shocks, and (2) illustrates the versatility of these methods in the numerical simulation of various steady and unsteady, complicated shock waves in perfect gases, equilibrium real gas, and nonequilibrium flows. One of the purposes of this formulation and overview is to facilitate the development of an efficient computer code in which the various methods can be included as separate modules that share many common operations and that can be called upon as needed.

First, the basic properties of hyperbolic partial differential equations and several schemes for the solution of linear hyperbolic partial differential equations are reviewed.

Then attention is focused upon the various aspects of shock-capturing schemes for the solution of nonlinear scalar hyperbolic partial differential equations based on conservation laws. Topics include monotone and first-order, explicit, upwind schemes; the deficiency of classical shock-capturing schemes; and methods of extending first-order total-variation-diminishing schemes to higher spatial orders. Some issues concerning the applicability of these schemes, which were designed for use with homogeneous hyperbolic conservation laws, to problems that include stiff source terms and shock waves are also discussed: It is important to investigate finite-difference methods for nonhomogeneous hyperbolic partial differential equations (those that contain source terms) because the equations that describe nonequilibrium flows (e.g., hypersonic and combustion flows) include coupled stiff source terms.

The performances of some of these schemes are illustrated by numerical examples that involve the dynamics of one-, two-, and three-dimensional flows of gases. The use of the Lax–Friedrichs numerical-flux method to obtain high-resolution shock-capturing schemes is generalized. Because this method can be extended to systems of nonlinear equations without the use of Riemann solvers or flux-vector-splitting approaches, it saves much time in computations of multimensional flows of real gases in thermodynamic equilibrium and nonequilibrium.

There is a discussion of the uniqueness, stability, and accuracy of finite-difference methods via the nonlinear dynamic approach equations — particularly nonhomogeneous hyperbolic partial differential equations that contain nonlinear source terms. The purpose of this discussion is to impress computational fluid dynamicists with the importance of the "nonlinear dynamic approach."

Formal extensions of nonlinear total-variation-diminishing schemes to systems of nonlinear hyperbolic conservation laws for multidimensional flows are reviewed. The generalization of these schemes to include steady and unsteady hypersonic flows of real gases in thermodynamic equilibrium and nonequilibrium are described. Examples of time-accurate and steady-state calculations of one-, two-, and three-dimensional flows are presented.

This work was done by H. C. Yee of **Ames Research Center**. *Further information may be found in NASA TM-101088 [N89-25652], "A Class of High-Resolution Explicit and Implicit Shock-Capturing Methods."*

Copies may be purchased [prepayment required] from the National Technical Information Service, Springfield, Virginia 22161, Telephone No. (703) 487-4650. Rush orders may be placed for an extra fee by calling (800) 336-4700. ARC-12667

Entropy-Based Approach to Nonlinear Stability

The second law of thermodynamics can suppress numerical oscillations in solutions to equations of flow.

A NASA technical memorandum suggests that schemes for the numerical solution of differential equations of flow can be made more accurate and robust by invoking the second law of thermodynamics. More specifically, the author proposes that instead of using artifical viscosity to suppress such unphysical solutions as spurious numerical oscillations and nonlinear instabilities, one should formulate the equations so that the rate of production of entropy within each cell of a computational grid be nonnegative, as required by the second law. The author conjectures that this approach may be necessary and sufficient to exclude unphysical solutions.

The first chapter introduces the general subject, beginning with remarks on the importance of nonlinear stability in computational fluid dynamics. The oscillations and nonlinear instabilities that have persisted since early work in this field are discussed, and a tentative connection between these unphysical phenomena and numerical decreases in entropy is established.

The second chapter makes the connection more explicit. It includes physical and mathematical descriptions of entropy and describes a relationship between physical and mathematical entropy. It shows some important properties of partial differential equations (PDE's) that come from conservation laws. The concept of nonlinear stability is introduced and these properties are exploited to show that solutions of scalar hyperbolic equations in multiple dimensions are bounded for all time. At this point, it is shown that the total entropy within a domain is bounded, and it is conjectured that if the entropy is bounded, the solution must also be bounded within a certain norm.

In the third chapter, the nonlinear-stability property of the PDE is extended to the semidiscrete (discrete in space but continuous in time) difference equations. The semidiscrete analog of the second law is derived. It is shown that the conjecture of the previous chapter is not affected by the semidiscrete approximation. The author explores ways to construct semidiscrete space-differencing schemes that satisfy the cell-entropy inequality. Such schemes can be constructed with accuracy to at least second order.

The fourth chapter discusses the effects of time-advancing schemes on the rates of production of entropy. The nonlinear-stability property of the PDE is extended to the fully discrete difference equations. It is shown that satisfying a semidiscrete cell-entropy inequality is sufficient to satisfy a fully discrete one, provided that implicit Euler time advance is used. A modified Crank-Nicolson time advance for scalar equations also has this property.

The next three chapters give examples of problems that increase in complexity up to the quasi-one-dimensional Euler equations. These include linear scalar equations in chapter 5, nonlinear scalar equations in chapter 6, and dynamics of one-dimensional flows of gas in chapter 7.

Chapter 8 reviews the basic concept of total-variation-diminishing (TVD) schemes. Where applicable, it explores the connections between the TVD approach and the new cell-entropy-inequality approach. Chapter 9 shows how the new approach relates to flux-splitting and to other previous schemes. Chapter 10 presents an outline of future research. Chapter 11 is a summary.

This work was done by Marshal L. Merriam of **Ames Research Center**. *Further information may be found in NASA TM-101086 [N90-17376], "An Entropy-Based Approach to Nonlinear Stability."*

Copies may be purchased [prepayment required] from the National Technical Information Service, Springfield, Virginia 22161, Telephone No. (703) 487-4650. Rush orders may be placed for an extra fee by calling (800) 336-4700.
ARC-12435

Machinery

Hardware, Techniques, and Processes

Probabilistic/Fracture-Mechanics Model for Service Life

Techniques of statistics, fracture mechanics, and other disciplines are combined into a cohesive mathematical model.

Marshall Space Flight Center, Alabama

A computer program makes probabilistic estimates of the lifetime of an engine and components thereof. Although the program is written specifically for the Space Shuttle main engine, the underlying concept may be applicable to other systems in which fractures of stressed parts can result in catastrophic failures. It can facilitate engineering tradeoff studies to optimize between service life and risk more accurately than can be done by conventional (nonprobabilistic) techniques.

Heretofore, fracture-mechanics analyses of critical components have sometimes yielded underestimates of lifetimes when they were based on worst-case values of parameters subject to statistical variations. The probability of occurrence for any individual worst-case condition is very low, while that of a combination of worst-case conditions is infinitesimal. Designs based on these underestimated lifetimes can result in inefficient uses of materials and/or excessive weights of components, with consequent reductions in payload capacities and increased costs of operation. At the other extreme, lifetimes can be overestimated assuming greater material/structural capabilities and/or less-severe operating conditions.

The probabilistic fracture-mechanics model and program were developed to fill the need for a more accurate life-assessment technique that will avoid errors in estimated lives and provide for the statistical assessment of the levels of risk created by engineering decisions in designing a system. The program implements a mathematical model that combines techniques of statistics, fatigue, fracture mechanics, nondestructive analysis, life-cycle cost analysis, and the management of engine parts. By use of statistical distributions of life-controlling parameters (see figure), the program computes rates of occurrence for such significant events as removals of parts, initiation of cracks, and rare failures in service. The program can be used to investigate the effects of such engine-component life-controlling parameters as return-to-service intervals, stresses, capabilities for nondestructive evaluation, and qualities of materials.

This work was done by T. Watkins, Jr., and C. G. Annis, Jr., of United Technologies Corp. for **Marshall Space Flight Center.** *For further information, Circle 1 on the TSP Request Card.*
MFS-27237

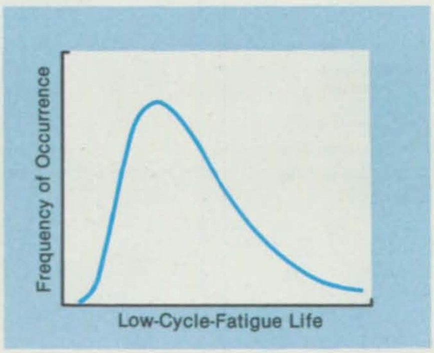

The **Frequency Distribution** of each life-controlling parameter — in this case, low-cycle-fatigue life of a component — is taken into account in a comprehensive statistical analysis of the lifetimes of the components and system.

Dishwasher for Earth or Outer Space

Features include a centrifugal tub and a novel blade filter.

Lyndon B. Johnson Space Center, Houston, Texas

A dishwashing machine (see Figure 1) cleans eating utensils in either Earth gravity or zero gravity of outer space. The dishwasher features a rotating tub that guides used washwater to a drain, a self-cleaning filter that removes food particles from the washwater without becoming clogged, and a separator that extracts air from the washwater so that both air and washwater can be recycled.

A priming pump purges air from spray-circuit plumbing. A spray pump circulates water containing detergent through a heater and a set of stationary nozzles in the rotating tub. The water impinges on the utensils and cleans them as they rotate through the spray on a rack that turns with the tub at 30 revolutions per minute.

The water and the entrained soil pass to the wall of the tub. There, the combination of centrifugal force and taper of the wall forces the waterflow down to a sump. From there, it is removed by suction from the spray pump. The water leaves the tub through a rotary seal in a central shaft.

The drained water enters a self-cleaning filter (see Figure 2). The water flows between parallel, closely spaced blades that catch and hold soil particles, preventing them from returning to the tub with the recirculated water.

When washing is finished, the spray pump is stopped, and a vacuum blower and evacuation valves are activated to pull the used washwater and outside air through the air/water separator. The outside air enters via the lid of the tub. This air is heated so that it dries the utensils.

At this time, the self-cleaning feature of the filter comes into play. A solenoid on the self-cleaning filter jiggles the blades in scissorlike motion, dislodging soil particles from them. The used washwater again flows through the blades, this time in reverse direction, and assists in dislodging the particles.

The separator is a centrifugal device similar to the dishwashing tub. The mixture of air, water, and soil enters through a central post in a bowl rotating at 100 revolutions per minute. The air flows axially through slotted disks (which collect droplets of water) and leaves the bowl. The water and soil flow radially outward from the central post and strike the wall of the bowl. The soil/water mixture flows outward along the tapered wall into a sump, from which a pump extracts it through a rotating seal. The soil/water mixture is then pumped to a wastewater system.

This work was done by Jon D. Tromble of Whirlpool Corp. for **Johnson Space Center**. *For further information, Circle 46 on the TSP Request Card.*
MSC-21442

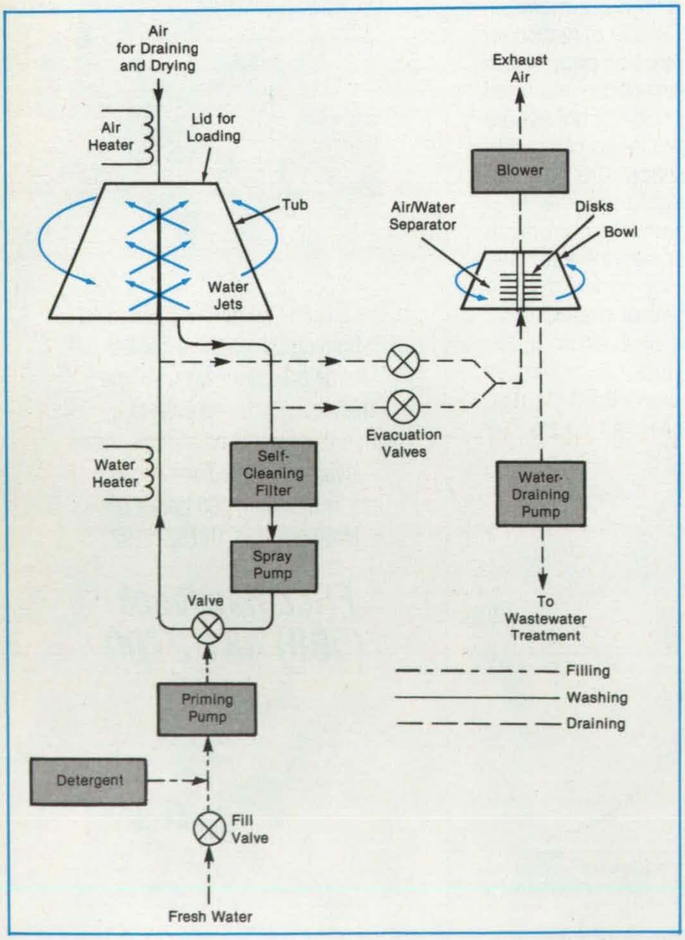

Figure 1. The **Dishwashing Cycle** consists of three phases: filling, washing, and draining. The rotation of the tub creates an artificial gravity that aids in the recirculation of water during the washing phase in the absence of true gravity. The centrifugal air/water separator also helps the system function in zero gravity.

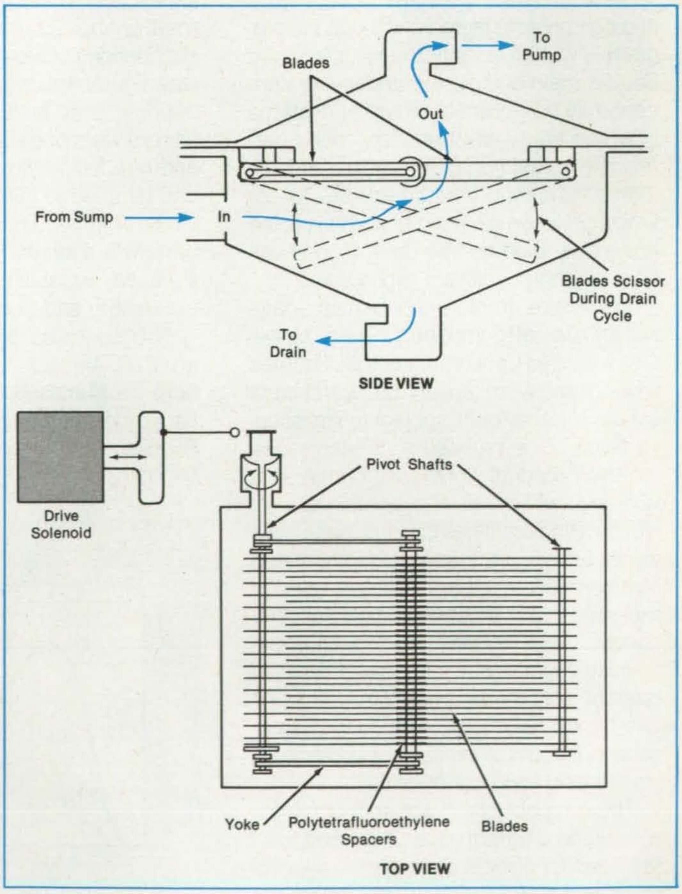

Figure 2. The **Self-Cleaning Filter** contains interdigitating blades that catch solid debris when the water flows between them. Later, the blades are moved back and forth in a scissor-like manner to disloge the debris, which are removed by a backflow of water.

TEM Pump With External Heat Source and Sink

An external hotter primary loop would drive a colder secondary loop.

NASA's Jet Propulsion Laboratory, Pasadena, California

A proposed thermoelectric/electromagnetic (TEM) pump would be driven by an external source of heat and by two or more heat pipe radiator heat sink(s). The thermoelectrics would generate electrical current to circulate liquid metal in the secondary loop of a two-fluid-loop system.

Pumps of this type are intended for use with space and terrestrial dual loop liquid metal nuclear reactors. Applications might include spacecraft on long missions or terrestrial beacons or scientific instruments that have to operate in remote areas for long times. In some previous versions of the TEM pump, the heat sources and the heat sinks were required to be the pumped fluids; thus, the temperature of the heat sink was constrained to be that of the radiator.

According to the new TEM pump concept, the two loops would be designed separately, yet the heat source would still be provided by the primary loop, which, in turn, would drive the secondary loop. The TEM pump would be reconfigured so that the heat source and the thermoelectric converters would be outside the magnetic field, yet still closely coupled. With the new configuration (see figure), an external source at any temperature high enough to provide the required current through the thermoelectrics would pump the liquid metal in the secondary loop, and a heat sink or sinks at any suitably lower temperature available could be attached to the thermoelectric cells.

The new configuration would decouple design parameters, thereby removing conflicting constraints and increasing the flexibility for design optimization. For example, the radiator, which heretofore has been the most massive and voluminous subsystem, could be optimized in terms of its own temperature, power, size, and mass constraints, without regard for the effect on the TEM pump. Similarly, the temperatures of the source and sink(s) could be optimized with respect to various TEM-pump parameters. The design of the TEM pump could be modified to include multiple radiators, converters, and ducts, as dictated by a particular application.

This work was done by Bill J. Nesmith of Caltech for **NASA's Jet Propulsion Laboratory**. *For further information, Circle 27 on the TSP Request Card. NPO-17864*

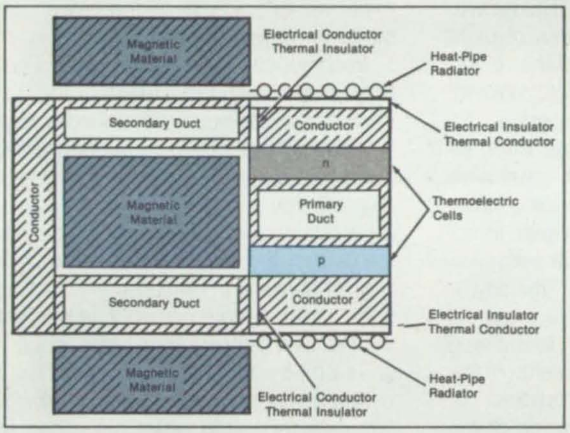

The **Two-Loop TEM Pump** concept offers greater flexibility of design in coupling to external heat sources and sinks.

Fabrication Technology

Hardware, Techniques, and Processes

Improved Boat for Liquid-Phase Epitaxy

Larger substrates and more uniform composition are obtained with a simpler, easier-to-use boat.

Langley Research Center, Hampton, Virginia

The liquid-phase epitaxial (LPE) growth process used in the fabrication of high-power channeled-substrate planar (CSP) lasers is typically a very-low-yield process. Consequently, it is desirable to perform the growth on a substrate of large area, increasing the number of laser chips available for evaluation and providing more usable devices from a given wafer. In addition, repeatability between growth runs has been traditionally poor. Typically, a change in the compositions of layers could be observed from one growth to the next without any change in the contents of the melts in the LPE boat. Thus, it is beneficial to reduce or eliminate the mixing of the melts within the boat as the growth substrate is moved through the boat.

In conjunction with the design of a new, fully automated LPE reactor, the LPE growth boat has been redesigned. It is still fabricated from ultra-high-purity graphite, but it has been modified to permit easy disassembly and cleaning, along with improved wiping action for more complete removal of the melt to reduce the carryover of gallium. In addition, the boat has been redesigned to accept larger substrates. The new substrate size is 1.0 in. (2.54 cm) by 1.25 in. (3.175 cm). This increased size provides approximately 3.3 times more usable wafer area than the previous substrates did. The growth melt for this boat amounts to 10 g, as compared with 3 g for the older design.

The LPE boat of the original design includes many components, including walls or partitions for separating the individual melts within the boat. In the new design, the walls are integrated with the sides of the boat to form a single unit. Thus, in a six-melt boat, the number of pieces is reduced from nine to one.

In the original design, the walls that separate the melts are positioned in channels within the sides of the boat, and, although their movement is limited by the top rails on the boat, they are subject to machining tolerances, which permit movement perpendicular to the slider direction. This small movement can seriously affect the carryover of melt from one growth bin to the next. The new design, with its one-piece melt container, fixes the walls in position, thereby eliminating movement and providing more-uniform wiping action from one bin to the next.

The reduction in the number of components has also reduced the time and difficulty in cleaning the boat. In addition, because the walls are fixed in position, less care is needed in handling the boat. The useful lifetime of the boat has also been increased. When the bottom of the partition walls becomes worn out, the bottom of the block can be reground to reveal a fresh surface, — a technique not possible with the old design.

The new boat design has permitted the growth of larger substrates than have been previously possible. The carryover of material between adjacent melts has been reduced, resulting in a more nearly uniform composition within each layer of the laser structure. The potential for the improved boat design may be extensive because of the wide use of LPE growth processes in the development and fabrication of solid-state devices.

This work was done by John C. Connolly of the David Sarnoff Research Center for **Langley Research Center**. *No further documentation is available.* *LAR-14199*

Smoother Turbine Blades Resist Thermal Shock Better

Smoothing removes small flaws where cracks start.

Marshall Space Flight Center, Alabama

A surface treatment increases the resistance of turbine blades to low-cycle fatigue. The treatment is intended for blades in turbines subject to the thermal shock of rapid starting. In a rocket engine, for example, the temperature rises from a cryogenic level to that of burning fuel. In conjunction with high film coefficients, the rapid increase in temperature causes low-cycle-fatigue cracks to appear prematurely at pits and scratches on the surfaces of turbine blades.

The treatment increases the resistance to low-cycle fatigue by a factor of more than 4. The treatment consists of two steps:

- The airfoil surface of the blade (see figure) is radially blended to remove superficial pits and scratches.
- The airfoil surface and the neck region are further smoothed by an automated blasting process.

The treatment removes only a thin layer — less than 3 mils (76 μm) — from the blade. No recrystallization occurs at rocket-turbine operating temperatures.

This work was done by Paul Czerniak, Kent Longenecker, Don Paulus, and Zane Ullman of United Technologies Corp. for **Marshall Space Flight Center**. *No further documentation is available.*
MFS-28472

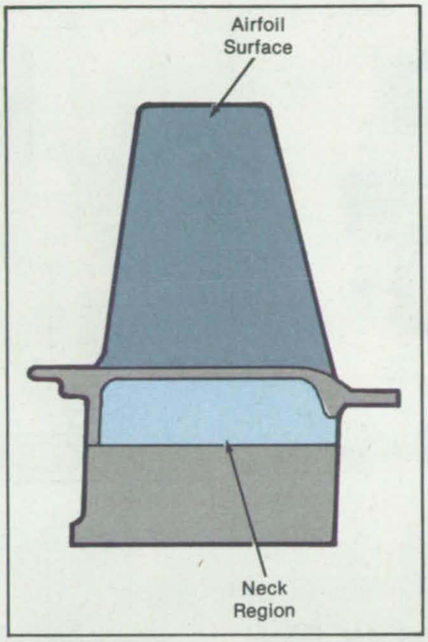

A **Turbine Blade** subject to severe thermal transients at startup quickly acquires fatigue cracks at superficial flaws. The incidence of cracking is reduced by smoothing the surfaces on the airfoil and the neck.

Reed Valve Regulates Welding Back-Purge Pressure

A simple modification yields welds of better quality.

Marshall Space Flight Center, Alabama

A reed valve halves the fluctuations in pressure in a back-purge chamber attached to a workpiece undergoing keyhole plasma arc welding. Without the reed valve, the rate of flow of the effluent purging gas is controlled, and this flow control exerts only indirect control over the pressure. The large fluctuations in pressure cause inconsistent, rough back beads and irregular penetration of the weld. With the reed valve, the backbead is smoother, and the weld penetrates more uniformly.

The valve is identical to one used in the fuel system of a two-cycle gasoline engine (see Figure 1). It is mounted on a plenum at the exhaust of the back-purge chamber (see Figure 2). Because the reed valve is unaffected by gravity, it is effective in any orientation; consequently, the workpiece and its back-purge chamber can, if necessary, be rolled during the welding procedure.

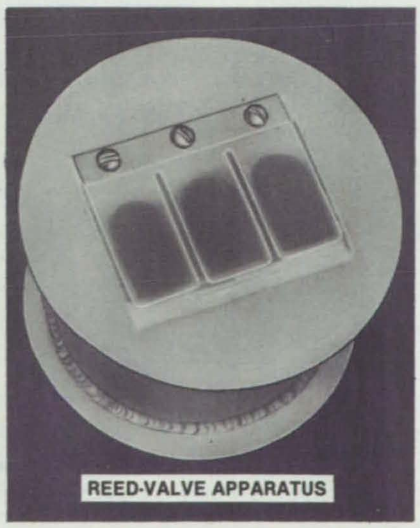

Figure 1. The **Reed Valve** is taken from the fuel system of a two-cycle gasoline engine.

This work was done by J. Ben Coby, Jr., and Jack L. Weeks of Rockwell International Corp. for **Marshall Space Flight Center**. *For further information, Circle 115 on the TSP Request Card.*

Inquiries concerning rights for the commercial use of this invention should be addressed to the Patent Counsel, Marshall Space Flight Center [see page 14]. Refer to MFS-29684.

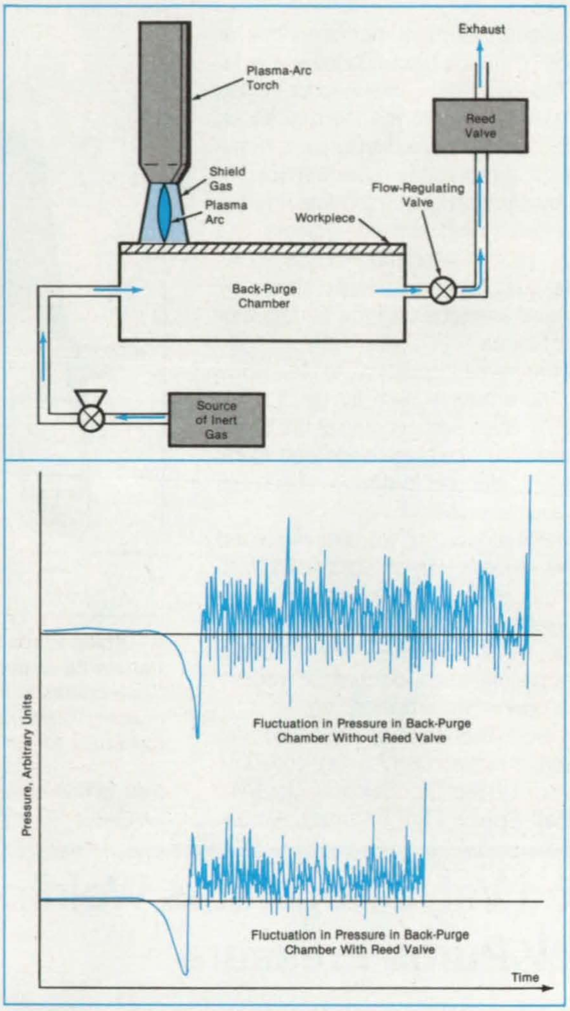

Figure 2. The **Pressure of an Inert Gas** in the back-purge chamber is kept more nearly constant by inserting a reed valve at the exhaust of the chamber. A smoother back weld bead and more uniform penetration of the weld result.

Thermosyphon Suspension for Growth of Crystals

The crystal is suspended by flow of the solution from which it precipitates.

Marshall Space Flight Center, Alabama

In a thermosyphon apparatus, the gentle upward flow of a supersaturated solution suspends a crystal growing from the solution. It is necessary to suspend a growing crystal because contact with a container can degrade its quality. The thermosyphon apparatus is intended principally for the growth of protein crystals, which are so fragile that they are easily damaged by the high-shear flows produced by pumps.

The apparatus includes a heating section, a cooling section, and an expansion-and-growth chamber in a closed flow loop (see figure). The flow is simple convection, and the rate of flow increases with the difference between the temperature, T_h, of the liquid in the heating section and the temperature, T_c, in the cooling section. The growing crystal is suspended at a point in the expansion-and-growth chamber where its settling speed equals the upward speed of the flow. As the crystal grows, it sinks lower to where the upward flow is faster, and, therefore, strong enough to suspend it. The expansion-and-growth chamber is designed to accommodate growing crystals in a wide range of sizes, and the range can be extended by choice of T_h and T_c to change the rate of flow.

Most of the tubing in the apparatus has an inside diameter of 6 mm. However, to obtain a flow of greater speed in the bottom of the expansion-and-growth chamber, a tube of 3 mm inside diameter is used to conduct the flow to the bottom of this chamber from the bottom of the cooling section. This helps to prevent crystals from settling in the lower part of the apparatus, and they are swept into the expansion section, where most of them are trapped. Crystalline nuclei that are small enough to be swept through the expansion section are dissolved as they pass through the heating section.

A thermistor is inserted through a filling port at the top to measure T_h. To initiate growth, seed crystals with typical sizes of 1 to 10 μm are suspended in a small amount (typically < 0.05 mL) of the saturated solution, which is then injected through the filling port. These crystals are small enough to travel around the loop while they grow slowly. Eventually, one becomes large enough to be trapped in the expansion section. Thereafter, T_h can be increased above the solution temperature so that the smaller crystals that are not trapped initially are dissolved in the heating section.

When a crystal has grown to the desired size, T_h is reduced to T_c to stop the flow. The crystal settles through the lower port of the apparatus into a flexible tube that is pinched closed at its bottom. The tube is then pinched closed at the top, and the

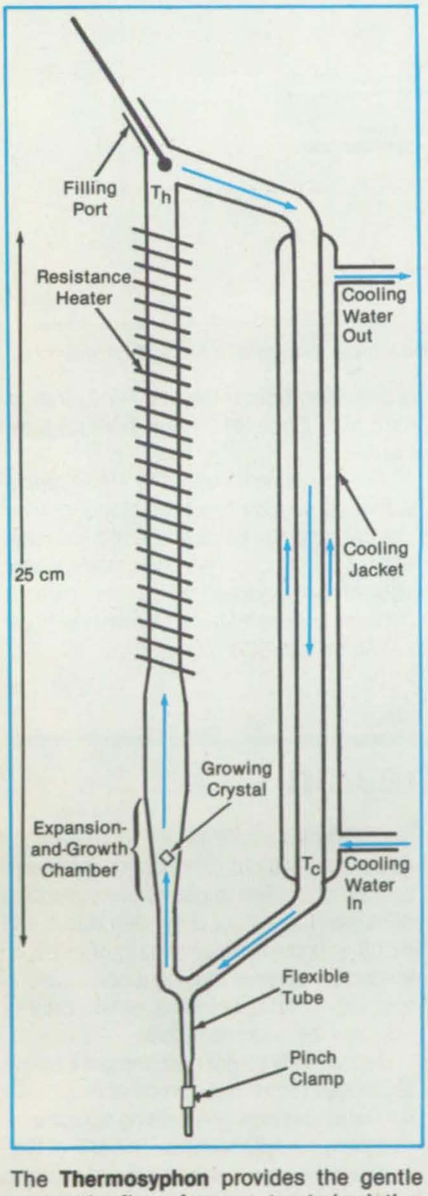

The **Thermosyphon** provides the gentle convective flow of supersaturated solution that both suspends and contributes material to the growing crystal.

bottom pinch is removed, allowing the crystal and the small amount of solution in the tube ($\approx$ 0.1 mL) to be removed.

This work was done by Thomas A. Nyce of the University of Alabama in Huntsville for **Marshall Space Flight Center**. *For further information, Circle 118 on the TSP Request Card.*

Inquiries concerning rights for the commercial use of this invention should be addressed to the Patent Counsel, Marshall Space Flight Center [see page 14]. Refer to MFS-26113.

Quick-Connect Truss Fastener

A robot or a heavily gloved technician could actuate this fastener without undue difficulty.

Lyndon B. Johnson Space Center, Houston, Texas

A quick-connect fastener will enable the assembly of a truss by a heavily gloved technician or by a robot. Originally designed for use by an Astronaut or robot assembling a truss in outer space, the fastener will also adapt to various connection applications that require quick assembly or disassembly. Previous truss-assembly-fastener designs of this general type included actuating tools on each assembly. This feature increased the complexity and made operation by robots difficult. The new, simplified design requires only the insertion and simple rotation of the actuating tool, making it easy for a robot or technician to operate.

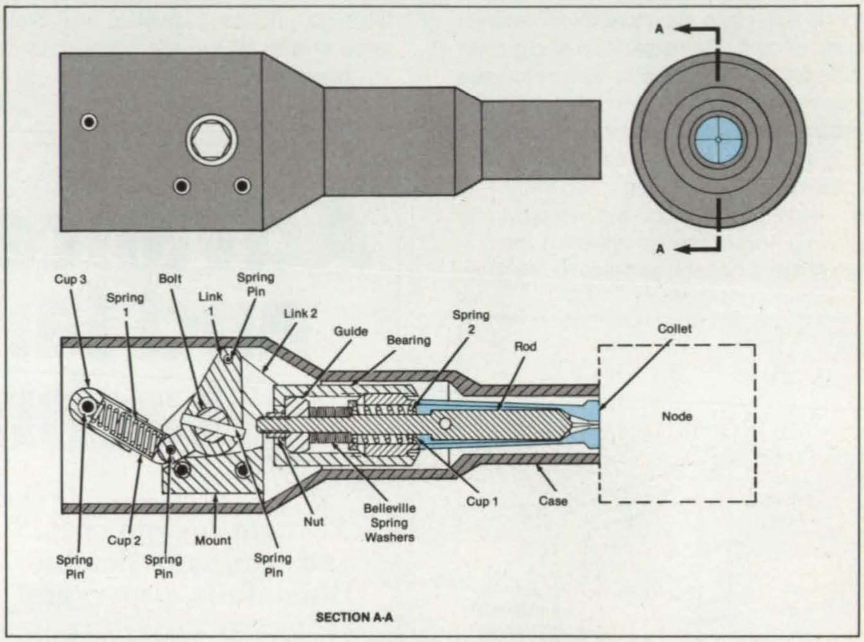

The **Quick-Connect Fastener** is actuated by the simple motion of a hexagonal wrench.

The connector (see figure) is 5.5 in. (14.0 cm) long and 1.8 in. (4.6 cm) in diameter at its largest end. To attach a strut to a node, the operator inserts a hexagonal shaft (Allen wrench) into a hexagonal hole in the head of the bolt and rotates the shaft 80° clockwise. This action rotates link 1, which pushes and rotates link 2. Link 2 pushes the guide to the right, thereby compressing Belleville spring washers, which, in turn, push on spring 2. The spring pushes the collet out of the case and into the node.

The collet is threaded into the bearing and so pulls it along until the bearing comes to a stop in the case. At this point, spring 2 begins to be compressed, allowing the rod to begin to spread the collet. When link 1 is 15° before center, the collet is spread out inside the node, preventing the rod from moving further. The Belleville spring washers then begin to be compressed as link 1 is rotated to 5° over the center, and maintain a preload of 250 to 300 lb (1,100 to 1,300 N) on the rod. This preload translates into a compressive load of approximately 1,000 lb (4,400 N) between the case and the node from an applied torque of only 50 to 100 lb•in (5.6 to 11.2 N•m). For detachment of the fastener from the node, it is necessary only to rotate the bolt 80° counterclockwise by use of the same tool.

This work was done by Philip L. Sheridan of **Johnson Space Center**. *For further information, Circle 11 on the TSP Request Card.*

This invention is owned by NASA, and a patent application has been filed. Inquiries concerning nonexclusive or exclusive license for its commercial development should be addressed to the Patent Counsel, Johnson Space Center [see page 14]. Refer to MSC-21504.

Grit Blasting Scribes Coats for Tests of Adhesion

Damage to substrates is reduced.

Marshall Space Flight Center, Alabama

A grit-blasting technique for cutting line gaps in paints, hard coats, lubricants, and other coating films is undergoing development. The line gaps are cut in chevron patterns, groups of parallel lines, or other prescribed patterns, in preparation for testing the adhesions of the coats to the substrates by attempting to peel the patterned areas off with adhesive tapes. Heretofore, the standard procedure has involved scoring the lines with razor blades or sharp knives.

Scoring with knife edges has several disadvantages. One is that the results of tape-peel tests can vary considerably because of variability in the cuts: it is difficult to make uniform, repeatable cuts, especially in tough coats. This is further complicated by variability in the hardnesses of substrates and variations among knife edges. Damage to substrates is another serious disadvantage. Ideally, the gap in a coat should extend down precisely to the surface of the substrate and no farther, but if the substrate is soft or otherwise vulnerable, the cut can extend far enough into the substrate to cause unacceptable damage. The risk of such damage could result in prohibition of testing of parts intended for service, making it necessary to test sacrificial specimens, which may or may not be representative.

As currently envisioned, the grit-blasting technique requires a combination of conventional and new grit-blasting equipment, materials, and procedures. The grit — typically, a mixture of fine particles of crushed glass, glass beads, and aluminum oxide — is entrained in a stream of compressed air and aimed at the workpiece through a

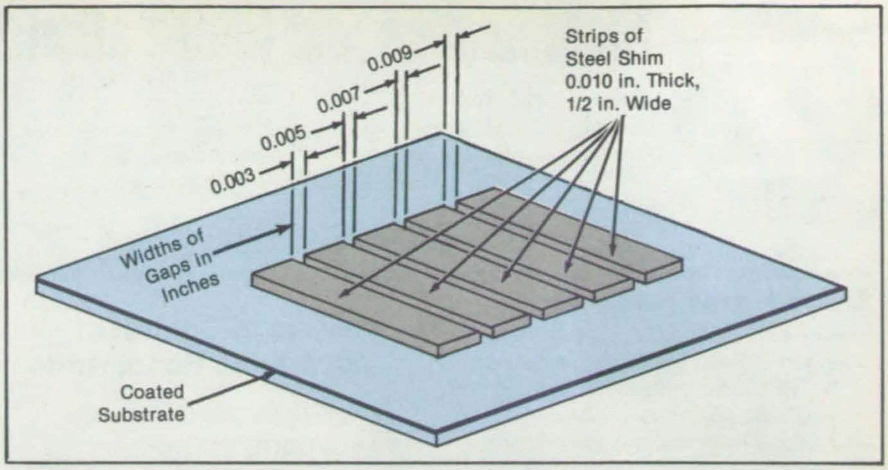

A Grit-Blasting Template of Steel Shim Stock was used to define areas to be protected and lines to be cut in a preliminary experiment on grit-blast scoring.

miniature grit-blasting nozzle. The type of material and size of the orifice in the nozzle are chosen to be compatible with the hardnesses and sizes of the particles in the grit mixture. The nozzle is mounted on a fixture that guides it along the desired cut line and maintains the standoff disance between the nozzle and the workpiece at the correct (and critical) value. Precise control of the air pressure and the shape of the orifice is also required to obtain consistent cuts. The lines to be cut can be defined, and the areas not to be cut can be protected by laying appropriately cut and spaced shim stock on the surface (see figure).

The grit is used only once. A vacuum-cleaner attachment mounted on the fixture with the nozzle removes the spent grit along with the coating and substrate debris, thereby keeping the work area clean and enabling the technician to perform the scribing operation safely. The vacuum-cleaner attachment is specially designed to be usable in any orientation, not to obstruct the view of the workpiece, and to preserve ease of manipulation of the nozzle.

The grit-blast technique results in very little damage to the substrate — usually, no more than a slight roughening. This may make it acceptable to test parts that previously could not be tested in this way for fear of damage. If the scribed and peeled areas of a part are to be recoated and the part placed in service after testing, the roughening is beneficial in that it increases the adhesion of the newly applied coat. With grits of diamond or ceramic powder, the grit-blasting technique can be used to scribe lines in advanced protective coats that, until now, have not been amenable to tape-peel adhesion tests because they are almost as hard as, or harder than, knives.

In some cases, grit-blast cutting of lines can cause separation of marginally adherent coats from substrates. In such cases, grit-blast tests may be better than tape tests. After further experimentation to define parameters, this phenomenon may be the basis for a new standard grit-blast test as an alternative to the tape-peel test of adhesion.

This work was done by Howard L. Novak of USBI Corp. — a Division of United Technologies for **Marshall Space Flight Center**. *For further information, Circle 6 on the TSP Request Card.*

Inquiries concerning rights for the commercial use of this invention should be addressed to the Patent Counsel, Marshall Space Flight Center [see page 14]. Refer to MFS-28452.

Books and Reports

These reports, studies, handbooks are available from NASA as Technical Support Packages (TSP's) when a Request Card number is cited; otherwise they are available from the National Technical Information Service.

Analysis of Control of Cooperating Robot Arms

The emphasis is on the full-dynamics approach.

A paper presents a theoretical analysis of the general problem of how to control the motions of, and the forces exerted by, several multiple-rigid-link robot arms that cooperatively manipulate a common rigid object. Such a robotic system can be viewed in various ways, depending on which variables are regarded as the control inputs. In the full-dynamics approach, the torques applied to the joints of the robot arms ("joint torques" for short) are considered to be the control inputs. In the arms-as-actuator approach, the forces applied by the tips of the robot arms to the manipulated object ("tip forces" for short) are regarded as the control inputs, and the joint torques necessary to produce the required forces are computed in a feedforward manner (this involves real-time measurements but no error-correction function). In the feedback-linearization approach, the control input is an acceleration in one of an infinite number of generalized-coordinate representations of the constrained dynamics of the system, and the joint torques necessary to produce the required accelerations are again computed in a feedforward manner.

The arms-as-actuator and feedback-linearization approaches require full information from dynamical models of the system to implement the feedforward functions. In principle, these two approaches yield simplification of the control laws and compensation for the nonlinear dynamics of the arms. In practice, these approaches entail considerable difficulties with regard to modeling, computation, and robustness.

In this paper, the emphasis is mainly on the construction, via the full-dynamics approach, of control laws that are relatively independent of dynamical models. In the dynamical analysis, the tip-force vector is decomposed into two orthogonal components: one that effects motion and is said to be in the "move" subspace and another that builds up internal forces and torques in the robot arms and manipulated object and is said to be in the "squeeze" subspace. This decomposition agrees with experience that squeeze forces can be applied without effecting motion. From the dynamical analysis, fixed- and moving-set-point laws (with and without transient shaping) for the control of motions are developed by use of a class of Lyapunov functions based on the total energy of the system to analyze the stability of the system. The combination of the "move/squeeze" decomposition and the energy-Lyapunov-function formulation provides the basic analytical framework within which the control of motions and the control of forces can be considered as two independent problems.

This class of control laws has a simple structure of proportional and derivative feedback, with compensation for the weights of the links in the arms and for the weight of the manipulated object. To control the joint torques and forces to a set point, either a feedforward strategy or, if sensor information is available, a feedback strategy can be used. The feedback strategy offers greater robustness and can yield tight force control if high integral-feedback gain is used.

For the control of motions, several choices of feedback variables are possible. These include the joint variable, the tip variable, and a generalized coordinate. In all three cases, the proportional/derivative/weight control law drives the system to a steady-state configuration. However, only in the case of the generalized coordinate does the steady-state configuration correspond to the desired one. In the joint- and tip-variable cases, one can conclude only that the configuration lies on a manifold on which the tip forces produced by the errors in the positions of the arms balance each other. The authors call this manifold the "jam manifold" and discuss some of its properties.

Computer simulations are performed for two three-link planar robot arms. From the results of these simulations, it is shown that (1) set-point control operates better with than without transient shaping and (2) feedback squeeze-force control gives smaller transient overshoot (better stability) than does feedforward squeeze-force control.

This work was done by Kenneth K. Kreutz of Caltech and John Ting-Yung Wen of Rensselaer Polytechnic Institute for **NASA's Jet Propulsion Laboratory**. *To obtain a copy of the report, "Stability Analysis of Multiple Rigid Robot Manipulators Holding a Common Rigid Object," Circle 41 on the TSP Request Card.*
NPO-17789

The History of the Kalman Filter

This widely used mathematical technique has evolved considerably since its introduction.

A paper presents a historical view of the adaptation of Kalman filtering techniques to aerospace applications and eventually to fields as diverse as exploration for oil and the control of powerplants. It describes the scientific breakthroughs and reformulations that transformed Kalman filtering techniques into a fundamental tool for analyzing and solving a broad class of estimation problems.

In 1960, R. E. Kalman published his now-famous paper, "A New Approach to Linear Filtering and Prediction Problems," in the *Transactions of the American Society of Mechanical Engineers*. That paper made a significant contribution to the field of linear filtering by removing the stationary requirements of the Weiner filter and presenting a sequential solution to the time-varying linear filtering problem.

The need for a filter like Kalman's arose during early feasibility studies from NASA's Apollo manned lunar mission. Kalman's work was introduced at a nearly perfect time but might have gone unnoticed except for a fortuitous meeting between a NASA scientist (one of the authors of the historical review) and Dr. Kalman. However, the usefulness of Kalman's work for the Apollo mission was limited by certain features of the formulation. A reformulation by NASA researchers transformed Kalman's method into the extremely useful tool now known as the extended Kalman filter.

The historical paper describes the development of navigation systems for the Apollo spacecraft and the Lockheed C-5A aircraft and the way in which these key systems led to a square-root formulation of the Kalman filter — a formulation that had features suitable for aircraft applications. The paper traces the development of the first known aircraft flight experiment in which the performance of a square-root formulation coded for an airborne computer was validated. The paper concludes with a discussion of the wide range of problems to which the extended and square-root Kalman filters are being applied.

This work was done by Leonard A. McGee of **Ames Research Center** *and Stanley F. Schmidt of Analytical Mechanics Associates. Further information may be found in NASA TM-86847 [N86-13311], "Discovery of the Kalman Filter as a Practical Tool for Aerospace and Industry."*

Copies may be purchased [prepayment required] from the National Technical Information Service, Springfield, Virginia 22161, Telephone No. (703) 487-4650. Rush orders may be placed for an extra fee by calling (800) 336-4700.
ARC-11734

Terminal Attractors in Neural Networks

Neural networks can be made to "learn" faster.

A report presents a theoretical study of terminal attractors in neural networks. A terminal attractor is a point of stability in a vector space that represents the state of a system; if the system is initially placed in a state sufficiently close to such a point (within a basin of attraction), the system will then proceed to that point. The concept of terminal attractors (and terminal repellers) was first introduced in 1970 in the analysis of nonlinear mechanical systems and is associated with such energy-cumulation effects as the snap of a whip. In 1988, terminal attractors were introduced into the analysis of content-addressable memories in neurodynamics.

Some previous studies of the dynamics of neural networks had involved the related but more-limited static-attractor concept and had revealed a number of limitations, including the existence of spurious equilibria, the requirement of infinite time (in principle) to reach a static attractor, low storage capacity, and no systematic way to find a synaptic-connection matrix that provides a desired set of attractors with prescribed basins. The purpose of this study was to remove some of these limitations.

In this study, the incorporation of terminal attractors into neurodynamics requires some revision of the classical theory of dynamical systems because (1) the classical theory is based on the Lipschitz condition, which is a restriction on derivatives that guarantees a unique solution for each set of initial conditions and prevents the system from reaching an attractor in a finite time, (2) in this study, it is desired to enable the system to reach an attractor in a finite time, and (3) this requires the violation of the Lipschitz condition at the points of equilibrium. The non-Lipschitzian dynamics exhibit new qualitative effects, including the existence of attracting trajectories that can be "remembered" by the system. Another new effect is a multiple-choice response to external excitations. This effect can be exploited to devise a neural network that would exhibit "creativity" in that it could be activated by internal rhythms as well as by external inputs.

The study includes a systematic analysis of applications of terminal attractors to the activation dynamics of neural networks. The starting point is the content-addressable memory and the recognition of patterns. Two basic properties of terminal attractors are exploited here: the finite time of transient dynamics and the infinite local stability of terminal attractors. It is demonstrated that because of the latter property, terminal attractors can be incorporated into a neural network such that any desired set of these attractors with prescribed basins (and without false attractors) is provided by an appropriate selection of the matrix of synaptic weights.

On the basis of the finite time of transient dynamics, one can obtain such advanced phenomena as complex associative memories and control of the basins of attractions by use of active terminal attractors (which temporarily leave their positions to "search" for transient solutions). The results are generalized to neural networks that are modeled by delay-differential equations. By incorporating terminal attractors in such a neural network, one can store patterns that are characterized not only by the vector of the state variables but also by durations of the exposures of its components.

Finally, the report discusses dynamical training by use of terminal attractors. This involves the introduction of a dynamical system that governs the relaxation of the matrix of synaptic-connection weights to the corresponding point of stable equilibrium represented by a terminal attractor.

This work was done by Michail A. Zak of Caltech for **NASA's Jet Propulsion Laboratory**. *To obtain a copy of the report, "Terminal Attractors in Neural Networks," Circle 149 on the TSP Request Card.* NPO-17832

Life Sciences

Hardware, Techniques, and Processes

Integrated Protein-Crystal-Growing Apparatus

The apparatus would contain the entire growth process.

Marshall Space Flight Center, Alabama

A proposed apparatus for research on the growth of protein crystals would dispense drops of protein and precipitating solutions, provide a controlled environment for crystallization, and store the crystals. Although the apparatus is intended for use in the microgravity of outer space, the concept of the apparatus may also be useful in the design of self-contained terrestrial experiments for remote and/or automatic execution.

The heart of the apparatus would be a hollow shaft made of polytetrafluoroethylene or other inert material. The shaft would contain sets of holes, channels, and chambers that would variously route pressure and vacuum supplies, accept mixed solutions from storage vials, dispense the solutions to crystal-growing chambers, and gather solidified crystals (see figure).

Before the start of a crystal-growing experiment, protein and precipitate solutions would be stored in adjacent pairs of sealed vials. An operator would turn the shaft by its handle to the position shown in the figure, aligning holes with the external pressure supply and with the drop dispensers on the pairs of vials. The pressure would act on a piston in each vial, driving it upward and thus forcing the solutions from their respective vials.

The protein and precipitating solutions from each pair of vials would enter a ball-type mixer. The mixed solution would continue through a channel in the shaft to a growth chamber, where it would form a precisely metered drop of liquid. The channel would be narrow, and the volume of the mixer would be small, so that little solution would wasted: probably only 5 to 10 microliters would remain in the dispensing system of each pair of vials after the formation of the drop.

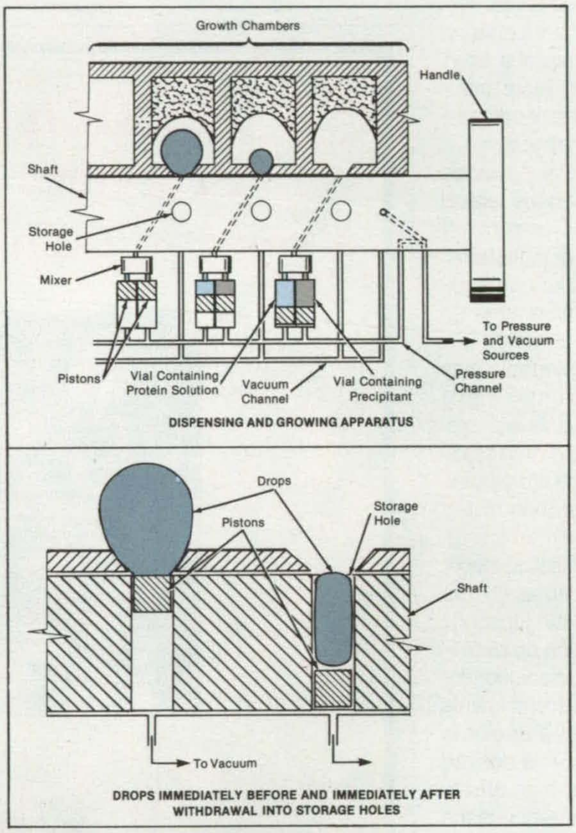

DISPENSING AND GROWING APPARATUS

DROPS IMMEDIATELY BEFORE AND IMMEDIATELY AFTER WITHDRAWAL INTO STORAGE HOLES

The **Hollow Shaft** is shown in a position in which the pressure supply would be connected to pistons in solution vials and solution mixers would be connected via small channels to growth chambers. Drops in chambers are shown at three stages: (1) before dispensing, (2) partly dispensed, and (3) fully dispensed. Actually, drops would be formed simultaneously in each chamber.

The operator would initiate the collection of the drops and the crystals that have precipitated in them by rotating the shaft to a position in which the hole in each growth chamber would be aligned with one end of a storage hole in the shaft and the other end of each storage hole would be aligned with a vacuum-supply port. The vacuum would pull pistons in the storage holes, sucking the drops into the storage holes.

The operator would then turn the shaft another 90° so that the drops would be sealed in the storage holes. Crystals could be observed through windows in the shaft and/or removed for analysis through access ports in the shaft.

This work was done by Percy H. Rhodes, Robert S. Snyder, and Marc L. Pusey of **Marshall Space Flight Center**. *For further information, Circle 101 on the TSP Request Card.*

Inquiries concerning rights for the commercial use of this invention should be addressed to the Patent Counsel, Marshall Space Flight Center [see page 14]. Refer to MFS-28422.

Closed-Cycle Nutrient Supply for Hydroponics

Dual pressurized bladders alternately store and release nutrient solution.

Lyndon B. Johnson Space Center, Houston, Texas

A hydroponic system controls the composition and feed rate of nutrient solution and recovers and recycles excess solution. The system uses air pressure in bladder tanks to transfer the solution to and from the hydroponic plant-growth chamber; this reduces the probability of leakage. The system was designed to operate in microgravity but may also be adaptable to hydroponic plant-growing systems on Earth.

The system operates cyclically. First, the bladder in tank 1 (see figure) is pressurized, forcing the nutrient solution from tank 1 through a sensor manifold, where its composition, pH, electrical conductivity, and temperature are measured. The solution continues its flow into a control manifold, where the measured quantities are adjusted by controlled addition of oxygen, carbon dioxide, potassium nitrate, water, nitric acid, and potassium hydroxide.

The adjusted solution flows into the hydroponic chamber. Unabsorbed solution continues through the chamber to a bladder in tank 2, where it accumulates. When tank 1 is empty, valves are switched and pressure is applied to the bladder in tank 2, forcing its contents back into tank 1. The feeding cycle then repeats.

The combination of a heater and flowing coolant in the control manifold maintain the flowing solution near the desired temperature. The coolant continues its flow through a heat exchanger, wherein it cools air flowing from the chamber to condense water that has evaporated from the solution and plants. The condensed water is returned to the water supply of the system.

This work was done by Steven H. Schwartzkopf of Lockheed Missiles and Space Co. for **Johnson Space Center**. *No further documentation is available.*

Inquiries concerning rights for the commercial use of this invention should be addressed to the Patent Counsel, Johnson Space Center *[see page 14].* *Refer to MSC-21655.*

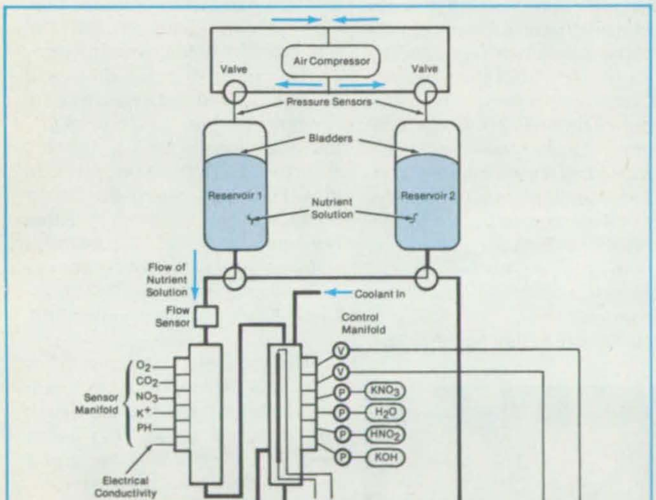

The **Nutrient Supply System** uses air pressure on bladders to transfer aqueous nutrient solution. The system measures and adjusts the composition of the solution before it goes to the hydroponic chamber. It eventually returns excess solution to one of the tanks.

New on the Market

Information Handling Services, Englewood, CO, is offering a new service which **integrates** the text of **IEEE standards**, including illustrations, diagrams, graphs, charts, and figures, **with CD-ROM technology** and high-speed search and retrieval software. It enables PC users with CD-ROM capability to locate IEEE standards documents in seconds, searching by keywords, organization names, and document numbers. Updated every 60 days, the service covers computers and electronics, instruments/terminology, communications, applications, and power.
Circle Reader Action Number 800.

The Ultraprobe 2000 **ultrasonic inspection system** from UE Systems Inc., Elmsford, NY, senses warning signals produced by operating mechanical equipment. Features such as frequency tuning and meter mode selection allow the portable, handheld instrument to be adapted to a wide variety of inspection situations. It detects all types of pressure or vacuum leakage, electrical arcs, blow-by in valves and steam traps, faults in motors, pumps, or compressors, and the beginning stage of bearing failure. By electronically converting a narrow range of ultrasound into the audible range, a user can hear subtle changes in equipment while observing these changes on a meter.
Circle Reader Action Number 792.

InfraRed Associates Inc., Cranbury, NJ, has introduced a thermally-stabilized, highly-sensitive **pyroelectric detector** that eliminates thermal drift problems. The device integrates a thermoelectric cooler, an FET preamplifier, and a temperature-sensing thermistor in a dry nitrogen backfilled TO-66 package. Applications include Fourier Transform spectroscopy and other analytical tasks where precise radiometric calibration is critical.
Circle Reader Action Number 796.

Sorbothane Inc., Kent, OH, has developed a **visco-elastic material** for shock absorption, vibration isolation, and acoustic damping applications. Its quasi-liquid properties enable high mechanical damping and energy absorption, while its faultless memory ensures return to original shape, even after repeated compressions. The material can be custom-molded to virtually any shape, color, and size specification.
Circle Reader Action Number 790.

A new MEGA 1 **robotic workcell** from Megamation Inc., Princeton, NJ, is accurate to ±.0005" and repeatable to ±.0002" over a 20" x 24" Cartesian workspace. Designed for close-tolerance SMT assembly and test in aerospace, communications, and other industries, the system features automated anti-collision technology and optional, fully-integrated machine vision. It allows up to four robotic heads to function independently in the same workspace.
Circle Reader Action Number 794.

A **"wearable" computer** has been developed by Park Engineering, Spokane, WA. Dubbed the CompCap™, the one-pound unit offers the speed and processing power of a 286 or 386 desktop computer, yet can be worn as part of a work uniform. A miniature screen positioned in front of the user's eyes displays graphics and text, and a voice data entry system enables hands-free computing.
Circle Reader Action Number 798.

The SSP-21110 **solid-state power controllers** from ILC Data Device Corp., Bohemia, NY, bring intelligent control to circuit breakers. Unlike conventional electromagnetic circuit breakers, the SSPCs can be digitally controlled and can report back the status of the controller and load. They respond in 10 µS for large overloads whereas less critical conditions conform to the I^2T curve.
Circle Reader Action Number 778.

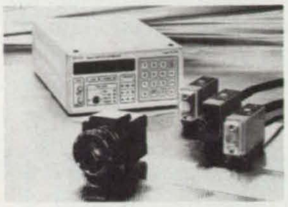

The SUNX IX series of **image sensors** from Ramco Electric Co., West Des Moines, IA, features two body styles and resolutions of 512, 2048, and 4096 bits. Use of a standard 35 mm camera lens provides flexibility of viewing fields. The programmable controller features pre-programmed functions for ease of operation and versatility. Serial, analog, and digital outputs are optional.
Circle Reader Action Number 776.

Colorado Video Inc., Boulder, CO, has introduced the model 493-4 video peak store, a **video memory instrument** that enables an operator to make a series of four different time exposures from a few seconds to several hours in length. The video output of these 512 x 480 x 8 bit memories can be viewed separately on individual TV monitors or connected to an RGB monitor for creation of a synthesized color image. Applications include capture of random transients, tracking of moving objects, and electro-optical scan conversion.
Circle Reader Action Number 784.

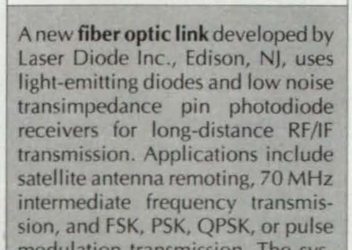

A new **fiber optic link** developed by Laser Diode Inc., Edison, NJ, uses light-emitting diodes and low noise transimpedance pin photodiode receivers for long-distance RF/IF transmission. Applications include satellite antenna remoting, 70 MHz intermediate frequency transmission, and FSK, PSK, QPSK, or pulse modulation transmission. The system is highly tolerant to EMI and EMP and provides excellent ground loop isolation, according to the manufacturer.
Circle Reader Action Number 782.

Pictured above is a compact remote head **CCD camera** that produces color images with a resolution of 330 horizontal lines. Developed by Chinon America Inc., Mountainside, NJ, the model CX-1000 consists of a 1.76" x .91" x .87" remote camera head, a 6-foot control cable, and a camera control unit. Applications include surveillance, industrial vision, and electronic and medical imaging.
Circle Reader Action Number 780.

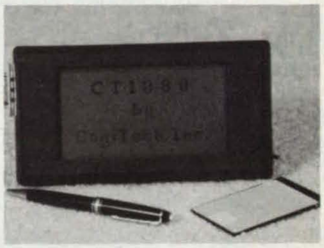

Weighing less than 1.5 pounds, the CT1000 **handheld computer** from CogiTech Inc., Goffstown, NH, offers 640K of RAM, uses memory cards in place of a disk drive, and has both a serial and a parallel port. It employs a clear resistive matrix touchpad over a 240 x 128 dot supertwist LCD. Programmed on an IBM PC using Microsoft C, the computer can be used in either horizontal or vertical mode and is software-switchable for 10 MHz or 4.77 MHz operation.
Circle Reader Action Number 788.

Ross-Hime Designs Inc., Minneapolis, MN, has produced a seven-axis **dexterous arm** that can reach into confined spaces. It features electric servo motor power and a modular design for high serviceability. Applications include telerobotics, hazardous materials handling, aerospace, and undersea operations.
Circle Reader Action Number 786.

An IR imaging and measurement system that needs no added cooling.

In R&D, NDT, or process monitoring measurements, Inframetrics' 700 Series' longwave IR accuracy makes your work easier, your results surer.

You get superior scan speed and spatial resolution —performance that won't "go south".

And there's *no LN_2 required*. Inframetrics' patented electric microcooler provides more sensitivity, greater resolution, and total freedom in scanner orientation. Design your experiment or test protocol without factoring in liquid nitrogen replenishment...or sacrificing image quality and uniformity.

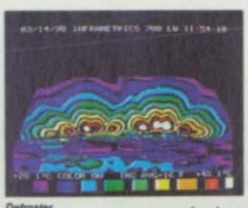

Defroster design thermal distribution

For your critical applications, there's no substitute for Inframetrics' precision temperature measurement and ultra-sharp imaging.

Other important features? Six measurement modes. Integral 3.5″ floppy disk image storage and analysis in lab or field. *Color* image viewing on a 4″ flip-up LCD. Backlit controls. RS232 remote control. And the industry's most versatile post-processing software.

Better still, Inframetrics offers unequalled applications support and training. Call our Commercial Products Division today for 700 Series information.

inframetrics

The Infrared Specialists

16 Esquire Road
North Billerica, MA 01862
Tel: 508/670-5555
Fax: 508/667-2702

Inframetrics Brussels
European Headquarters
Mechelse Steenweg 277, B-1800 Belgium
Tel: 32 2 252 5712
Fax: 358 200 740 760 or 32 2 252 5388

Circle Reader Action No. 370

New on the Market

Autodesk Inc., Sausalito, CA, has announced Release 11 of its AutoCAD **computer-aided design software**, now available for 80386- and 80486-based computers. Release 11 incorporates the new AutoCAD Development System, a C language programming environment that helps developers create specialized application programs. Another innovation is a multi-view plotting feature that enables the user to quickly lay out, organize, annotate, and plot AutoCAD drawings.
Circle Reader Action Number 774.

A new **3D laser digitizing system** has been introduced by Laser Design Inc., Minneapolis, MN, for rapid prototyping, reverse engineering, CNC duplicating, stereolithography, and inspection applications. The system is engineered for small to large parts using three-, four-, or five-axis scanning motions, and is computer-controlled for automatic scanning. It has an accuracy of ±.001" in standard work envelopes up to 36" x 60" x 24".
Circle Reader Action Number 772.

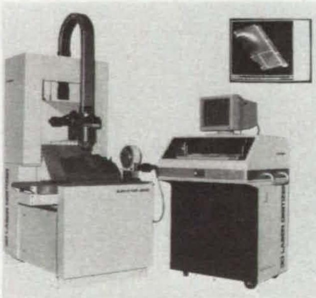

The RD 4030 series **hybrid recorder** from Omega Engineering Inc., Stamford, CT, offers high-speed scanning of 30 channels for recording, data logging, or digital storage. Multiple functions include ten-color recording on a 250 mm chart, data storage, and a variety of interface and alarm options. Optional features include RS232 or GPIB communications interfaces, math computation ability, DC power source, and remote control.
Circle Reader Action Number 762.

Optronics Engineering, Goleta, CA, has introduced the DC-450, a remote head **CCD color video camera** with auto exposure. Its microprocessor controls the electronic shutter and the camera's AGC to match available light. Shutter speeds range from 1/60 to 1/10,000 of a second. The DC-450's image sensor contains 378,624 active pixels which produce over 450 TV lines of horizontal resolution.
Circle Reader Action Number 768.

An **epoxy resin** with a 90-minute standard curing cycle at 121°C has been developed by CIBA-GEIGY Composite Materials, Anaheim, CA. Designated the R6264, the resin is preimpregnated into graphite fabric or unidirectional graphite tape. Available in a variety of area fiber weights, it features a 24°C out-time over two weeks, easy processing characteristics, and a high tolerance to variations in production technique.
Circle Reader Action Number 766.

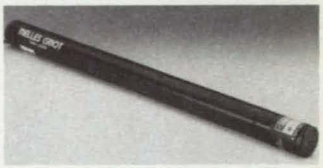

Melles Griot, Carlsbad, CA, has developed a high-power, compact 17 mW TEM_{00} **HeNe laser head** for the OEM, industrial, and research markets. The smallest HeNe laser available in this power range, the model 05 LHR 925 is housed in an industry-standard cylinder 25" long and 1.75" in diameter. Its high intensity per unit area results in a brighter beam and more power.
Circle Reader Action Number 770.

LiCONiX, Santa Clara, CA, is offering the IP series of internally-polarized, hard-sealed **helium cadmium (HeCd) lasers** for plane polarized 442 nm operation. Targeted for the optical disk and holography markets, the lasers are designed for maximum power output and minimum maintenance.
Circle Reader Action Number 764.

New Literature

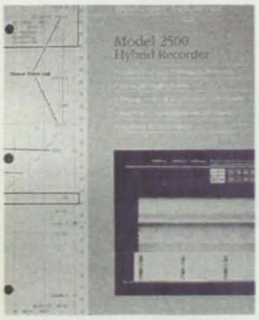

A full-color brochure distributed by Beckman Industrial Corp., San Diego, CA, showcases the model 2500 **hybrid recorder**, which combines the functions of a chart recorder and a datalogger. The instrument accepts up to 36 inputs of thermocouple, DC volts, or RTDs. It has six-color trend recording capability with digital printout, up to 80 alarm outputs, and automatic program lock.
Circle Reader Action Number 726.

Shock and vibration control products for the defense industry are spotlighted in a new catalog from Barry Controls, Brighton, MA. It contains instructions on mount selection and features a product specification section that simplifies the evaluation, comparison, and selection of isolation products.
Circle Reader Action Number 724.

A free brochure from GAF Chemicals Corp., Wayne, NJ, describes the various types of **polyvinyl pyrrolidone (PVP) polymers** and their physical and chemical properties. It also discusses commercial applications such as personal care products, plastics, inks and coatings, paper, and ceramics.
Circle Reader Action Number 718.

QK Genwave Corp., Newburyport, MA, has released a 12-page catalog containing specifications for miniature ovenized **oscillators**. It discusses frequency, phase noise, thermal and short-term stability, aging, and tuning ranges. Electrical properties and outlines for precision resonators are also covered.
Circle Reader Action Number 716.

A 32-page product directory from United Technologies Microelectronics Center, Colorado Springs, CO, features **integrated circuits** and **rad-hard technology** for the high-reliability aerospace and defense markets. Included are semicustom ICs, 1553 military-standard products, monolithic bus transceivers, rad-hard memories, and digital signal processors.
Circle Reader Action Number 722.

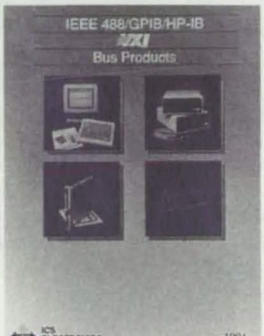

ICS Electronics Corp., Milpitas, CA, is offering a catalog of **IEEE 488/GPIB bus controllers, extenders, and expanders**, as well as VXIbus products. Over 40 hardware, software, and accessory items for GPIB and VXIbus installations are described. New products include the model 4811 IEEE 488/GPIB bus analyzer, a complete diagnostic, test, and debug tool; the model 4889A/B long-distance, fiber optic 488 bus extender; and GPIB controller cards with UNIX V and XENIX drivers for UNIX systems.
Circle Reader Action Number 720.

A new **electronic photography system** that captures and stores sharp black and white or color digital images is described in a brochure from Eastman Kodak's Government Systems Div., Rochester, NY. Using a standard Nikon F-3 camera and an advanced CCD imager, the unit captures six images in one burst at up to 2.5 images per second, and provides 1.3-million-pixel resolution. It can store up to 158 uncompressed images or 600 compressed images.
Circle Reader Action Number 728.

New Literature

Advanced Alloys Inc., Commack, NY, has published a six-page brochure describing a variety of **standard and specialty metals** in semi-finished and fabricated forms. Certification is to US federal, military, and aerospace specifications, as well as OEM requirements. The company also provides forgings, castings, and extrusions in rough, near-net, or finished dimensions.
Circle Reader Action Number 706.

The EFR 1000 **fiber recoater** from Amherst International, Burbank, CA, replaces the primary coating on spliced optical fibers and tests tensile strength. As described in a new color brochure, the microprocessor-controlled unit features an integral UV curing lamp and a flexible mold construction that prevents the bare fiber from touching the walls of the mold. Curing time ranges from 15 to 45 seconds.
Circle Reader Action Number 710.

Thermally-conductive adhesives are described in a literature package from Thermoset Plastics Inc., Indianapolis, IN. The adhesives are used to bond heat sinks, ceramic substrates, and plastic and metal lids, and offer various applications in multi-chip modules. The literature lists technical data such as cure temperature, density, viscosity, and thermal conductivity.
Circle Reader Action Number 712.

Concurrent Engineering: Issues-Technology-Practice, from Auerbach Publishers, New York City, details the experiences of companies that are applying **concurrent engineering**, including the obstacles they face and the strategies and techniques they employ. The publication analyzes technical tools such as tolerance packages and data management systems which can help engineers implement concurrent engineering.
Circle Reader Action Number 714.

A color brochure from Tinius Olsen, Willow Grove, PA, features **equipment for determining the mechanical properties of metals, plastics, composites**, and other materials. Featured products include electroluminescent digital indicating systems, floor model and benchtop universal testing machines, automated melt indexers, and fully-automated robotic testing systems.
Circle Reader Action Number 708.

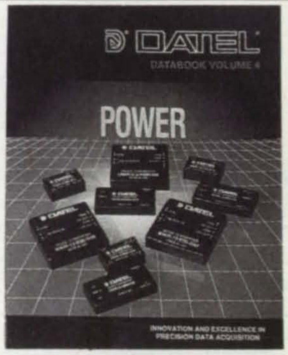

A 148-page catalog from Datel Inc., Mansfield, MA, includes specifications, data sheets, and applications for over 170 **power conversion** products. It covers wide-range-input DC-to-DC converter modules, data conversion hybrids, PC/AT and VMEbus board-level products, and panel-mount instrumentation. The publication contains a glossary of power supply terms and a section reporting recent innovations in power converter design.
Circle Reader Action Number 702.

Vibration, shock, and motion control products for military and commercial electronics applications are highlighted in a new catalog from Lord Aerospace Products, Erie, PA. The 132-page publication features low-profile avionics, plate-form, multiplane, high-deflection, and shipping container mounts. It devotes a section to vibration, shock, and motion control theory used in isolator selection.
Circle Reader Action Number 704.

Subject Index

Schnell Publishing Company

Chemical Marketing Reporter • Chemical Business

announce the election of

EDGAR S. WOOLARD, JR.

Chairman and C.E.O. / DuPont Company

to receive

The 1991 Kavaler Award

for

Chief Executive Excellence in the Chemical Industry

The Award

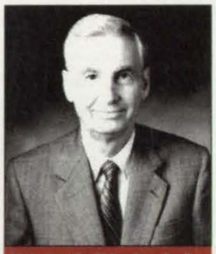

Edgar S. Woolard, Jr.

Mr. Woolard has been selected by the votes of an international Selection Committee of 50 chemical investment research analysts as being "the chemical industry chief executive who, by his vision and management skills, has made the most unique contribution to his company's success."

The industry's highest honor for executive achievement, the Kavaler Award was created by Schnell to recognize the accomplishments of chemical chief executive officers — those individuals who make it possible for the industry to function, succeed and grow.

The Selection Committee

Eleanor Barker, Sanwa McCarthy Securities Ltd.
Michael Binette, Burns Fry Ltd.
Leonard Bogner, Prudential Securities
Dr. Peter E. Butler, First Boston Corp.
Andrew W. Cash, First Manhattan Co.
Dr. Aris P. Christodolou, Mayfair Capital Partners
Jeffrey Cianci, Bear Stearns & Co.
Dr. Allan H. Cohen, Kemper Securities Group
Jean-Pierre Conreur, Tocqueville Asset Management
Tony Cox, Kleinwort Benson Securities
Melvin Cutler, Cutler Associates Investments
John L. Garcia, Wertheim Schroder
David V. Goacher, Allstate Insurance Co.
Robert D. Hardiman, Merrill Lynch Capital Markets
Jay R. Harris, Goldsmith & Harris
Michael Hoffman, Salomon Brothers
Warren J. Isabelle, Pioneering Management Corp.
Samuel Kanes, Scotia McLeod Inc.
Nicholas J. Kovich, Miller Anderson Sherrerd
George Krug, Oppenheimer & Co.
David S. Leibowitz, American Securities Corp.
John Lowry, Buckingham Research
Paul Miles, Neuberger & Berman
C. J. Milton, Research Capital Corporation
Avi M. Nash, Goldman Sachs
Kenneth R. Nover, Nover Associates
Richard O'Reilly, Standard & Poor's Corp.
Donald A. Pattison, C. J. Lawrence, Morgan Grenfell
Robert A. Payne, Citibank N.A.
Stuart Pulvirent, Shearson Lehman Brothers
Anantha K. S. Raman, Anantha Raman & Co.
Leslie C. Ravitz, Salomon Brothers
Robert S. Reitzes, Mabon Nugent & Co.
Dr. Albert Richards, Credit Suisse First Boston
Matthew D. Robbins, Duff & Phelps/MCM
John E. Roberts, Kidder, Peabody & Co.
Amy Ryan, Fred Alger & Co., Inc.
Joseph Salvani, E G S Partners
Regis W. Schultis Jr., J. P. Morgan Securities
Theodore Semegran, Shearson Lehman Brothers
Fred H. Siemer, Siemer Company
James F. Spencer, Wertheim Schroder
Edward J. Stavetski, Radnor Capital Management
Harvey Stober, Dean Witter Reynolds
James H. Wilbur, Smith Barney, Harris Upham
Luke F. Williams, Ingalls & Snyder
Christopher H. Willis, Brown Brothers Harriman
Thomas G. Wolfe, Standard & Poor's Corp.
Dr. William R. Young, Donaldson, Lufkin & Jenrette

The Event

Mr. Woolard will accept the Kavaler Award as the culmination of the Chief Executive Award Dinner at CHEM/EVENT 91, the annual black-tie Washington affair for chemical industry chief executives, their primary associates, and selected senior members of the executive and legislative branches of the federal government.

The recipient of the 1990 Award, Frank P. Popoff, President and C.E.O., The Dow Chemical Company will be on hand to take part in the presentation to Mr. Woolard.

The 1991 affair will further the high standards of last year's event, hailed as "terrific," "spectacular," and a "most memorable evening," by industry and government executives attending.

The new date for the Dinner is September 24th, changed from the previously announced September 25th.

Mark your calendar and plan now to reserve your table.

THE CHIEF EXECUTIVE AWARD DINNER
September 24, 1991
The Capital Hilton
Washington, D.C.

For information and reservations, contact
CHEM/EVENT 91, Box 1025, Wall Street Station, New York, NY 10268-1025, Telephone: 212-966-3100

CHEM EVENT 91

The Chief Executive Award Dinner
September 24, 1991
The Capital Hilton
Washington, D.C.

About Reservations

The Dinner is a business program for chemical industry executives and their guests and, as such, has no fund-raising or political purposes.

Please use the attached form to place your reservations for the Dinner. A check for the total amount of fees, or a corporate purchase order, must be enclosed with the form.

The earlier the reservation, the better the table location. Reservations will be processed in the order received, and promptly acknowledged. Further advisories will be sent as the event approaches.

Reservation Fees

For the Dinner, per person: $250
For the Dinner, per table of ten: $2,500

Please note that spouses and companions are most welcome to attend at the fees listed above.

The CHEM/EVENT 91 office may be reached at 212/966-3100 for information and assistance between 9 a.m. and 5 p.m. (Eastern Time)

Cancellation Policy

Substitutions may be made at any time up to September 24th. After September 17th, however, we cannot guarantee that the name of the substitute will be listed in the official seating or attendance lists.

Cancellations received at the CHEM/EVENT 91 office prior to 5:00 p.m. August 30th will be refunded in full. Cancellations received between August 30th and September 13th will result in a penalty of 50% of the refund. No refunds can be made for cancellations after September 13th.

About Accommodations

A block of rooms has been reserved at special rates for CHEM/EVENT 91 Dinner attendees at The Capital Hilton Hotel for the evenings of September 23rd and 24th. Requests for dates other than the 23rd and 24th will be on an "as available" basis.

Please reserve at an early date in order to avoid disappointment. Use the attached form to deal directly with the Reservations Department.

The Capital Hilton
Telephone: 202-393-1000
Fax: 202-639-5784

Circle Reader Action No. 483

HOTEL RESERVATION FORM

MAIL TO: Reservations Manager/The Capital Hilton Hotel
16th & K Streets N.W./Washington, DC 20036

RE: CHEM/EVENT 91 Chief Executive Award Dinner
September 24, 1991

ARR: 9/____/91 **DEP:** 9/____/91

ROOM:
________ Deluxe Single @ $175.00*
________ Superior Single @ $200.00*
________ Deluxe Double @ $190.00*
________ Superior Double @ $215.00*
________ Suite @ $400.00 (and up)*

(*All rates subject to Sales Tax of 11% and Occupancy Tax of $1.50. Room type subject to availability at time reservation received.)

NAME: ____________________

COMPANY: ____________________

ADDRESS: ____________________

CITY: __________ ST: ______ ZIP: ________

To Guarantee Your Reservation

If this reservation is not cancelled before 6:00 p.m. on arrival date, and I do not occupy the accommodations, I authorize billing of a one-night room charge to my:

_____ American Express _____ Diners Club _____ Visa
_____ Carte Blanche _____ MasterCard

Card #: ____________________ Exp.: ________

Signature: ____________________

NOTE: The cut-off date for reservations at the rates given is September 3,1991.

DINNER RESERVATION FORM

MAIL TO: CHEM/EVENT 91 / Box 1025
Wall Street Station / New York, NY 10268-1025

(Telephone Inquiries & Automatic Fax Reception: 212-966-3100)

______ Please reserve _____ place (s) @ $250 for the Chief Executive Award Dinner.

______ Please reserve _____ table (s) for ten people @ $2,500 for the Chief Executive Award Dinner.

NOTE: THE DINNER IS A BLACK-TIE AFFAIR.

Payment

______ A check in the amount of $__________ is enclosed to the order of Schnell Publishing Co.

______ A corporate purchase order in the amount of $__________ is enclosed.

NAME: ____________________

TITLE: ____________________

COMPANY: ____________________

ADDRESS: ____________________

CITY: __________ ST: ______ ZIP: ________

TEL #: __________ FAX #: __________

In submitting this form, I agree to be bound by the terms of cancellation as outlined in the information supplied.

Advertisers Index

***RAC** stands for **Reader Action Card.** For further information on these advertisers, please circle the RAC number on the Reader Action Card in this issue. This index has been compiled as a service to our readers and advertisers. Every precaution is taken to insure its accuracy, but the publiser assumes no liability for errors or omissions.

NASA Tech Briefs, ISSN 0145-319X, USPS 750-070, copyright © 1991 in U.S., is published monthly by Associated Business Publications Co., Ltd., 41 E. 42nd St., New York, NY 10017-5391. The copyrighted information does not include the individual tech briefs which are supplied by NASA. Editorial, sales, production and circulation offices at 41 East 42nd Street, New York, NY 10017-5391. Subscription for non-qualified subscribers in the U.S. , Panama Canal Zone, and Puerto Rico, $75.00 for 1 year; $125.00 for 2 years; $200.00 for 3 years. Single copies $10.00. Foreign subscriptions one-year U.S. Funds $150.00. Remit by check, draft, postal, express orders or VISA, MasterCard, and American Express. Other remittances at sender's risk. Address all communications for subscriptions or circulation to NASA Tech Briefs, 41 East 42nd Street, New York, NY 10017-5391. Second-class postage paid at New York, NY and additional mailing offices.

POSTMASTER: please send address changes to NASA Tech Briefs, 41 East 42nd Street, Suite 921, New York, NY 10017-5391

Modular Computers ®

LEA

in VME

POWERFUL FAMILY OF 16/32-BIT CMOS CPUs

PRODUCT	CPU/FPCP	MIPS (Max.)	SPEED (MHz)	CMOS-RAM (MByte)	RAM Back-up Source	ROM (MB)	RTC/ Watch-dog	Serial I/O	Misc. Features	Power Cons. (Watts)	Max Temp. (°C)
VM40	68040	20	50	4/8/16/32/ DRAM	Ext.	1	●	2	EEPROM LXB	5 – 8	-40 to +85
VM20	68020/68882	4	16/25	1/2/4/8 DRAM	Ext.	2	●	2		4 – 6	-55 to +125
VMPM 68KD	68030/68882	6	16/25	0.5–3 SRAM	Ext. or Battery	0,5	●	2		10 – 12	-55 to +125
VMPM 68KC-2	68020/68882	4	12/16/25	0.5–3 SRAM	Ext. or Battery	0,5	●	2		9 – 11	-55 to +125
VSBC-1	68HC000	1	12/16	0.1–1 SRAM	Ext. or Battery	0,5	●	2	SCSI	4	-40 to +85
VSBC-2	68HC000	1	16	0.1–1 SRAM	Ext. or Battery	1	●	6		2	-55 to +125
VSBC-3	68HC000	1	16	0.1–1 SRAM	Ext. or Battery	1	●	4	20 x TTL	3	-55 to +125

HIGH PERFORMANCE CONTROLLERS

★ ETHERNET/CHEAPERNET IEEE 802.3.w TCP/IP ★ TELNET/FTP
★ X.25, X.21 ★ MIL1553B ★ BITBUS ★ SCSI ★ GRAPHICS
★ 2 AXIS MOTION CONTROLLER ★ STEPPER MOTOR INTERFACE

INDUSTRIAL I/OS

★ ISOLATED DIGITAL I/OS ★ RELAYS ★ SERIAL I/O ★ 12/14/16-BIT A/D, D/A ★ SIGNAL CONDITIONING ★ PT100/J/K TEMP. SENSORS
★ ENCODER/COUNTER ★ PLUGGABLE-SCREW TERMINALS

PLC LANGUAGES

★ IEC 848 GRAFCET ★ LADDER DIAGRAM ★ FUNCTION PLAN
★ GRAPHICS EDITOR ★ WINDOW DEBUGGING
★ PROJECT MANAGEMENT ★ ON-LINE DOCUMENTATION

PEP Modular Computers Inc.
600 North Bell Avenue
Pittsburgh, PA 15106
Tel: ++1 (412) 2 79 66 61
Fax: ++1 (412) 2 79 68 60
Call tollfree:
(outside PA) 1- 800 -228 -17 37
(inside PA) 1- 800 -255 -17 37

★ Germany ★ Kaufbeuren Call ++49 (83 41) 4 30 20
★ France ★ Sèvres Call ++33 (1) 45 34 60 60
★ Sweden ★ Täby Call ++46 (8) 7 56 72 60
★ Benelux ★ Brussels Call ++32 (2) 4 78 34 16
★ UK ★ Brighton Call ++44 (273) 42 39 15

★ USA ★ GERMANY ★ FRANCE ★ UK ★ SWEDEN ★ BENELUX ★
★ CHINA ★ NORWAY ★ DENMARK ★ FINLAND ★ ITALY ★ SPAI

ADERSHIP
Single Height Systems
RE·SUPPORT·SERVICES
★68040
★20 MIPS
★3,5 MFLOPS
★32 MB RAM
★1 MB ROM
★EEPROM
★EXT. I/O
VM40
VIX.25
VMEbus
locity
TXvelocity
Circle Reader Action No. 533
TZERLAND ★ AUSTRIA ★ USSR
APAN ★ POLAND ★ CSFR ★ HUNGARY
Modular Computers